Doctoral Dissertation

Development of low temperature curable Cu inks with high conductivity and reliability for printed flexible electronics

Wanli Li

July 2018

Department of Adaptive Machine Systems,

Graduate school of Engineering,

Osaka University

Abstract

Printable and flexible electronics have attracted much attention because of their eco-friendly manufacturing processes and advantageous features such as light-weight, bendable, and foldable. With the market expansion, the development of abundant Cu inks instead of expensive Ag/Au nanoparticles inks becomes increasingly inevitable. However, the high preparation cost and oxidation of Cu nanoparticles as well as the poor stability of printed Cu patterns are insurmountable obstacles for their practical applications.

This dissertation provides three strategies: using submicron Cu particles instead of Cu nanoparticles, utilizing intense pulsed light (IPL) sintering, and introducing anti-oxidation Ag element, to address the oxidation problem of Cu inks and improve the conductivity and reliability of printed Cu patterns, enabling them to replace or partly replace the noble Ag and Au inks in the application of printable and flexible electronics.

At first, the concept that using in-situ formed fresh Cu nanoparticles to help sintering the submicron Cu particles has proved feasible by the developed submicron Cu particle/Cu complex inks. During the low temperature heat treatment of 140 °C, fresh Cu nanoparticles decomposed from Cu complex can attach to the submicron Cu particles and activate their surface, which contributes to sintering and neck-growth among these submicron Cu particles to achieve conductive pathways. With the reinforcement of IPL sintering, the microstructure of printed Cu patterns become denser and robust, and a resistivity below 5.8×10^{-6} Ω·cm is successfully achieved, which is superior to those obtained from Cu nanoparticle inks. Importantly, the method opens a new way for making highly reliable and highly conductive Cu patterns with large Cu particles instead of nanoparticles, which can largely decrease the cost and enhance the application of Cu inks for flexible electronic devices.

In order to improve the oxidation resistance of printed Cu patterns, printable and flexible Cu-Ag alloy patterns with high conductivity and ultrahigh oxidation resistance were successfully fabricated by using a newly developed Cu particle/Ag complex ink and employing a two-step sintering method. At the first step, the Cu particle/Ag complex ink transforms into a Cu-Ag nanoparticle core-shell structure under a low temperature of 140 °C in air and then further transforms into Cu-Ag alloy under IPL sintering which induces rapid diffusion between

the Cu core and the Ag nanoparticle shell. It was revealed that the obtained Cu-Ag alloy patterns have a bulk-like microstructure and show a very low resistivity of 3.4×10^{-6} Ω·cm (50 % of the bulk conductivity of Cu). It was clearly determined that the Cu-Ag alloy has a special core-shell structure with a Cu-rich phase in the core and an Ag-rich phase in the shell, showing high stability. The printed flexible patterns of the Cu-Ag alloy have ultrahigh oxidation resistance, remaining stable in air at 180 and 200 °C and demonstrating great potential for practical use in the fabrication of highly reliable and cost-effective printed electronic devices.

Finally, for printing electronics on heat-sensitive PET or paper substrates, Cu-Ag complex inks were put forward to fabricate highly oxidation-resistant and conductive patterns at a low temperature below 100 °C. The inks show an obvious self-catalyzed characteristic due to the in-situ formation of fresh metal nanoparticles which promote rapid decomposition and sintering of the inks at a low temperature below 100 °C. The process temperature is 40-60 °C lower than those of general Cu complex inks and 100-120 °C lower than those of general Cu/Ag particle inks. Highly conductive Cu-Ag patterns of 2.8×10^{-5} Ω·cm and 6.4×10^{-5} Ω·cm had been easily realized by sintering at 100 °C and 80 °C, respectively. In addition, the printed Cu-based patterns show high oxidation resistance not only at high temperatures of up to 140 °C (the maximum tolerable temperature of current PET substrate) but also at high humidity of 85 % because of the uniform Cu-Ag hybrid structure. The printable patterns exhibit great potential for applications in various wearable devices fabricated on textiles, papers, and other heat-sensitive substrates.

The dissertation confirms that developing novel Cu inks with anti-oxidation property, and corresponding curing methods can greatly improve the conductivity and reliability of printed Cu patterns, enabling them to be acceptable in various printed electronics.

Contents

List of figures

Figure 3.15 (a) Changes of relative resistance of sintered Cu patterns on PET, PEN and PI substrates as function of the outer bending radius. (Inset) Photograph of the specimen for outer bending test. (b)-(d) Changes of relative resistance of sintered Cu patterns during a repeated bending test at a bending radius of 10 mm on PET, PEN and PI substrates, respectively. Low temperature welding of 140 °C for 10 min and subsequent IPL using energy of 1080 mJ/cm^2, 1273 mJ/cm^2, and 2073 mJ/cm^2 were used to make sintered Cu patterns on PET, PEN, and PI substrates, respectively.

Figure 3.16 Relationship between bending radius and moving distance.

Figure3.17 Softening phenomenon of sintered Cu pattern on PEN substrate.

Figure 3.18 Change of relative resistance (R/R_0) of printed Cu films at temperatures of (a) 140 °C, (b) 180 °C, and (c) 220 °C, respectively, in air. R_0 is the original resistance of the printed patterns and R is the resistance of the printed patterns after oxidation at high temperatures. (d) XRD patterns of printed Cu films after oxidation in high temperatures for 5 hours. Low temperature heating of 140 °C for 10 min and IPL sintering using energy of 3300 mJ/cm^2 were used to fabricate printed Cu patterns.

Figure 3.19 Surface microstructures of printed Cu patterns after oxidation for 5h at (a, d) 140 °C, (b, e) 180 °C, and (c, f) 220 °C, respectively. The printed Cu patterns prepared from Cu particle ink with an average size of 350 nm are shown in a-c and those prepared from Cu particle ink with an average size of 800 nm are shown in d-f.

Figure 3.20 Mass fractions of CuO, Cu_2O and Cu in printed Cu patterns as a function of time, oxidized at (a) 140 °C, (b) 180 °C, and (c) 220 °C, respectively. Sample A and Sample B mean the printed Cu patterns prepared from Cu particles with average sizes of 350 nm and 800 nm, respectively.

Figure 3.21 Cross-sectional microstructures of printed Cu patterns after oxidation for 5h at (a, d) 140 °C, (b, e) 180 °C, and (c, f) 220 °C, respectively. The printed Cu patterns prepared from Cu particles with an average size of 350 nm are shown in a-c and that prepared from Cu particles with an average size of 800 nm are shown in d-f.

Figure 3.22 Photographs of the LED circuit with a 20 mm-long printed conductive pattern on PET, PEN, and PI substrates during the bending, folding, and twisting tests.

resistivity of patterns using Cu-46Ag complex ink. The dashed line in Figure 5.2a indicates the resistivity of bulk Ag.

Figure 5.3 Microstructure of patterns prepared from (a) pure Cu, (b) Cu-30Ag, (c) Cu-46Ag, (d) Cu-63Ag, and (e) pure Ag complex inks; (f) corresponding XRD patterns. Insets in Figure 5.3a-e are corresponding cross-sections of patterns, respectively, which were taken on an angle of 30°. The scale bar in insets is 200 nm. The annealing process is 100 °C for 30 min.

Figure 5.4 (a) XRD patterns of Cu pattern annealed at different temperatures for 30 min and (b) microstructure of Cu pattern annealed at 140 °C for 30 min.

Figure 5.5 (a) TEM image of pattern prepared from Cu-46Ag ink, (b) magnified TEM image, and (c) corresponding HR-TEM image. (d) STEM image and corresponding mapping images of (e) Cu and Ag, (f) Cu, and (g) Ag element.

Figure 5.6 (a) DSC results of pure Cu and Ag inks; (b) DSC, (c) TG, and (d) differential TG (DTG) results of all inks.

Figure 5.7 XRD patterns of (a) pure Cu, (b) pure Ag, and (c) Cu-46Ag complex inks; (d) TEM image and their HR-TEM image (inset) of in-situ formed Ag nanoparticles in Cu-46Ag complex ink.

Figure 5.8 XRD patterns of Ag complex ink after storage in ambient conditions for one month and Ag complex ink with addition of 5 wt. % formate acid.

Figure 5.9 Schematic illustration of self-catalyzed decomposition and sintering of Cu-Ag complex inks.

Figure 5.10 Changes in the relative resistance (R/R_0) of patterns prepared from pure Cu, Cu-30Ag, Cu-46Ag and Cu-63Ag complex inks in air at (a) 80 °C, (b) 110 °C, (c) 140 °C, and (d) 85 °C-85 % RH.

Figure 5.11 Microstructures of (a) original Cu-63Ag-100 pattern and (b) Cu-63Ag-100 pattern after aging at 80 for 2 h.

Figure 5.12 XRD patterns of printed patterns after oxidation at 140 °C for 64 h.

Figure 5.13 Photographs of the LED circuit with a 100 mm-long metal pattern prepared from (a) pure Cu and (b) Cu-46Ag complex inks on PET substrate after oxidation at 140 °C.

Figure 5.14 Change of relative resistance of the Cu-46Ag pattern during bending test. The

bending radius is 7 mm. Inset graph shows the real-time relative resistance during the last ten cycles of bending and releasing process.

List of tables

Chapter 1

Research background

1.1 Printed electronics

1.1.1 Definition and advantages of printed electronics

There are many kinds of definitions about printed electronics (PE). For example, PE is a set of printing methods used to create electrical devices [1]; PE uses traditional printing techniques to make electronic devices or circuits [2]; PE is a type of electronics that are created by printing technology [3]. To be sure, PE is closely related to the electronic manufacturing and printing technology. Here, based on our understanding, we define PE as a technology that merges electronic manufacturing technologies and traditional printing technologies to fabricate electronic devices and systems [4].

Compared with traditional electronic manufacturing technology, PE technology brings about the possibility of manufacturing electronic devices in a much simpler, faster, more cost-effective and more eco-friendly way [5]. As shown in **Figure 1.1**, to turn a functional material into a functional structure or pattern on a substrate, traditional manufacturing has to go through thin film deposition, spincoating photoresist layer, baking, photolithography, baking, developing, etching, and stripping of the photoresist masking layer [3]. In contrast, if the PE technology is employed, the functional material can be directly printed as patterns onto the substrate, followed by a simple post-treatment such as drying, annealing or sintering process. For a more complex device such as a field-effect transistor, the source, drain, and gate patterns, as well as semiconductor and insulating layers, can also be printed layer by layer onto a substrate [3]. It is clear that PE technology simplifies the manufacturing processes of electronics and saves a lot of materials as well as energy, showing huge potential in the field of manufacturing industry for electronic devices.

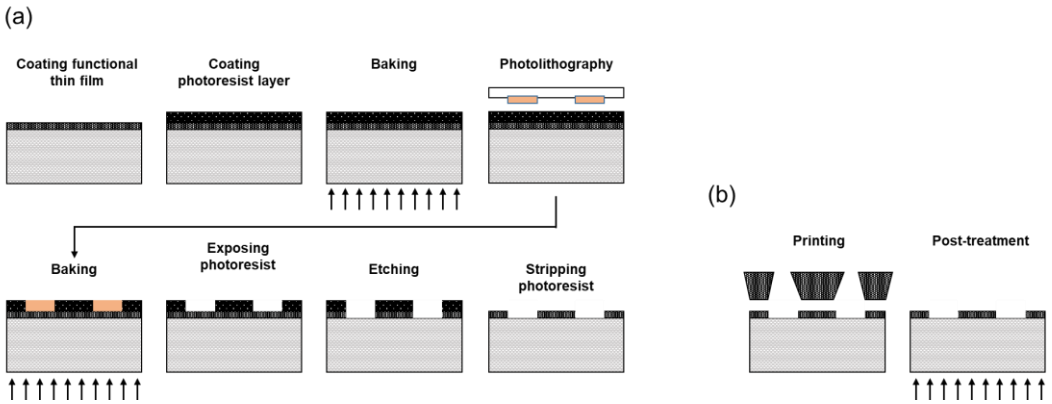

Figure 1.1 Comparison between (a) conventional microfabrication and (b) printing fabrication for integrated circuits [3].

Another advantage of PE technology is that electronic devices can be printed on various substrate materials rather than only on silicon wafers or on printed circuit board, which endow printed electronics with some unconventional features [5]. For example, when transparent plastic films are used as substrates, electronic devices become flexible, more lightweight, and even transparent; when the paper is used as substrates, the electronic devices become more environmentally friendly; when our skin or clothes are used as substrates, the electronics become wearable. **Figure 1.2** show some examples of printed electronic circuits or devices on plastic substrate, paper substrate, and our skin. It is believed that with the development of technologies, these novel electronics will change our daily life and have a big impact on our society.

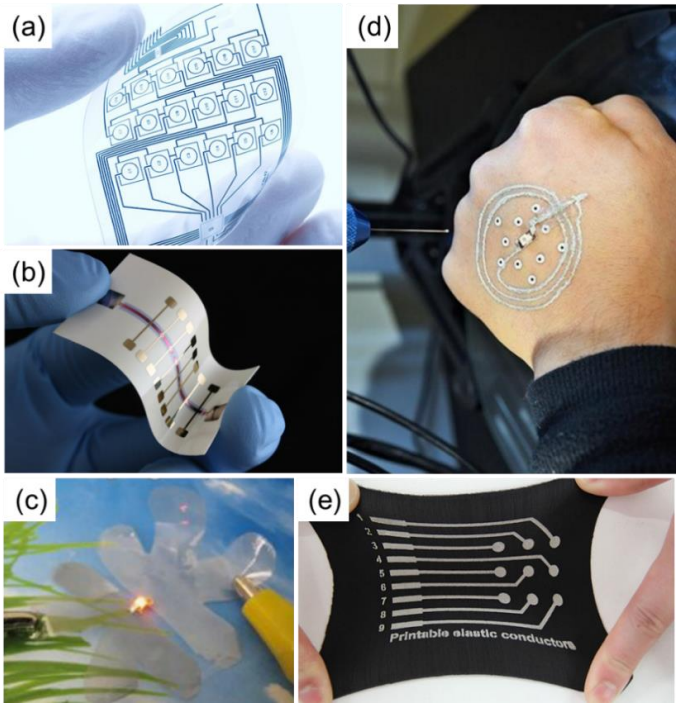

Figure 1.2 Examples of printed electronic circuits or devices on (a) plastic substrate [6], (b) paper substrate [7], (c) transparent paper [8], (d) skin [9], and (e) textile [10].

1.1.2 Three elements of PE

PE technology contains three basic elements: printable materials, printing methods, and post-treatment methods. Printable materials, also called as inks, are one of the foundations of printed electronics [3]. They will play roles of conductors, semiconductors, dielectric, or insulators and so on in the printed electronics. Printable materials mainly include organic materials and inorganic materials. Organic materials with perfect solubility can be naturally made into ink forms, thus they were firstly studied in detail and used for printed electronics, especially in organic photovoltaic cells (OPVs) and organic light-emitting diodes (OLEDs) [11, 12]. On the other hand, inorganic materials are usually insoluble solid, which need to change the morphology and size, and mix with a variety of additives (e.g., binders and surface tension modifiers) for improving the stability and printability [13-15]. However, both of them have advantages and disadvantages, as shown in **Table 1.1**. Much more researches are needed to improve these printable materials for fabrication of high performance printed electronics.

Table 1.1 Advantages and disadvantages of organic and inorganic materials for printed

electronics [3].

Materials	**Advantages**	**Disadvantages**
Organic materials	Better printability Low annealing temperature Flexibility	Low charge mobility Poor environment stability Batch to batch inconsistency
Inorganic materials	High charge mobility Environmental stability Mature manufacturing technology	Difficulty in ink formulation Impurity due to surfactants High post-processing temperature

Printing methods are manufacturing technologies of printed electronics, derived from traditional media printing industry [3]. To meet the different requirements such as compatibility with inks, printing resolution, speed, and cost, a wide variety of printing methods have been developed and used for printed electronics, such as screen printing, inkjet printing, flexographic printing, and offset-gravure printing [4]. The features and requirements of these printing methods are summarized in **Figure1.3**. The choice of a printing method is sometimes a major issue before launching research projects or before building up production lines. It should be suitable matching with inks, substrates, and quality of expected printed electronics.

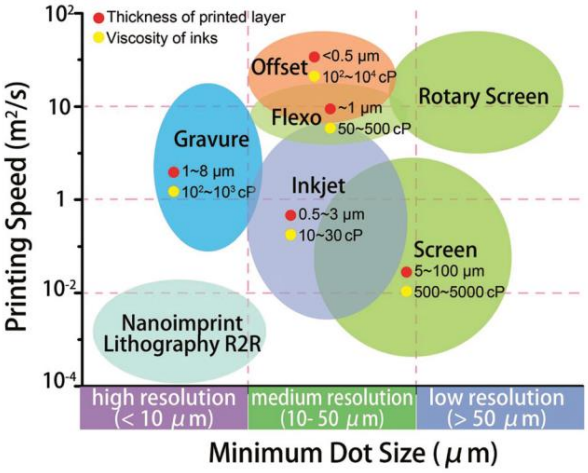

Figure 1.3 Resolution and throughput for various printing technologies [2].

After printing, a necessary post-treatment such as drying, curing or sintering, is required for the printed ink patterns or devices to acquire specific electronic properties [4, 15, 16]. For instance, printed patterns from Ag nanoparticle inks need a high temperature sintering above 150 °C to achieve a low resistivity with the order of 10^{-6} Ω·cm [17, 18]; Cu nanoparticle inks require a higher temperature above 200 °C and also an inert atmosphere for preventing them from severe oxidation [19]; semiconductor thin films made from oxide nanoparticles require a much higher treatment temperature above 300 °C to improve their charge mobility [20, 21]. It should be noted that the traditional thermal treatment, heating printed ink patterns or devices at such high temperatures, will damage most plastic (such as Polyethylene terephthalate (PET) and Polyethylene naphthalate (PEN)) and paper substrates, which inescapability hinders the application of these printable materials in flexible electronics. To overcome this problems, some specific post-treatment methods have been put forward, such as photonic sintering [22-28], plasma sintering [29-31], and microwave sintering [32]. Photonic sintering technology includes laser sintering, intense pulsed light (IPL) sintering, infra-red (IR) sintering, ultra-violet (UV) assisted sintering. By matching the emission spectrum of the light source with the absorption spectrum of the printable materials, light is mainly absorbed by the printable materials to realize their sintering without damaging the substrates [16, 33, 34]. Plasma sintering uses the ionized gas to bombard the printable materials and realize the decomposition/evaporation of organic stabilizers as well as the sintering of nanoparticles [31, 35]. In addition, if the hydrogen is used as feed gas, the plasma can have a reducing property [36]. Microwave sintering means that microwave is absorbed by printable materials and activate the evaporation of organic stabilizers as well as the sintering of materials [16, 37]. **Table 1.2** summarizes the advantages and disadvantages of these post-treatment approaches. Since every post-treatment approach uses a different equipment and has a different mechanism, it is difficult to appoint one technology which is suitable for every ink, every substrate, and every application.

Table 1.2 Advantages and disadvantages of various post-treatment methods.

Treatment	Advantages	Disadvantages
Thermal	Low cost, high throughput	Damaging the substrates, time-consuming
Laser	Selective heating, high resolution	Low throughput, complicated operation
IR/UV/IPL	Selective heating, high throughput	Complicated operation
Plasma	Temperature as low as possible	Low throughput, surface effect, etching of the surface of substrate
Microwave	Fast and volumetric heating	Low throughput, small penetration depth, local overheating

1.1.3 Applications

Due to the inherent advantages of large area, flexibility, and low cost and so on, PE technology has been employed to fabricate various electronic devices, such as transistors [38, 39], solar cells [40], sensors [41], and even integrated smart systems [42].

A transistor generally consists of a source pattern, a drain pattern, a gate pattern, an active layer (semiconductor), and a dielectric layer. The active layer is connected to the source pattern and the drain pattern. The dielectric layer is positioned between the active layer and the gate pattern. As shown in **Figure 1.4**, a transistor can be fabricated by four printers with pre- and post-treatment equipment, just like a full-color gravure printing of graphics products. The first printer is used to fabricate source and drain conductors on a film. The second printer is responsible for the printing of a semiconductor layer connected to the source pattern and the drain pattern. The third printer creates a dielectric layer on them. Finally, a gate pattern is printed on the dielectric layer by the fourth printer. At each printer, pre-treatment and post-treatment are done in a short time. Because of the fast roll-to-roll printing speed, the time is much shorter than that using traditional Si semiconductor manufacturing. In addition, the fabricated transistor is possible to be flexible because a flexible PET substrate is used.

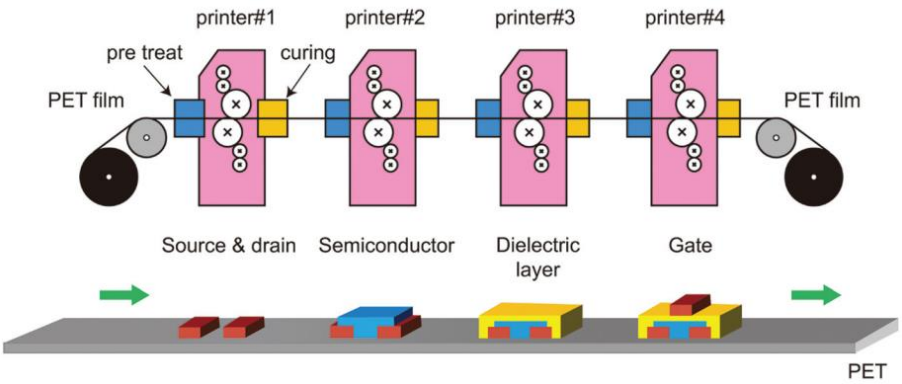

Figure 1.4 Schematic diagram of fabricating transistors by four printers [4].

A solar cell, or photovoltaic cell, can convert the energy of light directly into electricity by the photovoltaic effect and function as a power source to support the working function of other electronic devices. Flexible printed solar cells make for a variety of possibilities in terms of their application scenarios. For example, we can hang it from a backpack to harvest light energy when we are traveling; we can fix it on clothes to support the working of wearable electronics; and if we do not need it, we can roll it up for saving space. An indispensable component in solar cells is the front and back conductive patterns, which can be fabricated by printing techniques. As shown in **Figure 1.5**, fully-printed Ag back patterns were prepared by using different printing techniques in polymer solar cells [43]. Even though the performance of printed Ag back patterns is related to printing methods, the fact is that these patterns in solar cells can be successfully prepared by using proper PE technology.

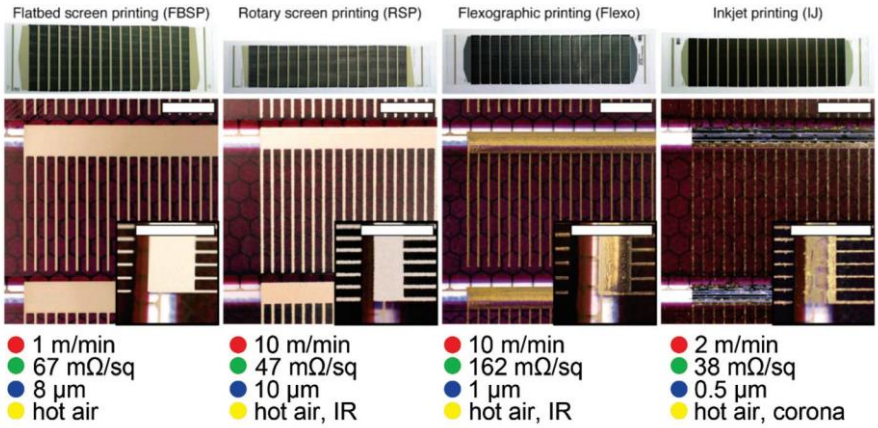

Figure 1.5 Printed Ag back electrodes by different printing techniques. The microphotographs

show the layer and edge quality and the areas of serial connection (scale bar is 5 mm). The printing speed, resistivity, thickness, and sintering parameters are shown below [2].

Sensors can detect events or changes in its environment and help people or robots to efficiently make a right response. Printable and flexible sensors containing many advantages such as lightweight, bendability, and foldability as well as low cost, have attracted much attention for a wide application. For instance, a fully-printed strain sensor array as shown in **Figure 1.6a** is a good example of a low-cost, flexible and lightweight system that can provide a reliable method for monitoring the structural health of aircraft [44]. A gas sensor shown in **Figure 1.6b** was fabricated by inkjet printing of polyaniline nanoparticle films with Ag-based conducting interdigitated pattern arrays on a PET film, having a stable logarithmic response to ammonia in a range of 1-100 ppm [45].

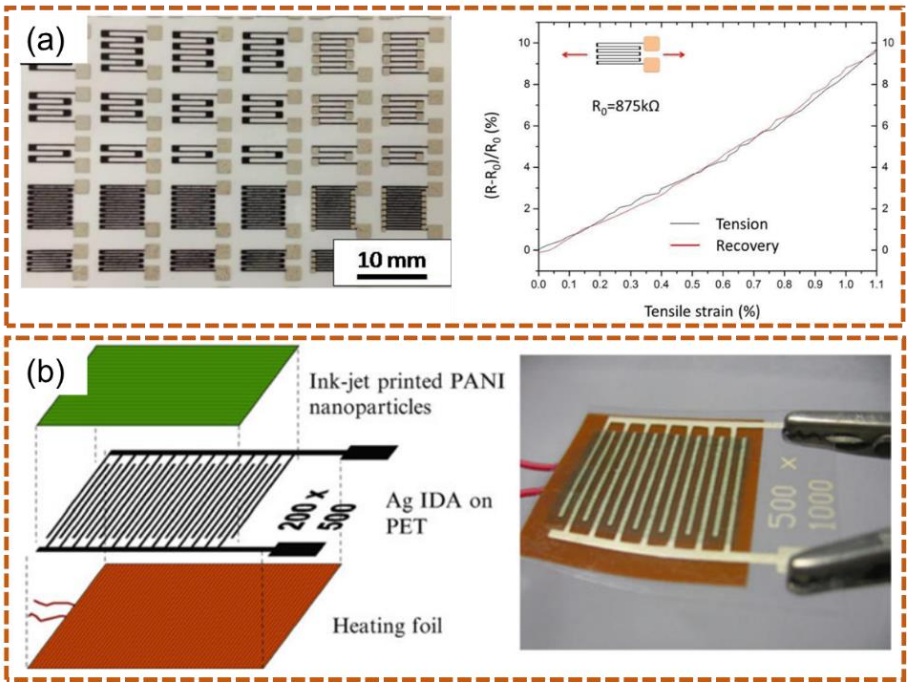

Figure 1.6 (a) Screen-printed strain sensors on PET substrates and their response to strain and (b) ink-jet printed ammonia gas sensor with polyaniline interdigitated electrodes [4, 44].

PE technology has also attracted increasing attention in the field of integrated smart systems that not only have electronic components such as transistors and sensors but also have power supply and data communication. As shown in **Figure 1.7**, all-printed smart temperature

sensor tags have been successfully developed by Thin Film Electronics company for medication control and food traceability. The smart tag integrates printed transistors for a logic, printed temperature sensor strip, a printed battery patch and an electro chromatic display, thus although PE technology has made great progress in recent years, it is still quite difficult to have everything printed for a smart system at present. PE technology as a new field will have a long way to go before becoming a mainstream industrial technology.

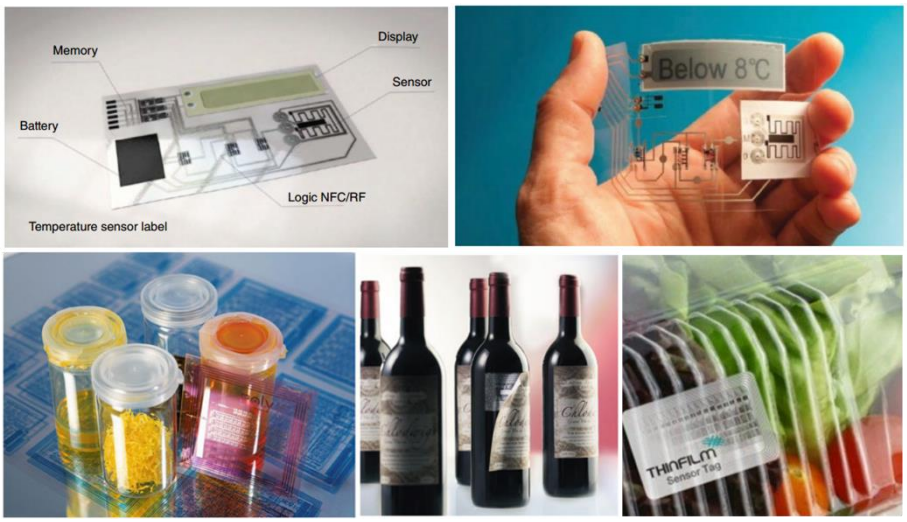

Figure 1.7 All-printed smart temperature sensor tag for medicine and food traceability management [3, 4].

1.2 Overview of conductive inks for printed electronics

As mentioned above, PE involves many aspects, such as printable materials, printing methods, and post-treatment methods, which is a comprehensive research field of physics, chemistry, materials, and electronics. Among them, printable materials are one of the key foundations of printed electronics, and especially printable conductive materials can be used to print various conductive patterns and circuits which are main components of electronic devices. So, in this section, I will summarize the development and application of printable conductive materials, including organic conductive polymers and metallic nanomaterials, metal complex inks, and other conductive inks. In addition, the corresponding post-treatment method will be simply introduced.

1.2.1 Organic conductive polymers

Organic conductive polymers include structural conductive polymers and composite conductive polymers. Structural conductive polymers (called charge transfer complexes at the beginning) were firstly discovered in 1954 [46], and their conductivity was greatly improved by Hideki Shirakawa, A. J. Heeger, and M. MacDiarmid using iodine doping in 1977 [47]. The mechanism of electron conduction in structural conductive polymers, as shown in **Figure 1.8**, is that electron can move along the π bond network when a polymer has conjugated double bonds. The more π bonds it has, the lower the activation energy of electrons will be, and the more easily these electrons can be delocalized, hence the better the electrical conductivity is [4]. In addition, doping of electron donors or acceptors can further improve the electrical conductivity of conjugated polymer [47]. For example, the doping of iodine or arsenic oxide (AsO_5) as electron acceptors in polyacetylene can facilitate the π bonds of polyacetylene to transfer to receptors, which increases the conductivity of the polymer to 10^4 $S \cdot cm^{-1}$, almost reaching the level of conductive metal [3]. To date, many kinds of structural conductive polymer have been developed. The most well-known conductive polymer is poly(3,4-ethylenedioxythiophene) or PEDOT. It is soluble in the presence of polystyrene sulfonic acid (PSS) and forms a colloidal dispersion (PEDOT: PSS). PEDOT: PSS has many advantages such as printable, flexible, lightweight, inexpensive, very compatible with organic and aqueous solvents [4]. These make it suitable as a transparent pattern for use in touchscreens, OLEDs, and electronic paper to replace the traditional indium tin oxide (ITO), the popular inorganic transparent pattern material. Due to the high conductivity-up to 1000 S/cm is possible-it can also be used as a cathode material in capacitors to replace manganese dioxide or liquid electrolytes [3].

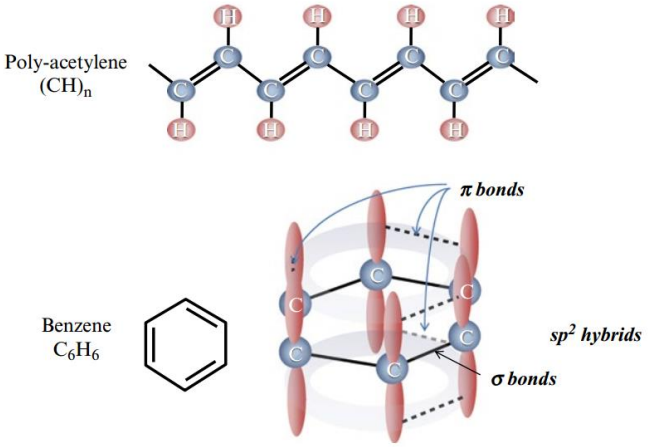

Figure 1.8 Conductive conjugated double bonds of polyacetylene and benzene [4].

Composite conductive polymers are another kind of organic conductive materials that incorporate a large number of conductive filler [48]. Unlike structural conductive polymers, the polymer material itself in a composite conductive polymer is not conductive; it only serves as a matrix. The conductivity is realized by conductive filler contained in the polymer, such as carbon nanotubes, graphene, metal powders, and metal nanowires as shown in **Figure 1.9**. Because of the simplicity and low cost to prepare, composite conductive polymers are widely used in conductive wiring, conductive coating, conductive adhesive, and antistatic material [3, 49].

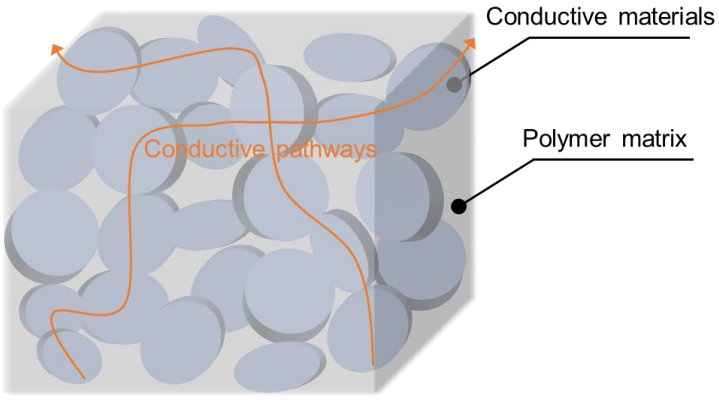

Figure 1.9 Schematic illustration of composite conductive polymers.

1.2.2 Metallic nanomaterials

Metallic materials are widely used in electronic devices as connectors, inductors, patterns,

and antennas because of because of their much higher electrical conductivity compared with inorganic conductive materials. Recently, the progress in the synthesis of nanomaterials, such as Au/Ag/Cu nanoparticles and nanowires, promote the development of metallic conductive inks for printed electronic devices [15]. These inks are normally made of metallic nanoparticles/nanorods/nanowires mixed with some volatile solvents and a small amount of surfactant. Because there is no polymer used, the printed metallic films are easy to achieve a high conductivity, only a few times lower than their bulk forms [3].

Ag nanoparticle inks are deemed as the most important and successful conductive inks because of their relatively low price compared to Au, relatively high environmental stability, and high conductivity of printed electronics. Ag nanoparticle inks can be easily produced and sintered in ambient to achieve high conductivity close to its bulk form. **Figure 1.10** shows a typical example of resistivity change of Ag nanoparticle ink as a function of heat-treatment temperature [4]. As seen, when the temperature is below 200 °C, the resistivity is quite high; when the temperature increases to 250 °C, the resistivity decreases rapidly and finally reaches a low value, about twice that of bulk Ag. This temperature boundary and the achieved resistivity are related to not only the Ag particle size and distribution but also the evaporation and decomposition temperatures of the solvent/surfactant used for stabilizing and dispersing the Ag particles [15]. Small size of metallic particles can reduce their melting point and facilitate the sintering of such particles at low temperatures [50]. As shown in **Figure 1.11**, the melting temperature of Au nanoparticles decreases below 300 °C when the size is less than 5 nm in diameter. The addition of surfactant and solvent in metallic nanoparticle inks can prevent the aggregation of the metallic nanoparticles and enable to be suitable for printing. However, these surfactant and solvent may hinder the sintering of metallic nanoparticles and increase the required temperatures, if they cannot be removed at low temperatures.

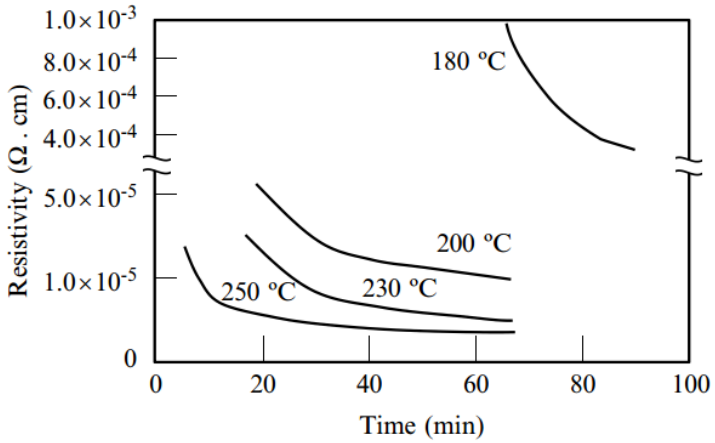

Figure 1.10 Typical resistivity change of Ag nanoparticle ink with alkylamine surfactant as a function of heating time [4].

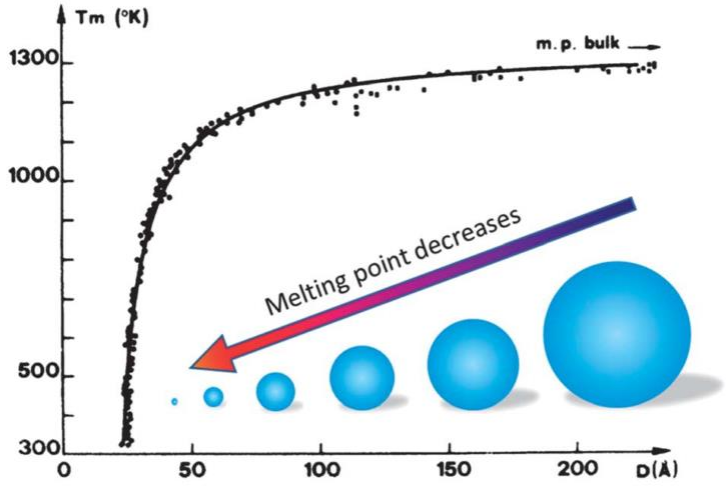

Figure 1.11 Melting point VS. particle diameter of gold nanoparticles. A schematic showing the melting point decreasing trend along with the particle size declining [51].

Many researches have been conducted to reduce the sintering temperature of Ag inks and enable them to be compatible with plastic substrates, such as reducing the size of as-synthesized Ag particles, finding alternative solvent and surfactant systems, or using novel sintering methods. **Table 1.3** summarizes the reported Ag particle inks with respect to particle size, post-treatment, and conductivity. As seen, Ag particle inks with a suitable size and solvent/stabilizing agent system can be successfully sintered below 200 °C or room temperature, and achieve a

low resistivity in the order of 10^{-6} Ω·cm. In addition, Ag nanowire inks have also been developed [52, 53]. Due to their one-dimensional high-aspect-ratio morphology, electrical connection between them is much smoother than that between nanoparticles.

Table 1.3 A brief overview of reported conductive Ag inks with respect to particle size, post-treatment, and conductivity.

Particle size	**Solvent/stabilizing agent**	**Post-treatment**	**Resistivity**	**Ref.**
7 nm	Toluene/Dodecylamine	Alcohol washing	7.3×10^{-5} Ω·cm	[54]
5-10 nm	Tetradecane/NA	Plasma sintering	5.0×10^{-6} Ω·cm	[31]
20 nm	Water/Polyacrylic acid	200 °C for 60 min	3.7×10^{-6} Ω·cm	[55]
50 nm	Water/Pluronic F-127	350 °C for 60 min	2×10^{-5} Ω·cm	[56]
15 nm	Water/Polyacrylic acid sodium	HCl vapors	3.8×10^{-6} Ω·cm	[57]
3.05 nm	Toluene/Thiolate	200 °C for 8 min	1.0×10^{-5} Ω·cm	[58]
30-50 nm	Ethanol/Polymer shell	Photonic sintering	1.0×10^{-5} Ω·cm	[59]
4.4 nm	Toluene/Carboxylic acid	140 °C for 210 min	5.8×10^{-6} Ω·cm	[17]
92 nm	Ethanol/Polyvinylpyrrolidone	160 °C for 75 min	3.8×10^{-6} Ω·cm	[60]

Recently, Cu nanoparticle inks have attracted increasing attention because of Cu is the most powerful commercializable material with sufficiently low price and high thermal/electrical conductivities, which can fully substitute expensive Au and Ag materials. Various Cu nanoparticle inks have been demonstrated to achieve Cu patterns with a high conductivity. **Table 1.4** summarizes the reported Cu particle inks with respect to particle size, post-treatment, and conductivity. As seen, in order to synthesize Cu nanoparticles with less oxidation, most of these Cu inks chose to use strong surfactants such as polyvinylpyrrolidone (PVP) and oleic acid which can better cover the surface of the Cu nanoparticles and assist in prolonging the oxidation process [61]. However, relatively high temperatures above 250°C are normally needed to remove these stronger surfactants before realizing the efficient sintering of

Cu nanoparticles. In addition, a vacuum condition, an inert atmosphere, or a reductive atmosphere is often required to prevent the Cu nanoparticles from oxidation during the sintering process, and enable them to be sintered to achieve a high conductivity of printed Cu patterns. Compared with Ag inks, Cu nanoparticle inks normally need a higher sintering temperature and an additional protective atmosphere which may have overshadowed the cost-effectiveness of these cheap Cu inks. Intense pulsed light (IPL) is a highly promising method to realize the effective sintering of Cu nanoparticle inks under ambient condition [22, 23, 62, 63]. The method involves the application of rapid intense pulses of light to induce heat and/or chemical reactions in an absorbing thin film [23, 24, 64]. The induced heat can reach up to several hundred degrees within a millisecond time frame [65]. Therefore, Cu nanoparticle inks can be sintered rapidly before the occurrence of oxidation. On other hand, Cu nanowire inks have also been developed and used successfully to fabricate flexible patterns and flexible transparent conductive films.

Table 1.4 A brief overview of reported conductive Cu inks with respect to particle size, post-treatment, and conductivity.

Particle size	Solvent/stabilizing agent	Post-treatment	Resistivity	Ref.
40-50 nm	Ethyleneglycol/ Polyvinylpyrrolidone	325 °C for 1 h in vacuum	1.7×10^{-5} Ω·cm	[66]
55 nm	2-(2-butoxyethoxy)ethanol /Polyvinylpyrrolidone	200 ◦C for 60 min, reductive atmosphere, Formic acid	3.6×10^{-6} Ω·cm	[67]
35-60 nm	Ethylene glycol/ Polyvinylpyrrolidone	275-325 ◦C for 60 min, vacuum	$9.2\text{-}1.2\times10^{-5}$ Ω·cm	[68]
5 nm	Non-polar solvent / Fatty acid	250 °C, reductive atmosphere, Formic acid	NA	[69]
40 nm	DI water/Oleic acid	250 °C for 30 min, vacuum	1.1×10^{-5} Ω·cm	[70]

42.3/108.3 nm	Toluene /Oleic acid	300 °C, Ar	5.9×10^{-6} Ω·cm	[71]
42.3/108.3 nm	Toluene /Oleic acid	300 °C, reductive atmosphere, H_2(4%)+Ar	3.5×10^{-6} Ω·cm	[71]
10 nm	Ethanol/Glycolic acid	200 °C for 60 min, N_2	9.1×10^{-6} Ω·cm	[19]
10-15 nm	Ethylene glycol /Tergitol	Photonic sintering	9.4×10^{-5} Ω·cm	[72]
135 ±30 nm	Ethylene glycol butyl ether, methylcellulose/ Polyethylene glycol 2000	250 °C for 30min in N_2	1.6×10^{-5} Ω·cm	[73]
Submicron	Ethanol/ Polyvinylpyrrolidone	Plasma sintering	1.6×10^{-5} Ω·cm	[74]
3.5± 1.0 nm	Propylene glycol, glycerol/ 1-amino-2-propanol	150 °C for 15 min, N2	3.0×10^{-5} Ω·cm	[75]
42.3/108.3 nm	Toluene /Oleic acid	Photonic sintering	4.6×10^{-6} Ω·cm	[76]
100 nm	Diethylene glycol/ Polyvinylpyrrolidone	Photonic sintering	6.97×10^{-6} Ω·cm	[77]
126 nm	Water and ethylene glycol/NA	Photonic sintering	1.0×10^{-5} Ω·cm	[78]

1.2.3 Metallic complex inks

Metal complex inks are another method for fabrication of conductive patterns and circuits on flexible substrates. They are different from particle-type inks which need a high annealing temperature to promote necking among particles. Metal complex inks made form specific metal salts and solvents can directly transform into pure metal patterns by a low temperature thermal decomposition process, normally including nucleation and growth with or without nanoparticle [79-84]. For example, Schubert et al. reported a kind of Ag complex ink decomposed at 130 °C for 60 min to form highly conductive patterns (6.8×10^{-6} Ω·cm) [85]; Yabuki et al. reported various Cu complex inks composed of Cu formate and different amine solvents which can be

annealed at 140 °C and achieved the lowest resistivity of 5.0×10^{-6} Ω·cm [86].

1.2.4 Other conductive inks

In addition, carbon nanomaterials such as carbon nanotube (CNT) [87-89], graphene (G) [90, 91], reduced graphene oxide (RGO) [92, 93], and some oxide ceramics such as indium tin oxide (ITO) [94, 95] can also be used as printable conductive materials. For example, random networks of CNTs have been an attractive choice for transparent conductive film applications due to their excellent stability [96]; ITO is one of the most widely used transparent conductive oxides because of its electrical conductivity and optical transparency [97]. However, due to the complicated fabrication process, intrinsic low conductivity or less flexibility, these conductive materials have a long way to go before their wide applications in flexible and printed electronics.

1.3 Motivation of present research

1.3.1 Issues associated with conductive inks

In the view of practical applications, there are six main aspects that can evaluate the printable conductive materials for flexible and printed electronics and they are: (1) Printability, (2) Post-treatment, (3) Cost, (4) Conductivity, (5) Flexibility, and (6) Reliability. Among them, the printability, the post-treatment, and the material cost can be identified as production factors; the conductivity, the flexibility, and the reliability can be seen as production factors. The currently available printable conductive materials are assigned into three levels of “Good”, “Fair” or “Poor” on each of the above aspects, as listed in **Table 1.5**. In the follows, we will discuss the major issues associated with these printable conductive materials. Finally, approaches for developing new printable conductive materials and corresponding post-treatments will be proposed.

Table 1.5 Comparison of various printable conductive materials

Materials	Production			Performance		
	Printability	Treatment	Cost	Conductivity	Flexibility	Reliability
Structural conductive polymers	Good	Good	Fair	Poor	Good	Poor
Composite conductive polymers	Good	Good	Optional	Fair	Good	Fair
Ag inks	Good	Good	Poor	Good	Fair	Fair
Cu inks	Good	Fair	Good	Good	Fair	Poor

Organic conductive materials have attracted much attention due to their super abilities of ink formulation and flexibility. They enable flexible conductive patterns to be made through low-cost roll-to-roll printing or coating processes, which can be integrated into radio frequency identification (RFID) tags, display backplanes, memory and sensor devices, and so on [3]. However, the conductivity of most organic conductive materials is not as good as metallic materials, as shown in **Table 1.6**. The lowest resistivity of commercial organic conductive materials is 10^{-3}-10^{0} Ω·cm, about 10^{3}-10^{6} times higher than those of metallic materials such as Ag and Cu. It should be noted that the electrical conductivity is the most important property for evaluation of conductive materials. Therefore, these organic conductive materials cannot satisfy the increasing requirement of high conductivity in printed electronics. In addition, the reliability of organic conductive materials is generally poor in the air [98]. Their conductivity will degrade with the increase of time, resulting the failure of the printed electronics. There are also other issues, such as the manufacturing costs, material inconsistencies, toxicity, poor solubility in solvents, and inability to melt. Therefore, more additional studies are required to improve the electrical conductivity and reliability of organic conductive materials.

Table 1.6 Electrical conductivity comparison of various conductive materials

Materials		Resistivity (10^{-6} Ω·cm)	Notes
Metallic	Au	2.44	Bulk properties at 20 °C
	Ag	1.59	
	Cu	1.68	
	Al	2.65	
	Ni	6.99	
	Sn	10.9	
Organic	PEDOT:PSS	10^3-10^6	Depends on doping/composition, oxygen defects, and crystallinity

Compared to the organic conductive materials, metallic materials show higher conductivities, as shown in **Table 1.6**. Ag inks are mature in terms of properties such as high conductivity and stability, and have been successfully applied to fabricate highly conductive patterns in some devices such as the transparent conductive film, transistors, and solar cells. However, their relatively high cost and severe problems of chemical migration and sulfur gas corrosion are still big hindrances to their widening applications in real commercial products [99]. Cu exhibits similar electrical resistivity to Ag, as shown in **Table 1.6**, but the cost of Cu is much lower than noble metal Ag. Concretely, the cost of Cu is about one hundredth that of Ag. Therefore, Cu inks are highly expected to replace or partly replace Ag inks for fabricating highly conductive patterns in printed electronics, especially in low-cost printed electronics. However, unlike Ag nanoparticles, Cu nanoparticles are easily oxidized not only during the sintering stage but also in the preparation and storage stages [68, 100]. The presence of Cu oxide layer will increase the required sintering temperature to over 250 °C, and a special reducing atmosphere will be required, which largely increases the cost of Cu inks and complicates their application process [69, 101, 102]. To overcome the oxidation of Cu inks during preparation and storage, air-stable Cu complex inks (not Cu nanoparticles) prepared by mixing specific Cu salts and amine-based solvents have been developed [81, 86]. These air-stable Cu complex inks can thermally decompose and self-reduce to pure Cu after a low-

temperature annealing process [25, 79, 86, 103]. However, the metal load is very low (about 15 wt. %), which increases the difficulty in making thick patterns [104]. Moreover, compared with bulk Cu patterns manufactured by traditional vacuum deposition, patternless plating, or forging molding methods, such printed Cu patterns show a porous structure composed of many small Cu particles with a low density [81]. In this structure, many particle boundaries are naturally exposed to the environment and will experience rapid oxidation due to their high Gibbs free energy [105, 106]. The continuous oxidation of Cu along grain boundaries will decrease the conductivity of the printed Cu patterns and eventually result in the failure of electronic devices. Introducing conductive and stable graphene into Cu inks can partly prevent Cu form oxidation; however, the addition of graphene destroys the purity of the metallic Cu pattern and results in high resistivity about 5 orders of magnitude higher than that of bulk Cu [107, 108]. Coating a nonoxidizable metal shell onto a Cu core is an another promising method that not only enhances the stability but also retains the high conductivity. For example, Cu-Ag core-shell nanoparticles have been formed by various chemical reduction and galvanic displacement methods [109-113]. These Cu-Ag core-shell nanoparticles can remain stable at room temperature; however, when they are used to make conductive patterns at high temperatures over 150 °C, the Ag shell is broken by simultaneous coalescence of the Cu cores and ripening of the Ag shell [111, 114, 115]. Hence, the sintered Cu patterns are not protected from oxidation over the long-term. Therefore, it is reasonable to deem that the development of low-temperature curable Cu inks for fabrication of highly reliable Cu patterns is very challenging.

1.3.2 Strategies for fabrication of highly conductive and reliable Cu patterns

According to the discussion in section 1.3.1, it can be concluded that, as a low cost and highly conductive material, Cu is very suitable for fabricating of metal conductive inks and creating conductive Cu patterns for flexible and printed electronics. However, the oxidation problem of Cu has heavily hindered their practical applications. How to solve the oxidation problem of Cu inks and print highly conductive and reliable Cu patterns using a low-temperature and a simple process is becoming increasingly urgent and crucial, which will determine whether these Cu inks can be practically applied in flexible and printed electronics.

With these in mind, we herein propose three strategies to address the oxidation problem of Cu inks and also improve the reliability of printed Cu patterns, enabling them to be really applied in practical applications. The first strategy is using submicron Cu particles instead of Cu nanoparticles to prepare Cu inks and print highly conductive patterns because such big Cu particles possess a higher oxidation resistance. The second strategy is utilizing intense pulsed light (IPL) to induce the efficient densification of printed Cu patterns at low temperatures in air and meanwhile strengthen the adhesion between sintered Cu patterns and substrates. The third strategy is introducing anti-oxidation Ag element to modify the surface of the Cu particles and fabricate Cu-Ag alloy patterns or Cu-Ag hybrid patterns. The detail of these strategies and experimental results will be discussed in *Chapter 2*-*Chapter 5*.

1.4 Purpose and scope of this study

The purpose of this study is to develop low-temperature curable Cu inks for fabrication of highly conductive and reliable Cu patterns, enabling these abundant and cheap Cu inks to replace or partly replace the noble Ag and Au inks in the application of printable and flexible electronics. Attempts are made to deal with the present challenges in Cu ink and printed Cu patterns. The dissertation presents three strategies to address the oxidation problem of Cu inks and also improve the reliability of printed Cu patterns. It mainly covers the studies of the ink formulation, post-treatment, property characterization, and reliability evaluation of submicron Cu particle/Cu complex ink, submicron Cu particle/Ag complex ink, and Cu complex/Ag complex ink, respectively.

In *Chapter 1*, a brief description of PE technology (definition, three elements of PE, and application), an overview of conductive inks, and existing issues of conductive inks are given. And a purpose of developing low-temperature curable Cu inks for fabrication of highly conductive and reliable Cu patterns in flexible electronics is suggested.

In *Chapter 2*, the concept using in-situ formed fresh Cu nanoparticles to help sinter the submicron Cu particles is proposed and Cu particle/Cu complex inks are developed. During the heat treatment, fresh Cu nuclei decomposed from Cu complex attach to the Cu particles, which plays a role of nano-welders in the realization of sintering these submicron Cu particles to

achieve high conductive Cu patterns. The effects of the size of Cu particles and the ratio of the amount of Cu complex to particles on the electrical resistivity and morphology of sintered Cu patterns are clarified, and the functions of the heat treatment temperature and holding time are investigated.

In *Chapter 3*, IPL is used to not only reinforce the bonding between submicron Cu particle and in-situ formed Cu nanoparticles but also improve the adhesion between films and substrates to fabricate highly conductive and reliable Cu patterns. The effects of substrates and particle sizes on the conductivity of achieved Cu patterns are investigated. The bending fatigue test and the oxidation resistance test are conducted to evaluate the reliability of printed Cu patterns. In addition, the potential applications of these Cu patterns were demonstrated with a flexible and folding LED circuit and a flexible dipole antenna for wireless power transmission.

In *Chapter 4*, considering the high oxidation resistance of Ag, Cu-Ag alloy patterns are fabricated by using a newly-developed Cu particle/Ag complex ink and a simple two-step sintering process consisting of low temperature pre-curing followed by rapid IPL sintering. The fabrication process of Cu-Ag alloy patterns is studied in detail. Especially, the alloying process is discussed and a possible mechanism is proposed. In addition, the long-term stabilities of Cu-Ag alloy patterns including high temperature oxidation resistance and bending fatigue property are studied.

In *Chapter 5*, for printing electronics on heat-sensitive PET or paper substrates, Cu-Ag complex inks were put forward to fabricate highly oxidation-resistant and conductive patterns low 100 °C. The ink formulation is optimized based on the conductivity, microstructure, and chemical composition of printed Cu-Ag hybrid patterns. The thermal behaviors of various complex inks were investigated in detail, the self-catalyzed characterics is discussed, and filannly the possible self-catalyzed mechanism is proposed. In addition, the oxidation resistance of printed Cu-Ag hybird patterns is evaluated.

In *Chapter 6*, the summary of the dissertation is presented.

Reference

1. https://en.wikipedia.org/wiki/Printed_electronics, 2018.06.12.

2. Wu, W., Inorganic nanomaterials for printed electronics: a review. *Nanoscale* **2017,** *9* (22), 7342-7372.

3. Cui, Z., Printed electronics: materials, technologies and applications. John Wiley & Sons: 2016.

4. Suganuma, K., Introduction to printed electronics. Springer New York: 2014.

5. M., L. M. A.; Volker, A.; Heiko, T.; Jürgen, S.; Ralf, A., Printable electronics: flexibility for the future. *physica status solidi (a)* **2009,** *206* (4), 588-597.

6. https://www.nasa.gov/ames-partnerships/technology/technology-opportunity-atmospheric-pressure-plasma-based-fabrication-of-printable, 2018.06.12.

7. https://spectrum.ieee.org/semiconductors/materials/electronics-on-paper, 2018.06.12.

8. Koga, H.; Nogi, M.; Komoda, N.; Nge, T. T.; Sugahara, T.; Suganuma, K., Uniformly connected conductive networks on cellulose nanofiber paper for transparent paper electronics. *Npg Asia Materials* **2014,** *6*, e93.

9. Zhijie, Z.; Shuang-Zhuang, G.; Tessa, H.; Cindy, E.; Xiaoxiao, F.; Jakub, T.; C., M. M., 3D printed functional and biological materials on moving freeform surfaces. *Advanced Materials* **2018,** *30* (23), 1707495.

10. https://www.printedelectronicsnow.com/issues/2015-10-01/view_features/universities-are-conducting-cutting-edge-research-on-flexible-and-printed-electronics/47772, 2018.06.12.

11. Chizu, S.; Yoshiaki, T.; Takeshi, Y.; Makoto, K.; Shuji, D., Recent progress of high performance polymer OLED and OPV materials for organic printed electronics. *Science and Technology of Advanced Materials* **2014,** *15* (3), 034203.

12. Berggren, M.; Nilsson, D.; Robinson, N. D., Organic materials for printed electronics. *Nature Materials* **2007,** *6*, 3.

13. Magdassi, S.; Kamyshny, A., Nanomaterials for 2D and 3D Printing. Wiley-VCH Verlag GmbH & Co. KGaA: 2017.

14. Perelaer, J.; Smith, P. J.; Mager, D.; Soltman, D.; Volkman, S. K.; Subramanian, V.; Korvink, J. G.; Schubert, U. S., Printed electronics: the challenges involved in printing devices, interconnects, and contacts based on inorganic materials. *Journal of Materials Chemistry* **2010,** *20* (39), 8446-8453.

15. Alexander, K.; Shlomo, M., Conductive Nanomaterials for Printed Electronics. *Small* **2014,** *10* (17), 3515-3535.

16. Wunscher, S.; Abbel, R.; Perelaer, J.; Schubert, U. S., Progress of alternative sintering approaches of inkjet-printed metal inks and their application for manufacturing of flexible electronic devices. *Journal of Materials Chemistry C* **2014,** *2* (48), 10232-10261.

17. Ankireddy, K.; Vunnam, S.; Kellar, J.; Cross, W., Highly conductive short chain carboxylic acid encapsulated silver nanoparticle based inks for direct write technology applications. *Journal of Materials Chemistry C* **2013,** *1* (3), 572-579.

18. Greer, J. R.; Street, R. A., Thermal cure effects on electrical performance of nanoparticle silver inks. *Acta Materialia* **2007,** *55* (18), 6345-6349.

19. Deng, D.; Jin, Y.; Cheng, Y.; Qi, T.; Xiao, F., Copper nanoparticles: aqueous phase synthesis and conductive films fabrication at low sintering temperature. *ACS Applied Materials & Interfaces* **2013,** *5* (9), 3839-3846.

20. Etienne, D.; Anshul, G.; Sylvain, B.; Sébastien, S.; Patrick, B., Characterization of sintered inkjet-printed silicon nanoparticle thin films for thermoelectric devices. *physica status solidi (a)* **2014,** *211* (6), 1301-1307.

21. Fukuda, N.; Watanabe, Y.; Uemura, S.; Yoshida, Y.; Nakamura, T.; Ushijima, H., In-Ga-Zn oxide nanoparticles acting as an oxide semiconductor material synthesized via a coprecipitation-based method. *Journal of Materials Chemistry C* **2014,** *2* (13), 2448-2454.

22. Kim, H.-S.; Dhage, S. R.; Shim, D.-E.; Hahn, H. T., Intense pulsed light sintering of copper nanoink for printed electronics. *Applied Physics A* **2009,** *97* (4), 791.

23. Li, W.; Hu, D.; Li, L.; Li, C.-F.; Jiu, J.; Chen, C.; Ishina, T.; Sugahara, T.; Suganuma, K., Printable and flexible copper–silver alloy electrodes with high conductivity and ultrahigh oxidation resistance. *ACS Applied Materials & Interfaces* **2017,** *9* (29), 24711-24721.

24. Lim, H. S.; Kim, S. J.; Jang, H. W.; Lim, J. A., Intense pulsed light for split-second structural development of nanomaterials. *Journal of Materials Chemistry C* **2017,** *5* (29), 7142-7160.

25. Lee, J.; Lee, B.; Jeong, S.; Kim, Y.; Lee, M., Microstructure and electrical property of laser-sintered Cu complex ink. *Applied Surface Science* **2014,** *307*, 42-45.

26. Han, S.; Hong, S.; Ham, J.; Yeo, J.; Lee, J.; Kang, B.; Lee, P.; Kwon, J.; Lee, S. S.; Yang, M. Y., Fast plasmonic laser nanowelding for a Cu-nanowire percolation network for flexible transparent conductors and stretchable electronics. *Adv Mater* **2014,** *26*.

27. Hwang, H.-J.; Oh, K.-H.; Kim, H.-S., All-photonic drying and sintering process via flash white light combined with deep-UV and near-infrared irradiation for highly conductive copper nano-ink. *Scientific Reports* **2016,** *6*, 19696.

28. Cherrington, M.; Claypole, T. C.; Deganello, D.; Mabbett, I.; Watson, T.; Worsley, D., Ultrafast near-infrared sintering of a slot-die coated nano-silver conducting ink. *Journal of Materials Chemistry* **2011,** *21* (21), 7562-7564.

29. Farraj, Y.; Smooha, A.; Kamyshny, A.; Magdassi, S., Plasma-induced decomposition of copper complex ink for the formation of highly conductive copper tracks on heat-sensitive substrates. *ACS Applied Materials & Interfaces* **2017,** *9* (10), 8766-8773.

30. Kwon, Y.-T.; Lee, Y.-I.; Kim, S.; Lee, K.-J.; Choa, Y.-H., Full densification of inkjet-printed copper conductive tracks on a flexible substrate utilizing a hydrogen plasma sintering. *Applied Surface Science* **2017,** *396*, 1239-1244.

31. Reinhold, I.; Hendriks, C. E.; Eckardt, R.; Kranenburg, J. M.; Perelaer, J.; Baumann, R. R.; Schubert, U. S., Argon plasma sintering of inkjet printed silver tracks on polymer substrates. *Journal of Materials Chemistry* **2009,** *19* (21), 3384-3388.

32. Perelaer, J.; de Gans, B. J.; Schubert, U. S., Ink-jet printing and microwave sintering of conductive silver tracks. *Advanced Materials* **2006,** *18* (16), 2101-2104.

33. Garnett, E. C.; Cai, W.; Cha, J. J.; Mahmood, F.; Connor, S. T.; Greyson Christoforo, M.; Cui, Y.; McGehee, M. D.; Brongersma, M. L., Self-limited plasmonic welding of silver nanowire junctions. *Nature Materials* **2012,** *11*, 241.

34. MacNeill, W.; Choi, C.-H.; Chang, C.-H.; Malhotra, R., On the self-damping nature of densification in photonic sintering of nanoparticles. *Scientific Reports* **2015,** *5*, 14845.

35. Bromberg, V.; Ma, S.; Egitto, F. D.; Singler, T. J., Highly conductive lines by plasma-induced conversion of inkjet-printed silver nitrate traces. *Journal of Materials Chemistry C* **2013,** *1* (41), 6842-6849.

36. Crowther, J. M.; Badyal, J. P. S., Non-isothermal plasma metallization of polymer-

supported gold (III) complexes. *Advanced Materials* **1998,** *10* (5), 407-411.

37. Fang, C. Y.; Randal, C. A.; Lanagan, M. T.; Agrawal, D. K., Microwave processing of electroceramic materials and devices. *Journal of Electroceramics* **2008,** *22* (1), 125.

38. Adrien, P.; Mahsa, S.; M., P. M.; Antonio, F.; E., A. J.; Claudia, A. A., All-printed flexible organic transistors enabled by surface tension-guided blade coating. *Advanced Materials* **2014,** *26* (32), 5722-5727.

39. Cai, L.; Zhang, S.; Miao, J.; Yu, Z.; Wang, C., Fully printed stretchable thin-film Transistors and integrated logic circuits. *ACS Nano* **2016,** *10* (12), 11459-11468.

40. Cheng, Y. B.; Pascoe, A.; Huang, F.; Peng, Y., Print flexible solar cells. *Nature* **2016,** *539* (7630), 488-489.

41. Khan, S.; Lorenzelli, L.; Dahiya, R. S., Technologies for printing sensors and electronics over large flexible substrates: a review. *IEEE Sensors Journal* **2015,** *15* (6), 3164-3185.

42. Street, R. A.; Ng, T. N.; Schwartz, D. E.; Whiting, G. L.; Lu, J. P.; Bringans, R. D.; Veres, J., From printed transistors to printed smart systems. *Proceedings of the IEEE* **2015,** *103* (4), 607-618.

43. Markus, H.; R., S. R.; Dechan, A.; C., K. F., Comparison of fast Roll-to-Roll flexographic, inkjet, flatbed, and rotary screen printing of metal back electrodes for polymer solar cells. *Advanced Engineering Materials* **2013,** *15* (10), 995-1001.

44. Zhang, Y.; Anderson, N.; Bland, S.; Nutt, S.; Jursich, G.; Joshi, S., All-printed strain sensors: Building blocks of the aircraft structural health monitoring system. *Sensors and Actuators A: Physical* **2017,** *253*, 165-172.

45. Crowley, K.; Morrin, A.; Hernandez, A.; O'Malley, E.; Whitten, P. G.; Wallace, G. G.; Smyth, M. R.; Killard, A. J., Fabrication of an ammonia gas sensor using inkjet-printed polyaniline nanoparticles. *Talanta* **2008,** *77* (2), 710-717.

46. Akamatu, H.; Inokuchi, H.; Matsunaga, Y., Electrical conductivity of the perylene-bromine complex. *Nature* **1954,** *173*, 168.

47. Chiang, C. K.; Fincher, C. R.; Park, Y. W.; Heeger, A. J.; Shirakawa, H.; Louis, E. J.; Gau, S. C.; MacDiarmid, A. G., Electrical conductivity in doped polyacetylene. *Physical Review Letters* **1977,** *39* (17), 1098-1101.

48. Park, M.; Park, J.; Jeong, U., Design of conductive composite elastomers for stretchable electronics. *Nano Today* **2014,** *9* (2), 244-260.

49. Matsuhisa, N.; Inoue, D.; Zalar, P.; Jin, H.; Matsuba, Y.; Itoh, A.; Yokota, T.; Hashizume, D.; Someya, T., Printable elastic conductors by in situ formation of silver nanoparticles from silver flakes. *Nature Materials* **2017,** *16*, 834.

50. Buffat, P.; Borel, J. P., Size effect on the melting temperature of gold particles. *Physical Review A* **1976,** *13* (6), 2287-2298.

51. Yang, C.; Wong, C. P.; Yuen, M. M. F., Printed electrically conductive composites: conductive filler designs and surface engineering. *Journal of Materials Chemistry C* **2013,** *1* (26), 4052-4069.

52. Wang, J.; Jiu, J.; Araki, T.; Nogi, M.; Sugahara, T.; Nagao, S.; Koga, H.; He, P.; Suganuma, K., Silver nanowire electrodes: conductivity improvement without post-treatment and application in capacitive pressure sensors. *Nano-Micro Letters* **2015,** *7* (1), 51-58.

53. Jiu, J.; Araki, T.; Wang, J.; Nogi, M.; Sugahara, T.; Nagao, S.; Koga, H.; Suganuma, K.; Nakazawa, E.; Hara, M.; Uchida, H.; Shinozaki, K., Facile synthesis of very-long silver nanowires for transparent electrodes. *Journal of Materials Chemistry A* **2014,** *2* (18), 6326-6330.

54. Wakuda, D.; Hatamura, M.; Suganuma, K., Novel method for room temperature sintering of Ag nanoparticle paste in air. *Chemical Physics Letters* **2007,** *441* (4), 305-308.

55. Jeong, S.; Song, H. C.; Lee, W. W.; Choi, Y.; Lee, S. S.; Ryu, B.-H., Combined role of well-dispersed aqueous Ag ink and the molecular adhesive layer in inkjet printing the narrow and highly conductive Ag features on a glass substrate. *The Journal of Physical Chemistry C* **2010,** *114* (50), 22277-22283.

56. Kosmala, A.; Wright, R.; Zhang, Q.; Kirby, P., Synthesis of silver nano particles and fabrication of aqueous Ag inks for inkjet printing. *Materials Chemistry and Physics* **2011,** *129* (3), 1075-1080.

57. Grouchko, M.; Kamyshny, A.; Mihailescu, C. F.; Anghel, D. F.; Magdassi, S., Conductive inks with a “Built-In” mechanism that enables sintering at room temperature. *ACS Nano* **2011,** *5* (4), 3354-3359.

58. Volkman, S. K.; Yin, S.; Bakhishev, T.; Puntambekar, K.; Subramanian, V.; Toney, M. F., Mechanistic studies on sintering of silver nanoparticles. *Chemistry of Materials* **2011,** *23* (20), 4634-4640.

59. Abbel, R.; van Lammeren, T.; Hendriks, R.; Ploegmakers, J.; Rubingh, E. J.; Meinders, E. R.; Groen, W. A., Photonic flash sintering of silver nanoparticle inks: a fast and convenient method for the preparation of highly conductive structures on foil. *MRS Communications* **2012,** *2* (4), 145-150.

60. Ding, J.; Liu, J.; Tian, Q.; Wu, Z.; Yao, W.; Dai, Z.; Liu, L.; Wu, W., Preparing of highly conductive patterns on flexible substrates by screen printing of silver nanoparticles with different size distribution. *Nanoscale Research Letters* **2016,** *11* (1), 412.

61. Ankireddy, K.; Druffel, T.; Vunnam, S.; Filipic, G.; Dharmadasa, R.; Amos, D. A., Seed mediated copper nanoparticle synthesis for fabricating oxidation free interdigitated electrodes using intense pulse light sintering for flexible printed chemical sensors. *Journal of Materials Chemistry C* **2017,** *5* (42), 11128-11137.

62. Ryu, J.; Kim, H.-S.; Hahn, H. T., Reactive sintering of copper nanoparticles using intense pulsed light for printed electronics. *Journal of Electronic Materials* **2011,** *40* (1), 42-50.

63. Araki, T.; Sugahara, T.; Jiu, J.; Nagao, S.; Nogi, M.; Koga, H.; Uchida, H.; Shinozaki, K.; Suganuma, K., Cu salt ink formulation for printed electronics using photonic sintering. *Langmuir* **2013,** *29* (35), 11192-11197.

64. Li, W.; Zhang, H.; Gao, Y.; Jiu, J.; Li, C.-F.; Chen, C.; Hu, D.; Goya, Y.; Wang, Y.; Koga, H.; Nagao, S.; Suganuma, K., Highly reliable and highly conductive submicron Cu particle patterns fabricated by low temperature heat-welding and subsequent flash light sinter-reinforcement. *Journal of Materials Chemistry C* **2017,** *5* (5), 1155-1164.

65. Park, S.-H.; Chung, W.-H.; Kim, H.-S., Temperature changes of copper nanoparticle ink during flash light sintering. *Journal of Materials Processing Technology* **2014,** *214* (11), 2730-2738.

66. Park, B. K.; Kim, D.; Jeong, S.; Moon, J.; Kim, J. S., Direct writing of copper conductive patterns by ink-jet printing. *Thin Solid Films* **2007,** *515* (19), 7706-7711.

67. Youngil, L.; Jun-rak, C.; Kwi Jong, L.; Nathan, E. S.; Donghoon, K., Large-scale synthesis

of copper nanoparticles by chemically controlled reduction for applications of inkjet-printed electronics. *Nanotechnology* **2008,** *19* (41), 415604.

68. Jeong, S.; Woo, K.; Kim, D.; Lim, S.; Kim, J. S.; Shin, H.; Xia, Y.; Moon, J., Controlling the thickness of the surface oxide layer on Cu nanoparticles for the fabrication of conductive structures by ink-jet printing. *Advanced Functional Materials* **2008,** *18* (5), 679-686.

69. Jang, S.; Seo, Y.; Choi, J.; Kim, T.; Cho, J.; Kim, S.; Kim, D., Sintering of inkjet printed copper nanoparticles for flexible electronics. *Scripta Materialia* **2010,** *62* (5), 258-261.

70. Jeong, S.; Song, H. C.; Lee, W. W.; Lee, S. S.; Choi, Y.; Son, W.; Kim, E. D.; Paik, C. H.; Oh, S. H.; Ryu, B.-H., Stable aqueous based Cu nanoparticle ink for printing well-defined highly conductive features on a plastic substrate. *Langmuir* **2011,** *27* (6), 3144-3149.

71. Jeong, S.; Lee, S. H.; Jo, Y.; Lee, S. S.; Seo, Y.-H.; Ahn, B. W.; Kim, G.; Jang, G.-E.; Park, J.-U.; Ryu, B.-H.; Choi, Y., Air-stable, surface-oxide free Cu nanoparticles for highly conductive Cu ink and their application to printed graphene transistors. *Journal of Materials Chemistry C* **2013,** *1* (15), 2704-2710.

72. Dharmadasa, R.; Jha, M.; Amos, D. A.; Druffel, T., Room temperature synthesis of a copper ink for the intense pulsed light sintering of conductive copper films. *ACS Applied Materials & Interfaces* **2013,** *5* (24), 13227-13234.

73. Zhang, Y.; Zhu, P.; Li, G.; Zhao, T.; Fu, X.; Sun, R.; Zhou, F.; Wong, C.-p., Facile preparation of monodisperse, impurity-Free, and antioxidation copper nanoparticles on a large scale for application in conductive ink. *ACS Applied Materials & Interfaces* **2014,** *6* (1), 560-567.

74. Gao, Y.; Zhang, H.; Jiu, J.; Nagao, S.; Sugahara, T.; Suganuma, K., Fabrication of a flexible copper pattern based on a sub-micro copper paste by a low temperature plasma technique. *RSC Advances* **2015,** *5* (109), 90202-90208.

75. Hokita, Y.; Kanzaki, M.; Sugiyama, T.; Arakawa, R.; Kawasaki, H., High-concentration synthesis of sub-10-nm copper nanoparticles for application to conductive nanoinks. *ACS Applied Materials & Interfaces* **2015,** *7* (34), 19382-19389.

76. Park, J. H.; Jeong, S.; Lee, E. J.; Lee, S. S.; Seok, J. Y.; Yang, M.; Choi, Y.; Kang, B., Transversally extended laser plasmonic welding for oxidation-free copper fabrication toward

high-fidelity optoelectronics. *Chemistry of Materials* **2016,** *28* (12), 4151-4159.

77. Hwang, Y.-T.; Chung, W.-H.; Jang, Y.-R.; Kim, H.-S., Intensive plasmonic flash light sintering of copper nanoinks using a band-pass light filter for highly electrically conductive electrodes in printed Electronics. *ACS Applied Materials & Interfaces* **2016,** *8* (13), 8591-8599.

78. Rager, M. S.; Aytug, T.; Veith, G. M.; Joshi, P., Low-thermal-budget photonic processing of highly conductive Cu interconnects based on CuO nanoinks: potential for flexible printed electronics. *ACS Applied Materials & Interfaces* **2016,** *8* (3), 2441-2448.

79. Farraj, Y.; Grouchko, M.; Magdassi, S., Self-reduction of a copper complex MOD ink for inkjet printing conductive patterns on plastics. *Chemical Communications* **2015,** *51* (9), 1587-1590.

80. Choi, Y.-H.; Hong, S.-H., Effect of the Amine Concentration on phase evolution and densification in printed films using Cu(II) complex ink. *Langmuir* **2015,** *31* (29), 8101-8110.

81. Shin, D.-H.; Woo, S.; Yem, H.; Cha, M.; Cho, S.; Kang, M.; Jeong, S.; Kim, Y.; Kang, K.; Piao, Y., A self-reducible and alcohol-soluble copper-based metal-organic decomposition ink for printed electronics. *ACS Applied Materials & Interfaces* **2014,** *6* (5), 3312-3319.

82. Li, W.; Li, C.-F.; Lang, F.; Jiu, J.; Ueshima, M.; Wang, H.; Liu, Z.-Q.; Suganuma, K., Self-catalyzed copper-silver complex inks for low-cost fabrication of highly oxidation-resistant and conductive copper-silver hybrid tracks at a low temperature below 100 °C. *Nanoscale* **2018**.

83. Hatamura, M.; Yamaguchi, S.; Takane, S.-y.; Chen, Y.; Suganuma, K., Decarboxylation and simultaneous reduction of silver(i)β-ketocarboxylates with three types of coordinations. *Dalton Transactions* **2015,** *44* (19), 8993-9003.

84. 廣瀬久美; 河染満; 関口卓也; 畑村眞理子; 菅沼克昭, β-ケトカルボン酸銀塩インクを利用した低温配線形成技術. *電子情報通信学会論文誌 C* **2012,** *95* (11), 394-399.

85. Jolke, P.; Chris, E. H.; Antonius, W. M. d. L.; Ulrich, S. S., One-step inkjet printing of conductive silver tracks on polymer substrates. *Nanotechnology* **2009,** *20* (16), 165303.

86. Yabuki, A.; Tanaka, S., Electrically conductive copper film prepared at low temperature by thermal decomposition of copper amine complexes with various amines. *Materials Research Bulletin* **2012,** *47* (12), 4107-4111.

87. Dinh, N. T.; Sowade, E.; Blaudeck, T.; Hermann, S.; Rodriguez, R. D.; Zahn, D. R. T.; Schulz, S. E.; Baumann, R. R.; Kanoun, O., High-resolution inkjet printing of conductive carbon nanotube twin lines utilizing evaporation-driven self-assembly. *Carbon* **2016,** *96*, 382-393.

88. Kwon, O.-S.; Kim, H.; Ko, H.; Lee, J.; Lee, B.; Jung, C.-H.; Choi, J.-H.; Shin, K., Fabrication and characterization of inkjet-printed carbon nanotube electrode patterns on paper. *Carbon* **2013,** *58*, 116-127.

89. Kholghi Eshkalak, S.; Chinnappan, A.; Jayathilaka, W. A. D. M.; Khatibzadeh, M.; Kowsari, E.; Ramakrishna, S., A review on inkjet printing of CNT composites for smart applications. *Applied Materials Today* **2017,** *9*, 372-386.

90. Zhang, D.; Chi, B.; Li, B.; Gao, Z.; Du, Y.; Guo, J.; Wei, J., Fabrication of highly conductive graphene flexible circuits by 3D printing. *Synthetic Metals* **2016,** *217*, 79-86.

91. Karagiannidis, P. G.; Hodge, S. A.; Lombardi, L.; Tomarchio, F.; Decorde, N.; Milana, S.; Goykhman, I.; Su, Y.; Mesite, S. V.; Johnstone, D. N.; Leary, R. K.; Midgley, P. A.; Pugno, N. M.; Torrisi, F.; Ferrari, A. C., Microfluidization of graphite and formulation of graphene-based conductive Inks. *ACS Nano* **2017,** *11* (3), 2742-2755.

92. Yol, J. S.; Hun, K. S.; Tark, H. J.; Jin, J. H.; Yeon, J. S.; Geon-Woong, L., Highly concentrated and conductive reduced graphene oxide nanosheets by monovalent cation–π interaction: toward printed electronics. *Advanced Functional Materials* **2012,** *22* (15), 3307-3314.

93. Lim, S.; Kang, B.; Kwak, D.; Lee, W. H.; Lim, J. A.; Cho, K., Inkjet-printed reduced graphene oxide/poly(vinyl alcohol) composite electrodes for flexible transparent organic field-effect transistors. *The Journal of Physical Chemistry C* **2012,** *116* (13), 7520-7525.

94. Hwang, M.-s.; Jeong, B.-y.; Moon, J.; Chun, S.-K.; Kim, J., Inkjet-printing of indium tin oxide (ITO) films for transparent conducting electrodes. *Materials Science and Engineering: B* **2011,** *176* (14), 1128-1131.

95. C., H. R.; Stefan, D.; J., S. J., Transparent indium tin oxide as inkjet-printed thin film electrodes for organic field-effect transistors. *physica status solidi (a)* **2011,** *208* (12), 2920-2925.

96. Wu, Z.; Chen, Z.; Du, X.; Logan, J. M.; Sippel, J.; Nikolou, M.; Kamaras, K.; Reynolds, J. R.; Tanner, D. B.; Hebard, A. F.; Rinzler, A. G., Transparent, conductive carbon nanotube films. *Science* **2004,** *305* (5688), 1273-1276.

97. Kim, H.; Gilmore, C. M.; Piqué, A.; Horwitz, J. S.; Mattoussi, H.; Murata, H.; Kafafi, Z. H.; Chrisey, D. B., Electrical, optical, and structural properties of indium–tin–oxide thin films for organic light-emitting devices. *Journal of Applied Physics* **1999,** *86* (11), 6451-6461.

98. Henning, S., Reliability of organic field-effect transistors. *Advanced Materials* **2009,** *21* (38-39), 3859-3873.

99. Kim, K.-S.; Bang, J.-O.; Jung, S.-B., Electrochemical migration behavior of silver nanopaste screen-printed for flexible and printable electronics. *Current Applied Physics* **2013,** *13*, S190-S194.

100. Magdassi, S.; Grouchko, M.; Kamyshny, A., Copper nanoparticles for printed electronics: routes towards achieving oxidation stability. *Materials* **2010,** *3* (9), 4626.

101. Woo, K.; Kim, Y.; Lee, B.; Kim, J.; Moon, J., Effect of carboxylic acid on sintering of inkjet-printed copper nanoparticulate films. *ACS Applied Materials & Interfaces* **2011,** *3* (7), 2377-2382.

102. Kim, I.; Kim, J., The effect of reduction atmospheres on the sintering behaviors of inkjet-printed Cu interconnectors. *Journal of Applied Physics* **2010,** *108* (10), 102807.

103. Yabuki, A.; Arriffin, N.; Yanase, M., Low-temperature synthesis of copper conductive film by thermal decomposition of copper–amine complexes. *Thin Solid Films* **2011,** *519* (19), 6530-6533.

104. Li, W.; Cong, S.; Jiu, J.; Nagao, S.; Suganuma, K., Self-reducible copper inks composed of copper-amino complexes and preset submicron copper seeds for thick conductive patterns on a flexible substrate. *Journal of Materials Chemistry C* **2016,** *4* (37), 8802-8809.

105. Li, W.; Li, L.; Gao, Y.; Hu, D.; Li, C.-F.; Zhang, H.; Jiu, J.; Nagao, S.; Suganuma, K., Highly conductive copper films based on submicron copper particles/copper complex inks for printed electronics: Microstructure, resistivity, oxidation resistance, and long-term stability. *Journal of Alloys and Compounds* **2018,** *732*, 240-247.

106. Ul-Hamid, A., A microstructural study of preferential oxidation at the grain boundaries

of Ni–Cr alloys. *Oxidation of Metals* **2002,** *57* (3), 217-230.

107. Wang, S.; Huang, X.; He, Y.; Huang, H.; Wu, Y.; Hou, L.; Liu, X.; Yang, T.; Zou, J.; Huang, B., Synthesis, growth mechanism and thermal stability of copper nanoparticles encapsulated by multi-layer graphene. *Carbon* **2012,** *50* (6), 2119-2125.

108. Norman, A. L.; Evagelos, K. A.; Wendelin, J. S., Graphene-stabilized copper nanoparticles as an air-stable substitute for silver and gold in low-cost ink-jet printable electronics. *Nanotechnology* **2008,** *19* (44), 445201.

109. Xu, X.; Luo, X.; Zhuang, H.; Li, W.; Zhang, B., Electroless silver coating on fine copper powder and its effects on oxidation resistance. *Materials Letters* **2003,** *57* (24), 3987-3991.

110. Muzikansky, A.; Nanikashvili, P.; Grinblat, J.; Zitoun, D., Ag dewetting in Cu@Ag monodisperse core–shell nanoparticles. *The Journal of Physical Chemistry C* **2013,** *117* (6), 3093-3100.

111. Grouchko, M.; Kamyshny, A.; Magdassi, S., Formation of air-stable copper-silver core-shell nanoparticles for inkjet printing. *Journal of Materials Chemistry* **2009,** *19* (19), 3057-3062.

112. Changsoo, L.; Na Rae, K.; Jahyun, K.; Yung Jong, L.; Hyuck Mo, L., Cu-Ag core–shell nanoparticles with enhanced oxidation stability for printed electronics. *Nanotechnology* **2015,** *26* (45), 455601.

113. Kim, N. R.; Shin, K.; Jung, I.; Shim, M.; Lee, H. M., Ag–Cu bimetallic nanoparticles with enhanced resistance to oxidation: a combined experimental and theoretical Study. *The Journal of Physical Chemistry C* **2014,** *118* (45), 26324-26331.

114. Tsai, C.-H.; Chen, S.-Y.; Song, J.-M.; Chen, I.-G.; Lee, H.-Y., Thermal stability of Cu@Ag core–shell nanoparticles. *Corrosion Science* **2013,** *74*, 123-129.

115. Hai, H. T.; Takamura, H.; Koike, J., Oxidation behavior of Cu–Ag core–shell particles for solar cell applications. *Journal of Alloys and Compounds* **2013,** *564*, 71-77.

Chapter 2

Low temperature sintering of submicron Cu particle/Cu complex inks

2.1 Introduction

Due to the high cost and poor oxidation resistance of synthesized Cu nanoparticles, commercially available micron/submicron Cu particles with higher oxidation resistance and lower cost (only 1/100-300 of the cost of Cu nanoparticles) are more suitable for fabrication of flexible and printed electronic devices. However, it is difficult to realize the efficient sintering/bonding of these large Cu particles and form conductive pathways because of their low driving force for densification [1, 2]. Several assisted methods have been attempted to realize the sintering or partly sintering of these big Cu particles, including high temperature and pressure [1], reductive atmosphere (formic acid or hydrogen) [3], a great amount of long-acting reductant (such as ascorbic acid) [4]; however, these methods are not compatible with either flexible substrates or printing methods. Using Cu nanoparticles to help bond micron/submicron Cu particles is recently proposed by H. S. Kim, and a conductive Cu pattern with the resistivity of $8.0\times10^{-5}\Omega\cdot$cm has been achieved on a polyimide (PI) substrate by using intense pulsed light (IPL) sintering [5]. However, the input energy of IPL was as high as 12500 mJ cm^{-2} which is dangerous to many flexible heat-sensitive substrates (PEN and PET). Moreover, the resistivity of achieved Cu patterns is far higher than that of bulk Cu patterns (1.68×10^{-6} $\Omega\cdot$cm). The possible reason is that the existence of Cu oxide shell on these Cu nanoparticles obstruct the efficient sintering of Cu particles.

In this chapter, the concept using in-situ formed fresh Cu nanoparticles to help sinter submicron Cu particles is proposed. Submicron Cu particle/Cu complex inks are developed, in which fresh and active metallic Cu nanoparticles resulted from the decomposition of Cu complex can avoid the oxidization like those pre-prepared Cu nanoparticles and in-situ bond large Cu particles to form highly conductive pathways at low temperatures. On the other hand, compared pure Cu complex inks, our Cu particle/Cu complex inks enable printed Cu patterns to have a high-qualitative surface morphology and favorable thickness. The influences of ink formulation and post-treatment on thickness, surface morphologies, microstructures, and

achieved conductivities of printed Cu patterns are studied and a possible low temperature sintering mechanism of the Cu particle/Cu complex inks is proposed. In addition, to evaluate the reliability of printed Cu patterns, they are used as conductive wires to light up a LED under the bending condition, twisting condition, and adhesive tape tests.

2.2 Experimental

2.2.1 Materials

Cu(II) formate tetrahydrate (Cuf, Wako, Japan) was used as the Cu precursor. 2-amino-2-methyl-1-propanol (AMP, Naclal tesque, Japan) was used as a complex agent or solvent. Three kinds of Cu particles (Mitsui Mining & Smelting Co., Ltd) were used as received. Particle A, particle B and flake particle C have an average size of 0.17 μm, 0.7 μm and 3.0 μm (determined by SEM, **Figure 2.1**), respectively. Polyethylene terephthalate (PET) substrate of 100 μm thick was purchased from Toray Industries, Inc.

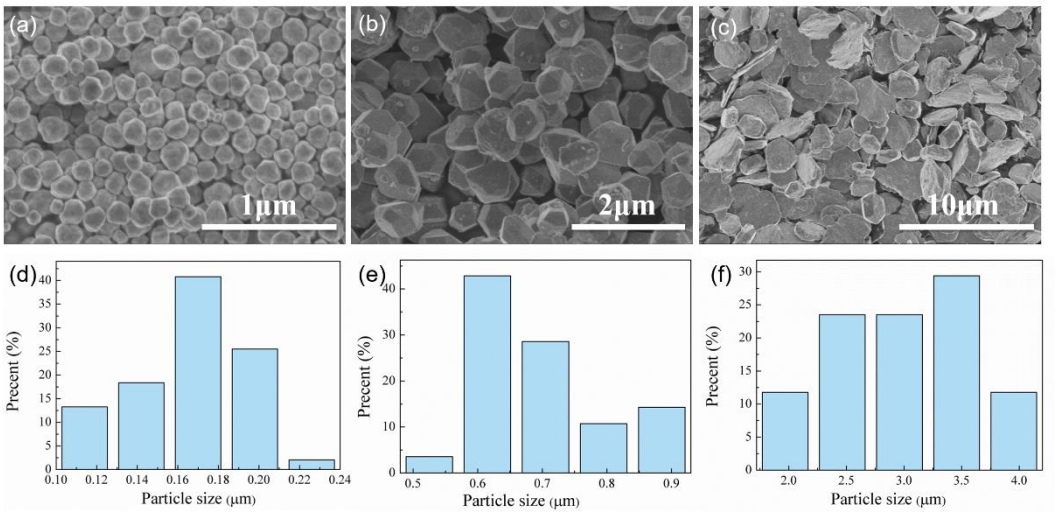

Figure 2.1 SEM images of received Cu particles: (a) particle A, (b) particle B, and (c) particle C; (d)-(f) are the corresponding particle size distribution.

2.2.2 Preparation of Cu particle/Cu complex inks, screen-printing, and thermal sintering

The standard fabrication process is shown in **Figure 2.2**. Firstly, the Cu(II) formate tetrahydrate (Cuf) powders were added to 2-amino-2-methyl-1-propanol (AMP) with a fixed

molar ratio of 1: 2 and then the mixture was stirred for 30 min at room temperature to ensure complete formation of the Cuf-AMP complex. The formation of the complex can be confirmed by the color change from the initial light blue color to dark blue [6]. After that, Cu particles were respectively introduced into the Cuf-AMP complex solutions with different mass ratios as shown in **Table 2.1**. Finally, these mixtures were uniformly mixed using a hybrid mixer (HM-500) for 30 min to obtain homogeneous Cu particle/Cu complex inks (Cuf-AMP-Cu particle inks).

To prepare conductive Cu patterns, the prepared Cu particle/Cu complex inks were deposited on glass or PET substrates by using a screen-printing method. Then, these ink-deposited glass or PET substrates were heated at a temperature ranging from 120 to 180 °C for 2 to 60 min in a nitrogen (99.99%) atmosphere. The heating rate was 10 °C min^{-1}. Prior to heating, the nitrogen gas flow was set as 5 L min^{-1} for 5 min to ensure washout of residual oxygen in a box furnace and then decreased to 1.5 L min^{-1} to prevent oxidation of Cu during annealing process.

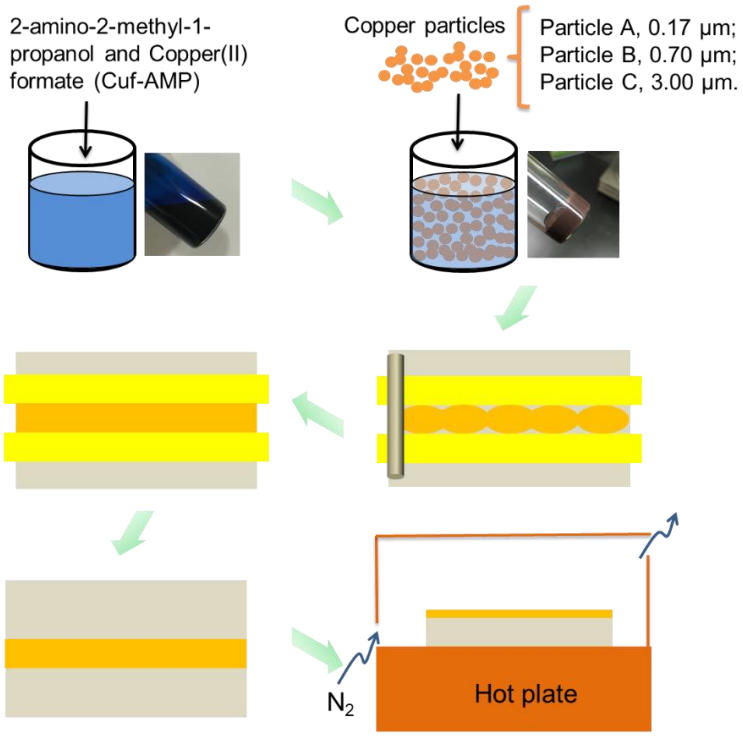

Figure 2.2 Diagram of Cuf-AMP-Cu particle ink fabrication, screen-printing, and thermal sintering process.

Table 2.1 Formulations and characteristics of Cu inks and sintered Cu patterns.

Inks (mass)	**Type of particle**	**Cu load (%)**	**Thickness (μm)**
Cuf-AMP: Cu particle =1:4	Particle A	83.1	49
	Particle B		47.7
	Particle C		51.87
Cuf-AMP: Cu particle =2:1	Particle A	43.7	11.94
	Particle B		13.87
	Particle C		16.80
Cuf-AMP: Cu particle =3:1	Particle A	36.8	10.12
	Particle B		10.7
	Particle C		14.3
Cuf-AMP: Cu particle =4:1	Particle A	32.6	8.30
	Particle B		10.29
	Particle C		12.30
Cuf-AMP: Cu particle =5:1	Particle A	29.7	7.52
	Particle B		8.98
	Particle C		11.16
Cuf-AMP	No particle	15.7	6.78

Thickness is obtained after sintering.

2.2.3 Characterization methods

The thermal behaviors of Cu(II) formate tetrahydrate and prepared Cu particle/Cu complex

inks were investigated by thermogravimetric-differential thermal analysis (TGA-DTA, Netzsch) at a heating rate of 10 °C min^{-1} in a nitrogen (99.99%) atmosphere. The phases of the formulated inks and sintered patterns were identified by using X-ray diffraction (XRD, Rigaku) with Cu Kα radiation. The surface and cross-section morphology of the sintered conductive patterns were observed by using a field emission scanning electron microscope (FE-SEM, SU8020, Hitachi). Focused ion beam (FIB, FB2100, Hitachi) was used to make the cross-section samples with a diameter of 150 mm at a standard current of 1.10-2.80 nA. The thickness of the sintered patterns was measured by using a three-dimensional laser microscope (VK-9500, Keyence), and the resistivity of the sintered Cu patterns was measured using a four-point probe analyzer (Loresta GP T610, Mitsubishi Chemical Analytech).

2.3 Characterization of Cu particle/Cu complex inks

The thermal behaviors of the Cuf-AMP complex ink and Cuf-AMP-Cu particle ink (Cuf-AMP: Cu particle B = 3: 1) were characterized using TGA-DTA, as shown in **Figure 2.3**. It is clear that the two kinds of inks have similar endothermic/exothermic peaks and mass loss trends, indicating that the decomposition and removal of Cuf-AMP complexes in the two inks is basically the same. The first endothermic peaks at about 130 °C are due to the evaporation of trace water and small molecular impurities in the inks. Subsequently, the exothermic peaks at about 150 °C are attributed to the decomposition of the Cuf-AMP complexes accompanied by a drastic mass loss. Farraj et al. investigated the mechanism of the decomposition process of the Cuf-AMP complexes by simultaneous thermal analysis coupled with mass spectrometry (STA-MS) and they found that the loss is because of the release of CO_2 and carbon [7]. The second endothermic peak at about 180 °C may be due to the crystallization of Cu or volatilization of carboxyl groups/AMP fragments in the complexes [7, 8]. It should be noted that the percentage of the remaining Cu loads in the Cuf-AMP complex ink and Cuf-AMP-Cu particle ink are 14.8 % and 37.6 %, respectively, which are consistent with the theoretical content of Cu in each (15.7% and 36.8%, **Table 2.1**).

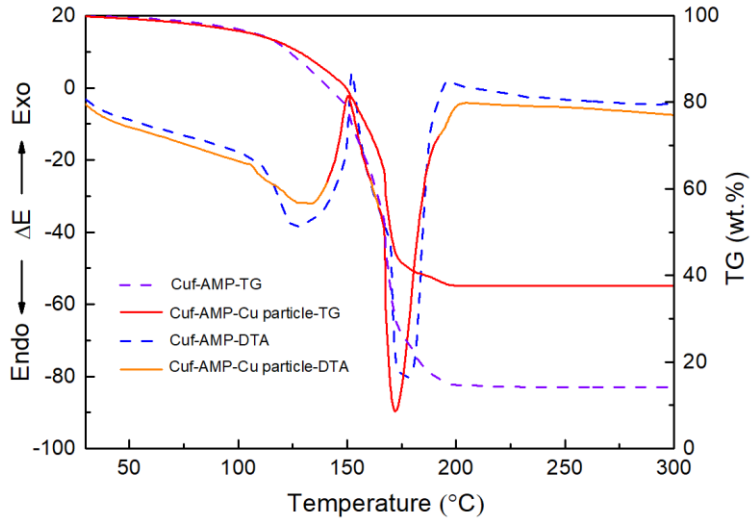

Figure 2.3 TG-DTA plots of (a) Cuf-AMP complex ink and (b) Cuf-AMP-Cu particle ink.

In addition, XRD analysis was conducted to identity the phase composition of the Cuf-AMP complex ink and Cuf-AMP-Cu particle ink after heat treatment at 140 °C for 15 min under a nitrogen atmosphere (**Figure 2.4**). The sintered patterns prepared from the two inks only show the peaks of metallic Cu. No other undesired substances (Cu_2O and CuO) are detected, indicating that Cuf-AMP complex is self-reducible to pure metallic Cu in a nitrogen atmosphere [6, 7], and preset Cu particles do not introduce impurities to Cu patterns.

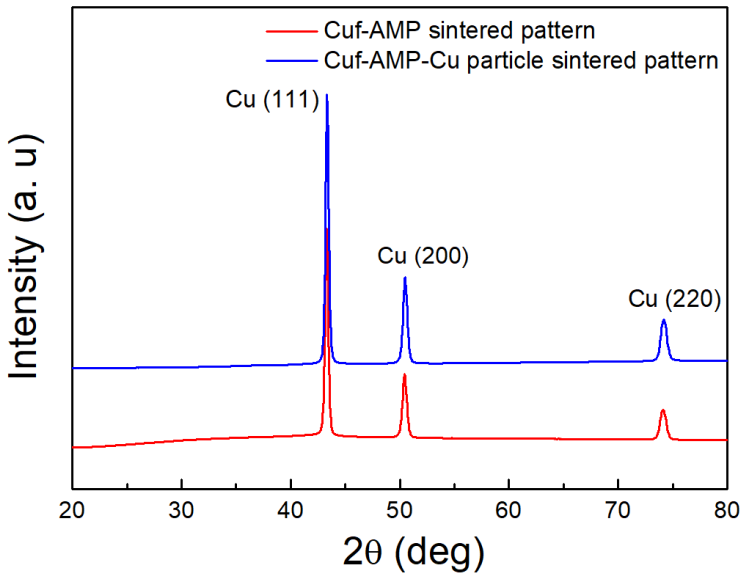

Figure 2.4 XRD patterns of Cuf-AMP complex ink and Cuf-AMP-Cu particle ink (Cuf-AMP:

Cu particle B=3:1) after heat treatment at 140 °C for 15 min in a nitrogen atmosphere.

2.4 Conductivity, microstructure, and surface morphology of printed Cu patterns

Figure 2.5 shows the electrical resistivity of the sintered Cu patterns fabricated from different Cuf-AMP-Cu particle inks. Based on the TG and XRD results discussed in section 2.3, all the printed inks were heated at 140 °C for fabrication of conductive patterns. As shown in Figure 2.5, the electrical resistivity of the sintered patterns prepared from the Cuf-AMP-Cu particle A ink and Cuf-AMP-Cu particle C ink decreases with an increasing content of Cu complex. On the other hand, the electrical resistivity of the sintered pattern prepared from the Cuf-AMP-Cu particle B ink first decreases and then increases with an increasing content of Cu complex. When the mass ratio of Cuf-AMP and Cu particle B is 3: 1 (about 36.8 wt.% Cu load), the sintered Cu pattern exhibits the lowest electrical resistivity of 1.13×10^{-5} Ω·cm, which is far superior to that of the pattern prepared from only these Cu particles (non-conductive, 1.66×10^{2} Ω·cm and 4.55×10^{1} Ω·cm for Cu particle A, B and C, respectively, after heat treatment at 140 °C for 15 min) and lower than that of the pattern prepared from pure Cuf-AMP complexes (1.4×10^{-5} Ω·cm). These results indicate that the Cu complex can enhance the sintering of all kinds of Cu particles and Cu particles with suitable size and amount can also improve the conductivity of printed Cu patterns prepared from Cuf-AMP complex.

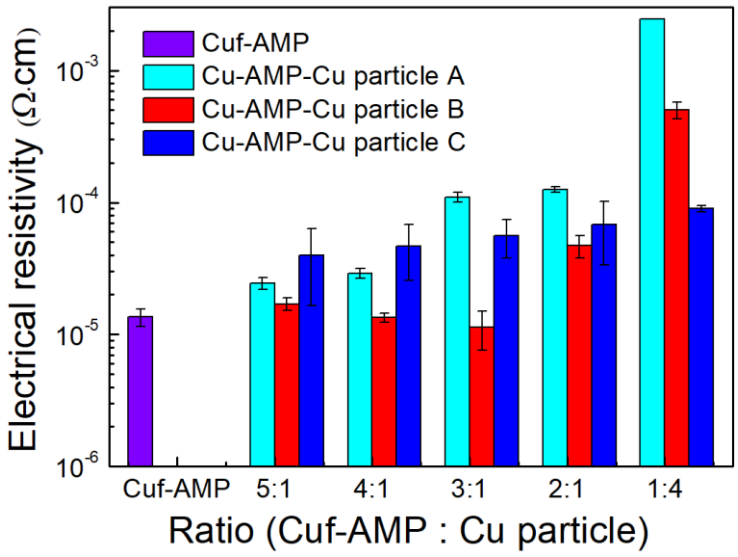

Figure 2.5 Electrical resistivity of the sintered Cu patterns with different Cu particle content

after heat treatment at 140 °C for 15 min in a nitrogen atmosphere.

The microstructure of the sintered patterns was studied to clarify their conductivity property. **Figure 2.6a** shows the SEM micrographs of patterns prepared from the pure Cuf-AMP complex. The Cuf-AMP complex is decomposed to form fresh Cu particles of different sizes over a wide range (0.04-0.66 μm), which are randomly stacked together with some large or small pores. In contrast, these large or small fresh Cu particles formed by the decomposition of the Cuf-AMP complex are difficult to observe when the Cu submicron particles are added into the complex (**Figure 2.6b–d**). This indicates that preset Cu particles may influence the nucleation process of metallic Cu generated from the decomposition of surrounding Cuf-AMP complex. Furthermore, compared with the size of the original Cu particles, the size of the particles in the sintered patterns has increased to 0.2 μm, 0.79 μm and 3.13 μm from the original sizes of 0.17, 0.7 and 3.0 μm, respectively. The TG and XRD results confirm that the Cuf-AMP complex has been decomposed into metallic Cu in the low temperature process. Therefore, the increase in size indicates that metallic Cu from the decomposition of Cuf-AMP complex might cover on the surface of these Cu particles to enlarge their size because these preset Cu particles act as heterogeneous nucleation sites for metallic Cu. Furthermore, these fresh and active Cu nuclei are expected to be beneficial for low-temperature sintering of these submicron Cu particles. As shown in Figure **2.6g and h**, the surfaces of the Cu particles are clearly rough due to the deposition of the Cu nuclei and an obvious connection between Cu particles is found. Some small particles (about 110 nm) clearly exist between the Cu particles (**Figure 2.6g and h**). These small particles come from the decomposition of Cu-AMP complex like a nano-welder to bond the Cu particles together to improve the sintering of the Cu particles. It can be expected that controlling the quantity of Cu-AMP complex is very important in these inks. If the content of Cuf-AMP is insufficient, the surface of the Cu particles will not be completely coated and connected together to realize the sintering at low temperatures. On the other hand, if there is an excess of Cuf-AMP, the density of the sintered patterns will be decreased due to the removal of a large amount of organics, which give a porous and rough microstructure [9, 10]. Therefore, a suitable ratio of Cu particles and Cuf-AMP complex is a key to achieving high performance Cu

patterns. In the present work, the optimal mass ratio of the Cuf-AMP complex and Cu particle B is determined as 3: 1.

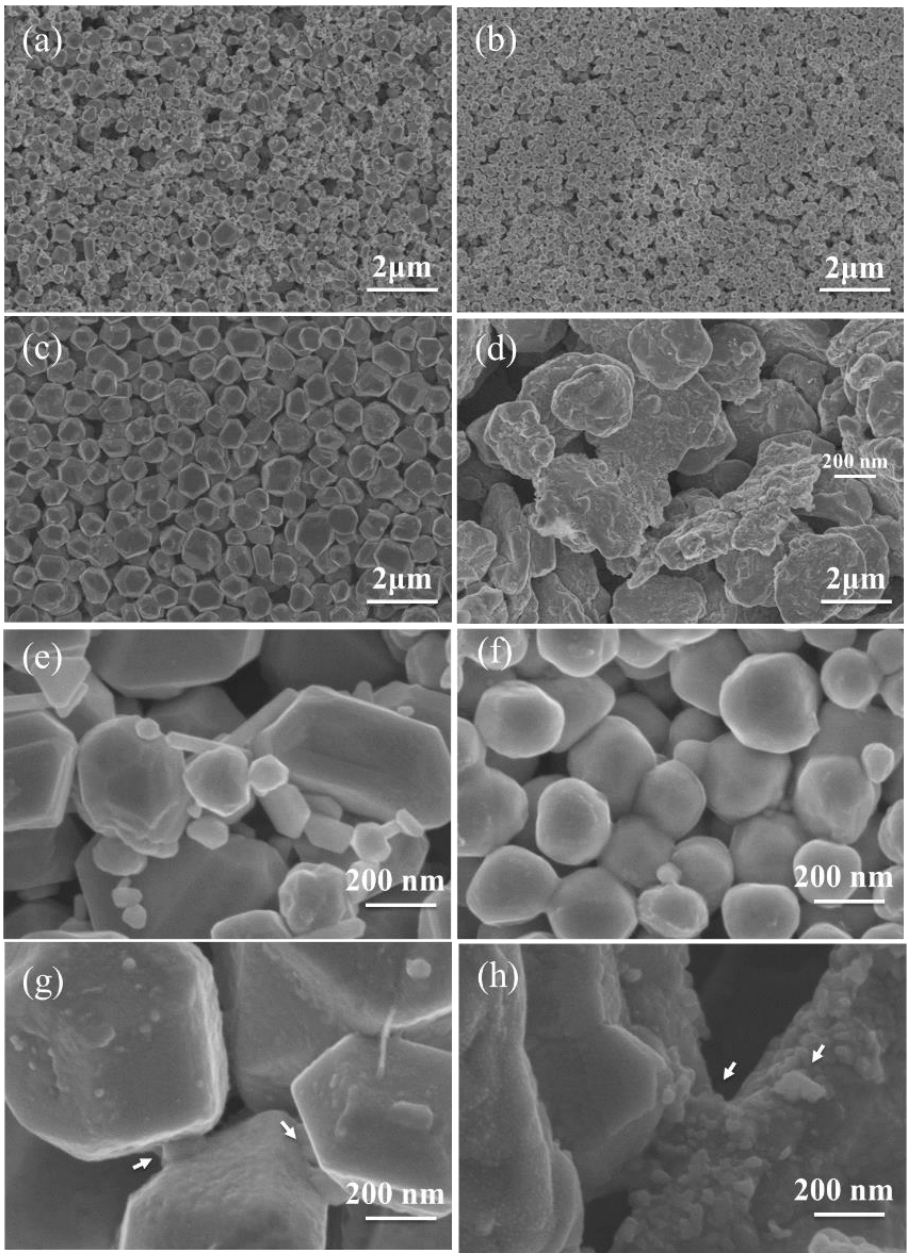

Figure 2.6 SEM images of (a) Cuf-AMP complex ink, (b) Cuf-AMP-Cu particle A ink, (c) Cuf-AMP-Cu particle B ink, and (d) Cuf-AMP-Cu particle C ink after heat treatment at 140 °C for 15 min in a nitrogen atmosphere; (e)-(h) High-magnification images of (a)-(d), respectively.

Figure 2.7 shows the cross-sectional images of the sintered patterns prepared from the

Cuf-AMP complex ink and optimal Cuf-AMP-Cu particle B ink. In the former, a porous structure is observed, and the grain size is small (**Figure 2.7a**). In the latter, a denser structure is observed with a large grain size (**Figure 2.7b**). Furthermore, an unclear thin Cu layer area between the big particles can be observed in some places (as indicated by the arrows in **Figure 2.7b**), which originates from Cu nuclei generated from the self-reduction of the Cuf-AMP complex mentioned above. Furthermore, in-situ formed Cu nuclei are completely assimilated by neighboring large Cu particles to form a big grain size in some places (as indicated by the cycle in Figure 2.7b). These results confirm that the decomposition of Cuf-AMP complex to form a thin Cu layer between Cu particles improves the sintering of large Cu particles to achieve high conductivity.

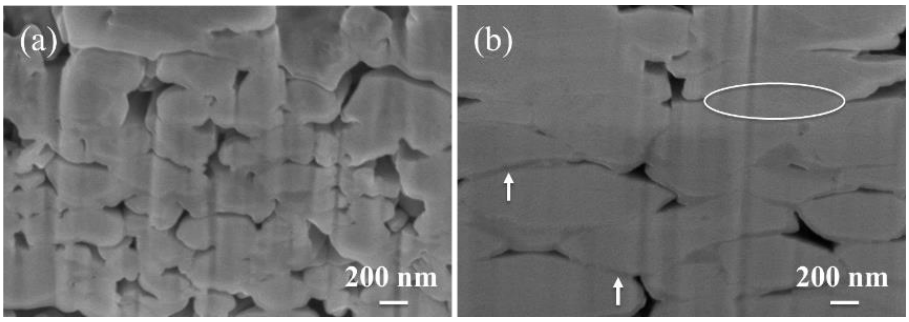

Figure 2.7 Cross-sectional morphology of (a) Cuf-AMP complex ink and (b) Cuf-AMP-Cu particle B ink after heat treatment at 140 °C for 15 min in a nitrogen atmosphere.

It has been mentioned that the Cuf-AMP complex ink always causes a rough surface of sintered patterns due to the low Cu load. When the Cu load is increased with the addition of Cu particles, the shape of the sintered Cu patterns is largely improved. **Figure 2.8a** shows the optical photos of the sintered patterns with/without Cu particles. Although these patterns show a brownish Cu color, there are significant differences. The sintered patterns prepared from the inks with Cu particle A, B or C show a uniform surface morphology with a relatively sharp edge without large cracks, while the sintered pattern prepared from the pure Cuf-AMP complex ink is non-uniform with some large cracks/pores and a rough edge. The cracks and pores seem to be formed by the violent decomposition and removal of organics in the complex due to low Cu load. **Figure 2.8b** shows the corresponding line profile of these sintered patterns with over

five positions. The Cuf-AMP complex ink gives a thin pattern with a thickness of about 6.78 μm. The pattern is uneven with a roughness of about 6.78 μm which is equivalent to the thickness of the pattern, indicating that some areas are missing showing a discontinuous Cu layer, as confirmed in Figure 2.8a. On the other hand, sintered patterns prepared from Cu complex/Cu particle A, B and C inks achieve thick patterns, and the thicknesses are about 10.12, 10.7 and 14.3 μm, respectively. The roughness of the sintered patterns prepared from Cu particle A and B is largely reduced to about 2.12 and 3.89 μm, respectively. This indicates that the morphology and roughness of the patterns has been improved by the additional Cu particles. However, the roughness of the sintered pattern prepared from Cu particle C is increased to 8.9 μm, which might correspond to the large diameter of the Cu particles used in the ink. As mentioned above, the average sizes of particles A, B, and C are 0.17, 0.7 and 3 μm, respectively, which correspond to the roughness values of 2.12, 3.89 and 8.9 μm, respectively. These results indicate that thickness and roughness of patterns closely agree with the size of Cu particles. A large size contributes to a big thickness and large roughness. To improve the morphology and thickness of the Cu patterns, a suitable diameter of Cu particle needs to be considered in order to make a uniform Cu pattern.

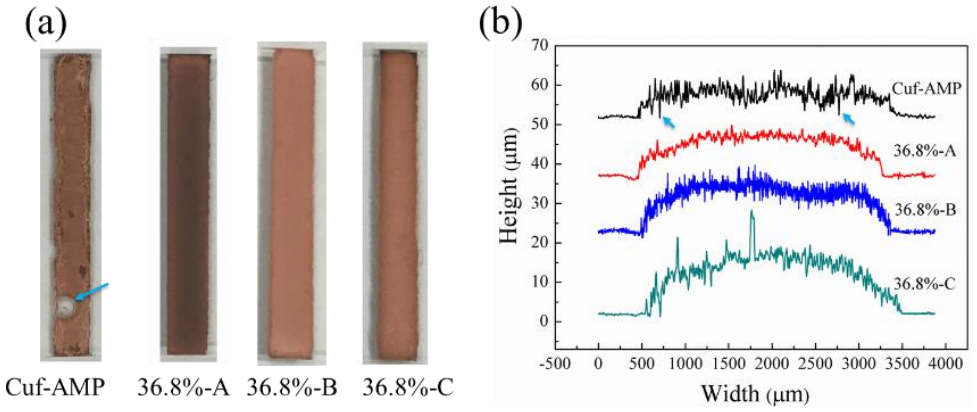

Figure 2.8 (a) Optical surface images and (b) cross-sectional morphology of the sintered patterns with/without Cu particle A, B or C heated at 140 °C for 15 min in a nitrogen atmosphere.

2.5 Sintering parameters of Cu inks and application

Figure 2.9 shows the electrical resistivity of sintered Cu patterns heat treatmented at various temperatures for one hour with a mass ratio of Cuf-AMP and Cu particle of 3: 1. The

electrical resistivity of the sintered patterns decreases as the heat treatment temperature increases. The decrease speed of electrical resistivity is fast in the case of the Cuf-AMP-Cu particle A ink. Over 140 °C, the decrease in electrical resistivity is very clear in the other three inks. It suggests that 140 °C might be enough for the decomposition of the Cuf-AMP complexes, which is in good agreement with the TG and XRD results mentioned above. The neck growth and connection among Cu particles can contribute to the decrease in electrical resistivity, which has been observed in the sintered patterns. It should be also noted that the size of the Cu particles influences the electrical resistivity of the sintered patterns. In general, small particles, especially nanoparticles, are easy to be sintered at a low temperature [11, 12]. However, as shown in the present work, small particles of 0.17 μm give the worst conductivity. There are two related reasons. One is the oxide on the surface of these particles which hinders the sintering of Cu particles at a low temperature. XRD analysis was performed on particles A, B, and C and a small peak of Cu_2O was found only in particle A (**Figure 2.10**). Second is the contact resistance between these small particles which determines the electrical resistivity of the sintered patterns [13]. Patterns containing many small particles tend to have a lot of contact resistance which causes high electrical resistivity. In contrast, large Cu particles seem to be beneficial to low electrical resistivity of the sintered patterns as seen in the present process. When these fresh Cu nuclei are coated on the surface of these large Cu particles, they can activate these particles to be sintered at a low temperature. Another important reason is that, compared with Cu nanoparticles, these large particles are antioxidants. However, Cu particles that are too large provide poor packing which will cause the decrease in electrical resistivity. Therefore, the selection of suitable Cu particles in the present ink is a key to achieving high conductivity, high packing density, appropriate thickness and sharp morphology.

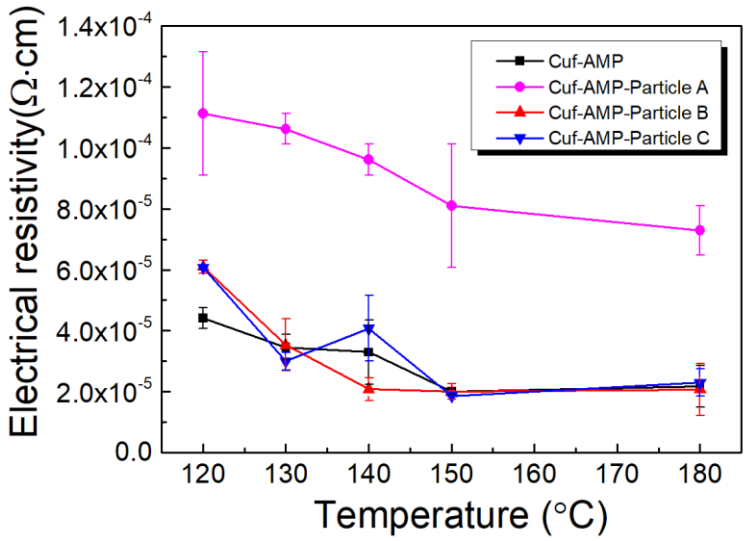

Figure 2.9 Electrical resistivity as a function of annealing temperature for one hour with a mass ratio of Cuf-AMP and Cu particles of 3: 1 in a nitrogen atmosphere.

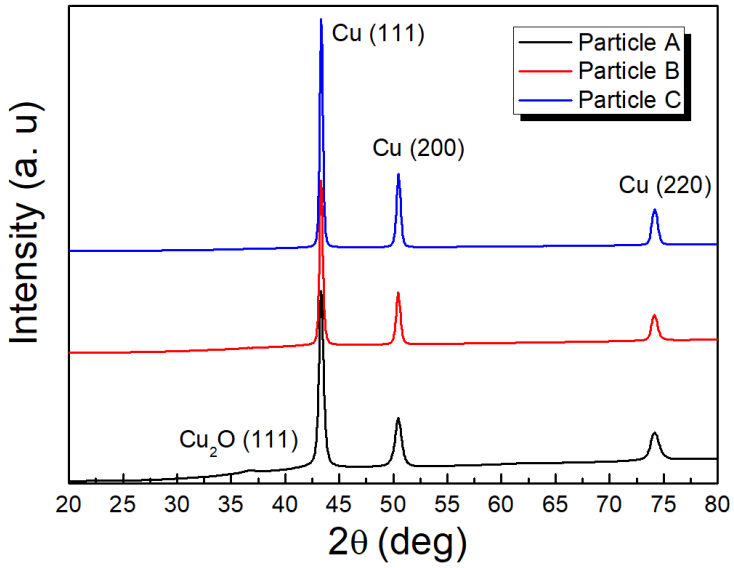

Figure 2.10 XRD patterns of Cu particle A, B, and C.

Figure 2.11 shows the relationship between the electrical resistivity of the sintered patterns and holding times. The electrical resistivity of the sintered patterns decreases with an increase of holding time until 15 min, after which a slight increase in electrical resistivity is observed. Therefore, the short 15 min sintering process is enough for these Cu inks even those with large particle sizes. A relative thermal decomposition also confirmed the results (**Figure 2.12**). The

Cuf-AMP-Cu particle B ink is heated to 140 °C and then held on to observe the decomposition evolution. Beyond holding time of 13 min, no significant weight-loss is observed, which indicates that the decomposition of the Cuf-AMP complexes and removal of the organics has been finished. The average electrical resistivity of the sintered Cu patterns is 1.4, 1.1 and 2.5×10^{-5} Ω·cm for Cuf-AMP complexes, Cuf-AMP-Cu particle B and Cuf-AMP-Cu particle C inks, respectively. Therefore, a low temperature of 140 °C and a short sintering time of 15 min is enough for these Cu inks. When the holding time is increased, a slight increase in electrical resistivity is still not clear, which might be related to the stress of the pattern or the oxide of the Cu nuclei formed from the in situ decomposition of the Cuf-AMP complex.

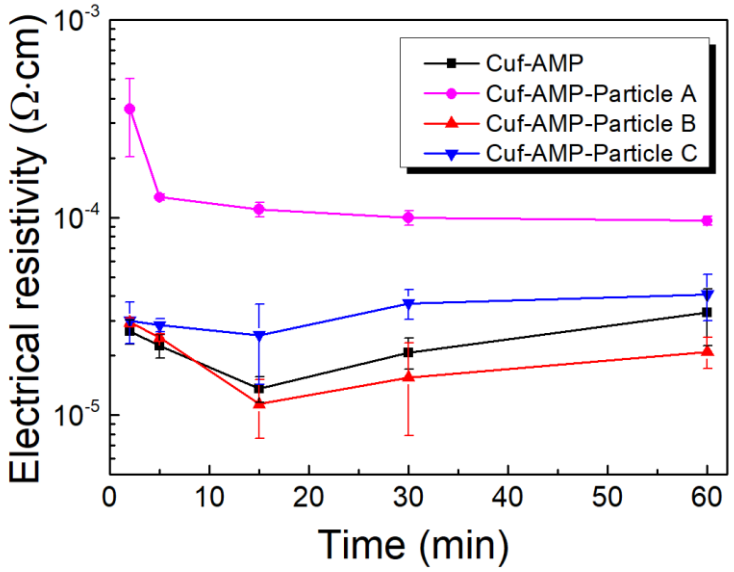

Figure 2.11 Electrical resistivity of the sintered Cu patterns as a function of the holding time at 140 °C in a nitrogen atmosphere.

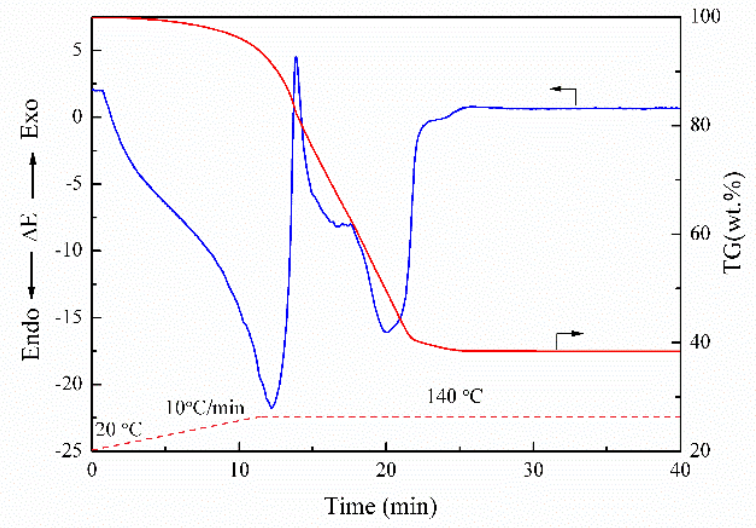

Figure 2.12 Relative thermal decomposition analysis using TGA-DAT.

2.6 Low-temperature sintering mechanism of Cuf-AMP-Cu particle inks

The decomposition mechanism of the Cuf-AMP complex has been investigated by Farraj *et al.* [7] who found that as the temperature increases, the decomposition of Cu(II) formate takes place in two stages.

$$Cu(HCOO)_2 \rightarrow Cu(HCOO) + CO_{2(g)} + 1/2H_{2(g)}$$

$$Cu(HCOO) \rightarrow Cu_{(s)} + CO_{2(g)} + 1/2H_{2(g)}$$

Based on their conclusions, the possible mechanism of the nucleation and sintering of Cuf-AMP-Cu particle inks is illustrated, as shown in **Figure 2.13**. The Cuf-AMP complex ink is transformed into pure metallic Cu by a continuous and homogeneous nucleation process. In the process, Cu ions are consumed to form nuclei, which randomly grow into particles. Nucleation formed in the early stage can grow into big particles, while nucleation at a late stage may grow into small particles because there are not enough materials for their growth. Therefore, Cu particles with different sizes can be observed as shown in Figure 2.14a and 2.6a, which is in agreement with the reported results [7, 13]. On the other hand, in the case of Cuf-AMP-Cu particle inks, these Cu particles are preset to provide nucleation sites as the nucleation of metallic Cu tends to occur on the surface of these Cu particles, which is called heterogeneous nucleation [14, 15]. Heterogeneous nucleation can be considered as a surface catalyzed or assisted nucleation process which can decrease the nucleation barrier of Cu ions. In other words,

the low interface energy between metallic Cu and the particles may facilitate the fast deposition of Cu on the surface of the particles [15]. Furthermore, these nuclei coated on the surface of the Cu particles can promote the sintering of the Cu particles to form electrical pathways. Based on this mechanism, high qualitative Cu patterns prepared from submicron or micron Cu particles can be obtained even by treatment at a low temperature and for a short time.

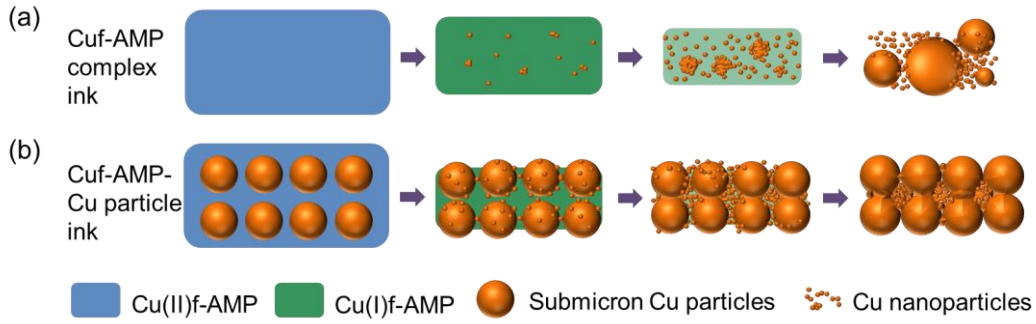

Figure 2.13 Schematic illustration of the nucleation and sintering behaviors of (a) Cuf-AMP complex ink and (b) Cuf-AMP-Cu particle ink.

2.7 Application

To demonstrate the application of printed conductive patterns for flexible electronic devices, the sintered Cu patterns were used as conductive wires to light up a LED during the bending, twisting and adhesive tape tests, as shown in **Figure 2.14**. The LED illumination intensity remains constant without significant degradation, strongly suggesting that the present inks with a high Cu load can be used in flexible printed electronic devices. Importantly, there are four advantages to using these inks for practical applications. Firstly, submicron Cu particles instead of Cu nanoparticles aer used. Cu submicron particles are very cheap compared with the Cu nanoparticles, 1/100-300, which can decrease the price of the inks significantly and increase the possibility for wide application in electronic devices. Secondly, in contrast with methods which need a reductive atmosphere to protect the pattern during heat treatment, the developed inks can be sintered and achieve a high conductivity under a nitrogen atmosphere. Thirdly, the developed inks do not need additional sintering agents for connecting the submicron Cu particles at a low temperature. During the heat treatment, the decomposition of self- reducible

Cu complex will create many fine Cu nuclei which can help connect the submicron Cu particles rapidly and create a high electronic pathway. Fourthly, the sintered patterns have a good thickness due to an increased Cu load. They can withstand a high carrying capability.

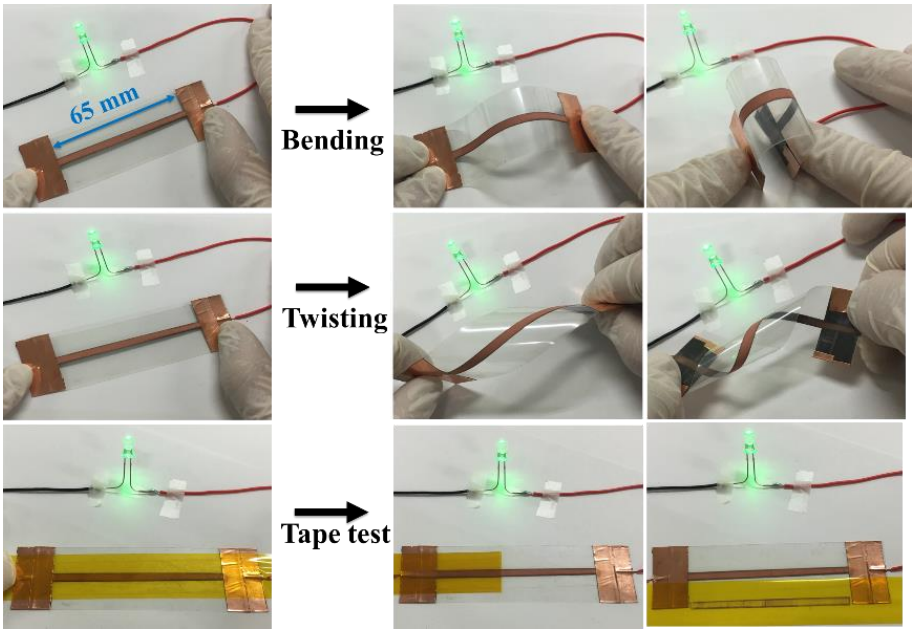

Figure 2.14 Photographs of the LED circuit with a 65 mm-long printed Cu pattern on PET substrate during the bending, twisting, and adhesive tape tests.

2.8 Conclusion

In this chapter, Cu particle/Cu complex inks are developed and the sintering of submicron Cu particles at low temperatures by using the in-situ formed fresh Cu nanoparticles is successfully realized. During the heat treatment, fresh Cu nuclei decomposed from Cu complex attach to the Cu particles to activate their surface, which contributes to the connection and neck-growth between these submicron Cu particles to achieve high conductive pathways. The effects of the size of Cu particles and the ratio of the amount of Cu complex to particles on the electrical resistivity and morphology of sintered Cu patterns are clarified, and the functions of the heat treatment temperature and holding time are investigated. The results show that Cu patterns with high conductivity of 1.1×10^{-5} Ω·cm can be easily achieved by using submicron Cu particle/Cu complex ink with heat treatment at a low temperature of 140 °C for only 15 min under a nitrogen

atmosphere. Furthermore, the sintered patterns maintain a high-qualitative surface morphology and favorable thickness, and also exhibit a strong adhesion to polymer substrates which will be advantageous for the fabrication of flexible electronic devices.

References

1. Wu, S. P.; Gao, R. Y.; Xu, L. H., Preparation of micron-sized flake copper powder for base-metal-electrode multi-layer ceramic capacitor. *Journal of Materials Processing Technology* **2009,** *209* (3), 1129-1133.

2. Tam, S. K.; Fung, K. Y.; Ng, K. M., Copper pastes using bimodal particles for flexible printed electronics. *Journal of Materials Science* **2016,** *51* (4), 1914-1922.

3. Liu, X.; Nishikawa, H., Low-pressure Cu-Cu bonding using in-situ surface-modified microscale Cu particles for power device packaging. *Scripta Materialia* **2016,** *120*, 80-84.

4. Wu, C.-J.; Sheng, Y.-J.; Tsao, H.-K., Copper conductive lines on flexible substrates fabricated at room temperature. *Journal of Materials Chemistry C* **2016,** *4* (15), 3274-3280.

5. Sung-Jun, J.; Hyun-Jun, H.; Hak-Sung, K., Highly conductive copper nano/microparticles ink via flash light sintering for printed electronics. *Nanotechnology* **2014,** *25* (26), 265601.

6. Shin, D.-H.; Woo, S.; Yem, H.; Cha, M.; Cho, S.; Kang, M.; Jeong, S.; Kim, Y.; Kang, K.; Piao, Y., A self-reducible and alcohol-soluble copper-based metal-organic decomposition ink for printed electronics. *ACS Applied Materials & Interfaces* **2014,** *6* (5), 3312-3319.

7. Farraj, Y.; Grouchko, M.; Magdassi, S., Self-reduction of a copper complex MOD ink for inkjet printing conductive patterns on plastics. *Chemical Communications* **2015,** *51* (9), 1587-1590.

8. Choi, Y.-H.; Hong, S.-H., Effect of the amine concentration on phase evolution and densification in printed films using Cu(II) complex Ink. *Langmuir* **2015,** *31* (29), 8101-8110.

9. Araki, T.; Sugahara, T.; Jiu, J.; Nagao, S.; Nogi, M.; Koga, H.; Uchida, H.; Shinozaki, K.; Suganuma, K., Cu Salt ink formulation for printed electronics using photonic sintering. *Langmuir* **2013,** *29* (35), 11192-11197.

10. Kim, S. J.; Lee, J.; Choi, Y.-H.; Yeon, D.-H.; Byun, Y., Effect of copper concentration in printable copper inks on film fabrication. *Thin Solid Films* **2012,** *520* (7), 2731-2734.

11. Jung, I.; Shin, K.; Kim, N. R.; Lee, H. M., Synthesis of low-temperature-processable and highly conductive Ag ink by a simple ligand modification: the role of adsorption energy. *Journal of Materials Chemistry C* **2013,** *1* (9), 1855-1862.

12. Deng, D.; Jin, Y.; Cheng, Y.; Qi, T.; Xiao, F., Copper nanoparticles: aqueous phase synthesis and conductive films fabrication at low sintering temperature. *ACS Applied Materials & Interfaces* **2013,** *5* (9), 3839-3846.

13. Yabuki, A.; Arriffin, N.; Yanase, M., Low-temperature synthesis of copper conductive film by thermal decomposition of copper–amine complexes. *Thin Solid Films* **2011,** *519* (19), 6530-6533.

14. Fletcher, N. H., Size effect in heterogeneous nucleation. *The Journal of Chemical Physics* **1958,** *29* (3), 572-576.

15. Kwon, S. G.; Krylova, G.; Phillips, P. J.; Klie, R. F.; Chattopadhyay, S.; Shibata, T.; Bunel, E. E.; Liu, Y.; Prakapenka, V. B.; Lee, B.; Shevchenko, E. V., Heterogeneous nucleation and shape transformation of multicomponent metallic nanostructures. *Nature Materials* **2014,** *14*, 215.

Chapter 3

Intense pulsed light reinforcement of printed Cu patterns

3.1 Introduction

In the chapter 2, the additive of the Cu complex made from Cu(II) formate and 2-amino-2-methyl-1-propanol could be decomposed into fresh Cu nanoparticles at low temperature of 140 °C and these fresh and active Cu nanoparticles can play a role of nano-welders in the realization of bonding those big Cu particles. However, the resistivity of achieved Cu patterns was not stable. And, the resistivity was rapidly increased after several bending cycles because of the insufficient sintering and weak adhesion between Cu patterns and substrates. Intense pulsed light (IPL) treatment is an effective photonic technology for structural reformation of various materials including metals, metal complex, ceramics and so on [1]. It has also been used to sinter various Cu nanoparticle inks to achieve highly conductive and stable Cu patterns on flexible substrates [2-6].

In this chapter, a two-step sintering method involving low-temperature heat-welding and subsequent IPL sinter-reinforcement is developed and optimized to realize highly reliable and highly conductive Cu patterns. The possible mechanism of the two-step sintering process is also discussed. In addition, the effects of substrates and particle sizes on the conductivity of achieved Cu patterns are investigated. The flexibility and oxidation resistance of achieved Cu patterns are evaluated. Results show that highly conductive and reliable Cu patterns can be easily achieved on even heat-sensitive PET substrate by using our Cu particle/Cu complex inks and two-stepping sintering process. Also, it should be noted that the printed Cu patterns from our submicron Cu particle/Cu complex exhibit excellent oxidation resistance and are superior to those from Cu nanoparticles.

3.2 Experimental

3.2.1 Materials

Cu (II) formate tetrahydrate ($C_2O_4H_2Cu{\cdot}4H_2O$, 98%) was purchased from Wako Pure Chemical Industries, Ltd. 2-amino-2-methyl-1-propanol ($C_4H_{11}NO$, 98%) was purchased form

Nacalai tesque, Inc. Submicron Cu particles with average sizes of 250 nm, 350 nm, and 800 nm were provided by Mitsui Mining & Smelting Co., Ltd. PI substrate was purchased from Du Pont Toray Co., Ltd. with a thickness of 50 μm while PEN and PET substrates were purchased from Toray Industries, Inc. with a thickness of 100 μm.

3.2.2 Ink preparation, screen-printing, and two-step sintering process

The standard fabrication process of the Cu particle/Cu complex inks has been described in section 2.2.2. The prepared inks were printed to form different patterns on PI, PEN and PET substrates by the screen-printing method. The thickness of the printed Cu ink is 50 μm. After that, the printed Cu inks would be transformed into conductive Cu patterns by using a two-step sintering process, as shown in **Figure 3.1**. The ink-printed substrates were heated at a low temperature of 140 ºC for 0-15 min under nitrogen (99.99%) atmosphere, followed by IPL sinter-reinforcement under an air atmosphere. The IPL system used in this study is PulseForge 3300 (Novacentrix, Austin, TX, USA) which covers broad band emission range from 200 to 1500 nm. The water-cooled xenon lamp, located 10 mm from the substrate stage, can create an optical energy as a function of the electrical voltage and duration time. In this study, in most cases, electrical voltage was fixed at 250 V and the duration time was changed from 550 μs to 2350 μs to supply optical energy from 471 mJ/cm^2 to 2073 mJ/cm^2. When studying the effect of Cu particle size on the conductivity of achieved Cu patterns, the irradiation duration was fixed at 2000 μs and the electrical voltage was changed from 240 V to 300 V to supply optical energy from 1700 mJ/cm^2 to 3300 mJ/cm^2.

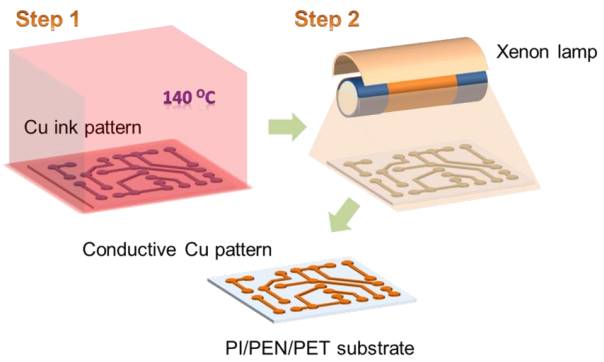

Figure 3.1 Schematic diagram of two-step sintering process including low temperature heat-

welding and IPL sinter-reinforcement.

3.2.3 Characterization methods

The surface and cross section of sintered Cu patterns were characterized by field-emission scanning electron microscopy (FESEM, Hitachi SU8020, Hitachi High Technologies America, Inc.) and transmission electron microscopy (TEM, JEOL-2100, JEOL Ltd). Focused ion beam (FIB, FB2100, Hitachi) was used to make cross-sectional samples with a diameter of 150 mm and a standard current of 1.10-2.80 nA. Crystal phase analysis of sintered Cu patterns was performed by X-ray diffraction (XRD, Rigaku) using Cu Kα. The electrical resistivity of the sintered submicron Cu particle patterns was measured using a four-probe analyzer (LorestaGP T610, Mitsubishi Chemical Analytech Co. Ltd). To test the mechanical reliability of sintered Cu patterns, two ends of samples were attached onto a pair of grips in a dynamic mechanical analyzer (EZ Test, Shimadzu) to measure the tensile (outer bending) and compressive (inner bending) performance with a constant speed of 60 mm min^{-1}. In the test, the bending radius (R) was calculated using equation 2.1, where L, dL, and Hs denote the initial length, the moving distances and the substrate thickness. The change in the electrical resistance of the samples during the testing was recorded using an Agilent Technologies 34410A multimeter and an Agilent Technologies 11059A Kelvin probe set (Agilent Technologies, Santa Clara, USA) through a four-point probe method. The long-term stability of printed Cu patterns without any encapsulation was evaluated by exposing them to high temperatures of 140 ºC, 180 ºC, and 220 ºC in air. The oxidation behaviors of printed Cu patterns were studied by observing their resistivity change and corresponding microstructure. The qualitative evaluation of Cu, Cu_2O, and CuO in printed Cu patterns was also performed by measuring the area under the peaks of Cu (111), Cu_2O (111), and CuO (111), respectively.

$$\text{Bending radius} = L/2\pi\left[\left(\frac{dL}{L}\right) - (\pi^2 H_s^2/12L^2)\right]^{1/2} \quad (2.1)$$

3.3 Two-step sintering of Cu particle/Cu complex inks

As mentioned in most reports, high heat-resistant polyimide (PI) substrate was firstly used to clarify the influence of two-step sintering process on the sintered Cu patterns. **Figure 3.2a**

shows the resistivity evolution of sintered Cu patterns. The patterns prepared from only IPL sintering without low temperature heat-welding process are insulating even though the supplied IPL energy is increased to 2073 mJ/cm^2. The color of the printed Cu pattern is kept deep blue, indicating the existence of lots of Cu ions corresponding to incomplete decomposition of Cuf-AMP complex. Cuf-AMP complex can decompose and react into fresh metallic Cu with necessary energy. For example, IPL energy as high as 16000-40000 mJ/cm^2 resulted in the decomposition of similar Cuf-AMP complex into metallic Cu [7], however, the instantaneous high energy seriously damaged the flexible substrate and caused a poor microstructure of sintered patterns due to large evaporation of organics in a short time [4, 5, 7]. In order to induce the mild and complete decomposition of Cuf-AMP complex in the ink in present work, a low temperature heat-welding process was firstly applied to form fresh Cu nanoparticles from Cuf-AMP complex. Three kinds of low temperature heat-welding processes were investigated, 140 °C for 5, 10 and 15 min, respectively. As shown in the result, the low temperature heat-welding process significantly improves the conductivity of the sintered Cu patterns. When the supplied IPL energy is increased to 1520 mJ/cm^2 and 2073 mJ/cm^2, the sintered Cu patterns with the low temperature welding of 140 °C for 10 min can achieve low resistivities of 1.5×10^{-5} Ω·cm and 7.2×10^{-6} Ω·cm, respectively. Further increase of the supply of energy results in partial delamination between sintered Cu patterns and the substrate, so the highest energy used in this study is limited to 2073 mJ/cm^2. It should be noticed that the low temperature heat-welding of 140 °C for 10 min is enough and a longer time of 15 min has no obvious benefit on the conductivity of the sintered Cu patterns. This can be explained by the thermogravimetric-differential thermal analysis (TG/DTA) result (**Figure 3.3**). When temperature is kept on 140 °C for about 10 min, no weight-loss is observed, which indicates the decomposition process has been completed.

Figure 3.2b shows the top-view image of the Cu pattern after low temperature heat-welding of 140 °C for 10 min. The shape of the Cu particles becomes irregular compared with that of original Cu particles, which indicates the decomposition product of Cuf-AMP may cover the surface of these original submicron Cu particles. And in some local region, the fresh metallic Cu from the decomposition of Cuf-AMP complex has helped bond the adjacent big Cu particles.

Figure3.2c shows the top-view image of the Cu pattern after low temperature heat-welding of 140 °C for 10 min and subsequent flash light sinter-reinforcement using energy of 2073 mJ/cm^2. The submicron Cu particles have been bonded with each other to form high conductive pathways, giving the low resistivity of the sintered Cu patterns (7.2×10^{-6} Ω·cm). In order to understand the bonding mechanism between these big Cu particles, the sintered Cu patterns were further observed by TEM. Many Cu nanoparticles cover on the surface of big Cu particles (**Figure3.2d**) and also exist between big particles (**Figure3.2e**). These Cu nanoparticles (5-20 nm) are easily sintered with low energy due to its high activity. Hence, these in-situ formed Cu nanoparticles can play a role of nano-welders in the connection of big Cu particles. On the other hand, although these nano-welders can improve the sintering of big Cu particles, prolonging the time of low temperature heat-welding does not give a decreased resistivity but a slight increased resistivity (**Figure 3.4**), which might be attributed to the intrinsic oxidation of such small Cu nanoparticles under a high temperature for a long time [8]. The rapid flash light sintering overcomes the oxidation problem to achieve high conductivity Cu patterns by competing with time. During flash light reinforcement, Cu pattern can experience an instantaneously high temperatures process and be sintered in very short time thus the process can prevent the Cu particles from oxidization. As shown in **Figure 3.5**, the mapping image of element O is uniform without difference between in-situ formed Cu nanoparticles and original submicron Cu particles, which proves that the oxidization of in-situ formed Cu nanoparticles is avoided by rapid flash light sintering process. Therefore, the low temperature heat-welding and subsequent IPL sinter-reinforcement process is a powerful candidate to sinter big Cu particles with in-situ nano-welders for highly conductive Cu patterns.

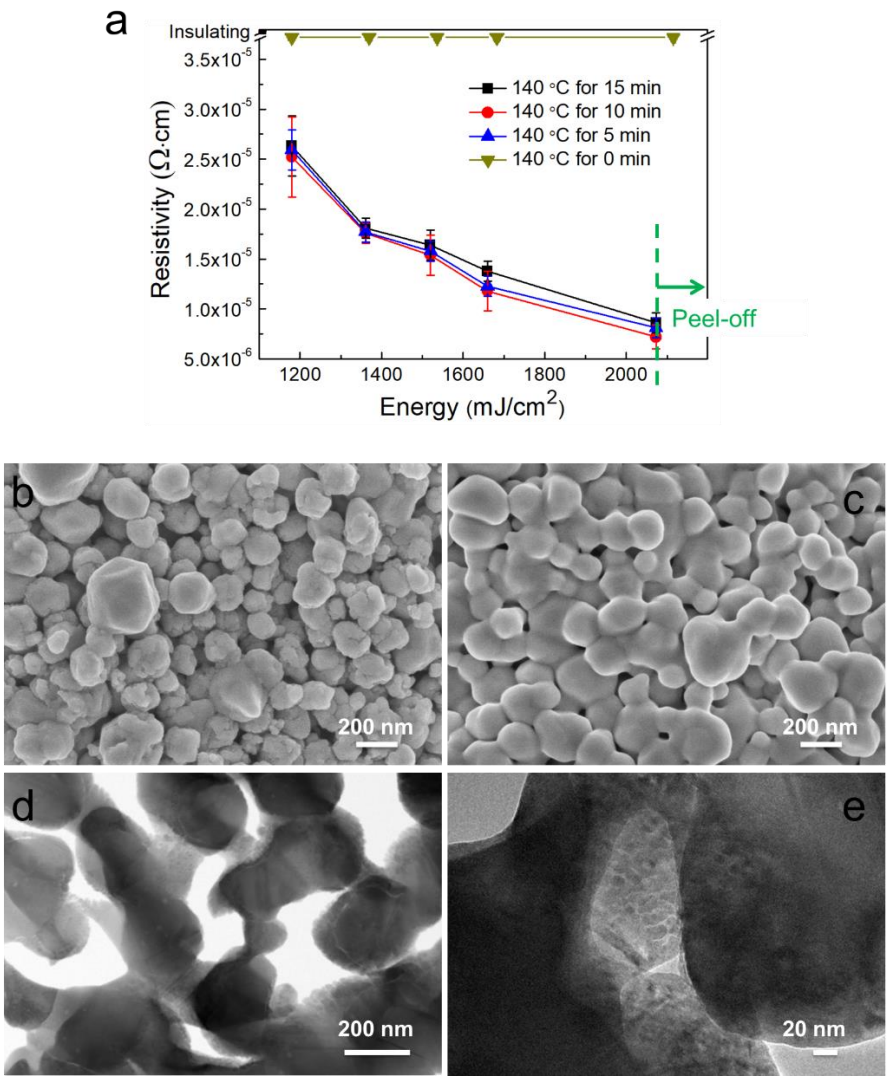

Figure 3.2 (a) Resistivity evolution of sintered Cu patterns as a function of the low temperature heat-welding and the input energy of IPL (under conditions with energy of >2182 mJ/cm^2, the sintered Cu patterns were partially peeled off from the substrate), (b) the top-view image of the Cu pattern after low temperature welding of 140 °C for 10 min, (c) the top-view image of the Cu pattern after low temperature welding of 140 °C for 10 min and subsequent IPL sinter-reinforcement using energy of 2073 mJ/cm^2, (d) scanning transmission electron microscope (STEM) image of sintered Cu patterns, and (e) TEM image of the interface between the sintered submicron Cu particles. Image c, d, and e are from the same sample. The size of original Cu particles is 250 nm.

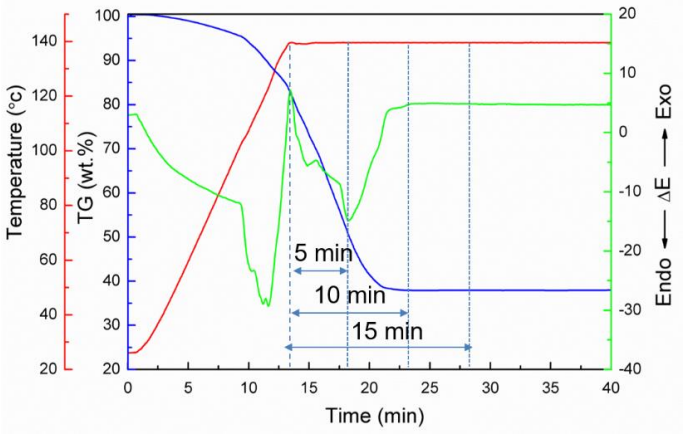

Figure 3.3 TG-DTA plots of submicron Cu particle ink in a nitrogen atmosphere; testing condition is that the temperature was heated to 140 °C and then kept on 140 °C for 30 min.

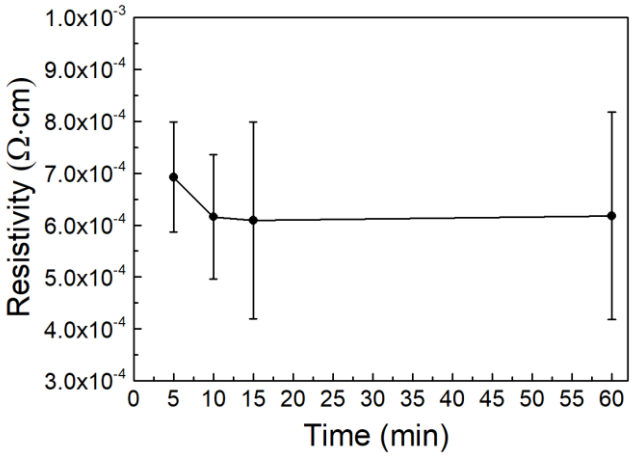

Figure 3.4 Resistivity of sintered Cu patterns depending on the holding time at 140 °C in a nitrogen atmosphere.

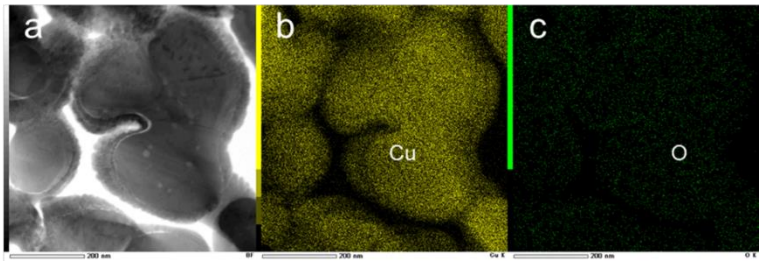

Figure 3.5 Element mapping of the sintered Cu pattern after low temperature welding of 140 °C for 10 min and subsequent IPL sinter-reinforcement using energy of 2073 mJ/cm^2. (a) Bright field image, (b) Cu mapping, and (c) O mapping.

Furthermore, in order to highlight the additive of Cuf-AMP complex, two-step sintering of Cu ink without Cuf-AMP complex was conducted for comparison (**Figure 3.6**). Result shows that sintered Cu patterns prepared from the Cu ink without Cuf-AMP complex have a resistivity as high as seven times of that prepared from Cu ink with Cuf-AMP complex. It is convinced that the importance of additive Cuf-AMP complex to improve the sintering of submicron Cu particles.

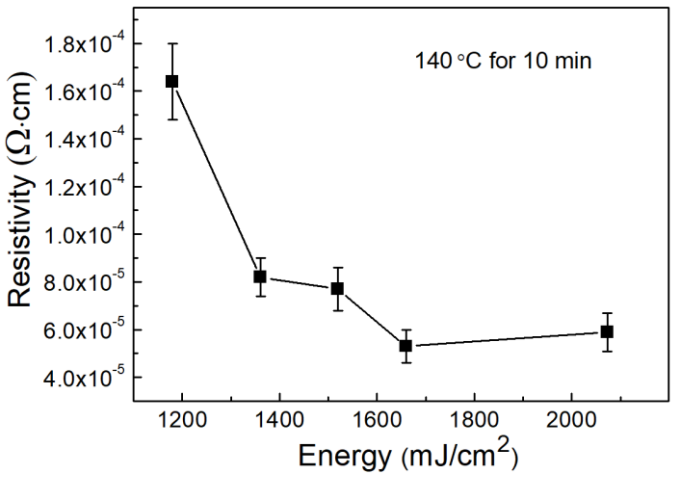

Figure 3.6 Resistivity evolution of sintered Cu patterns prepared from Cu ink without Cuf-AMP complex as function of supply IPL energy.

The microstructural transformation and crystal phase analysis of sintered Cu patterns during two-step sintering were further investigated. **Figure 3.7** shows the SEM images of sintered Cu patterns after two-step sintering with low temperature welding of 140 °C for 10 min and subsequent IPL sinter-reinforcement using different energy. For a low energy of 1180 mJ/cm^2, local sintering between adjacent Cu particles is clearly observed although these particles still keep the original morphology (**Figure 3.7a**). The cross-section image also confirms that a network structure in small range with small grains size has occurred including some clear pores (**Figure 3.7d**). With the increase of the supply of energy, the contact area between adjacent Cu particles is enhanced clearly with distorted particles morphology (**Figure 3.7b**). The huge grain size in the network structures is observed clearly in large range, and an

evolved dense microstructure is formed even with a few pores (**Figure 3.7e**), which well corresponds to the resistivity evolution of sintered Cu patterns with the increasing supply of energy in Figure 3.2a. When the supply of energy increases to 2073 mJ/cm^2, the tight connect between Cu particles seems to be no change from the surface images, however, some small particles are almost disappeared (**Figure 3.7c**). The cross-section image shows the microstructure is largely densified, and the grain size in the network structures is also further grown to form a dense and bulk-like microstructure (**Figure 3.7f**). It corresponds to the low resistivity of 7.2×10^{-6} Ω·cm sintered Cu pattern mentioned above. The resistivity, slightly higher than that of pure bulk Cu, is attributed to the denser structure with a small amount of voids [9].

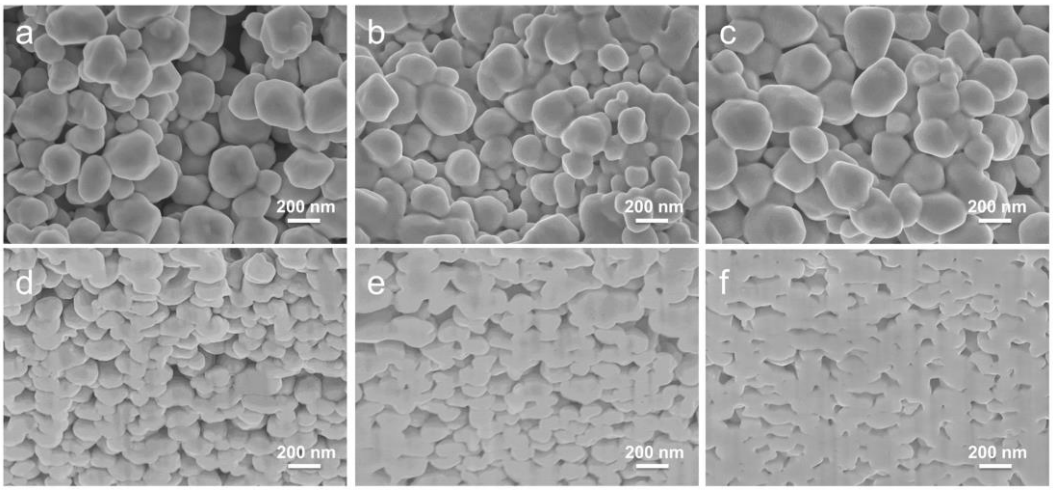

Figure 3.7 SEM images of sintered Cu patterns after low temperature welding of 140 °C for 10 min and subsequent IPL sinter-reinforcement with energy of 1180 mJ/cm^2, 1520 mJ/cm^2, and 2073 mJ/cm^2 respectively. Top-view images of patterns are shown in a-c and corresponding cross sections are shown in d-f. The size of original Cu particles is 250 nm.

Figure 3.8 shows the XRD results of Cu patterns before and after low temperature heat-welding and subsequent IPL reinforcement. The weak Cu_2O phase is observed in the ink (a line) and Cu patterns after low temperature heat-welding process (b line). The XRD analysis of pure Cuf-AMP pattern after low temperature heat-welding was also conducted and in the result no Cu_2O phase can be found (Figure 2.4). It suggests that the weak Cu_2O phase in a line and b line

comes from the original submicron Cu particles. It confirms the reason that the high conductivity did not be achieved with only heat-treatment due to the existence of oxides[8]. When Cu pattern is further treated by IPL, the intensity of Cu_2O phase is largely decreased to negligible (c line). As the applied flash light energy increases, the Cu_2O phase diminishes, leaving the Cu phase only. The reduction of Cu_2O phase to pure Cu during IPL sintering is a complex reaction of photochemical reaction and thermal reaction, which has been deeply studied in many previous researches [5, 10-15]. The existence of organics in ink is the crucial factor to reduce Cu_2O phase to pure Cu.

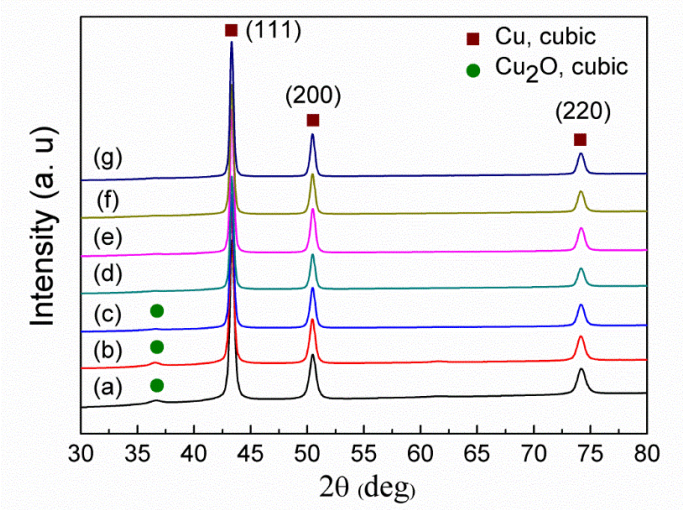

Figure 3.8 XRD patterns of (a) the submicron Cu particle ink, (b) the sintered Cu pattern after low temperature welding of 140 °C for 10 min and low temperature welding of 140 °C for 10 min with IPL sinter-reinforcement using energy of (c) 1180 mJ/cm^2, (d) 1361 mJ/cm^2, (e) 1520 mJ/cm^2, (f) 1660 mJ/cm^2, and (g) 2073 mJ/cm^2.

3.4 Effect of substrates on the conductivity of achieved Cu patterns

As mentioned above, the PI substrate is colorful and opaque closing to the ultraviolet region (**Figure 3.9**). Transparent and cheap PET and PEN substrates are preferred substrates for most flexible devices. Due to heat-sensitive property of PET and PEN substrates, Cu patterns are seldom fabricated successfully on these substrates considering the high energy treatment process of oxidized Cu ink. Here, the two-step process can overcome the weak-point of high energy.

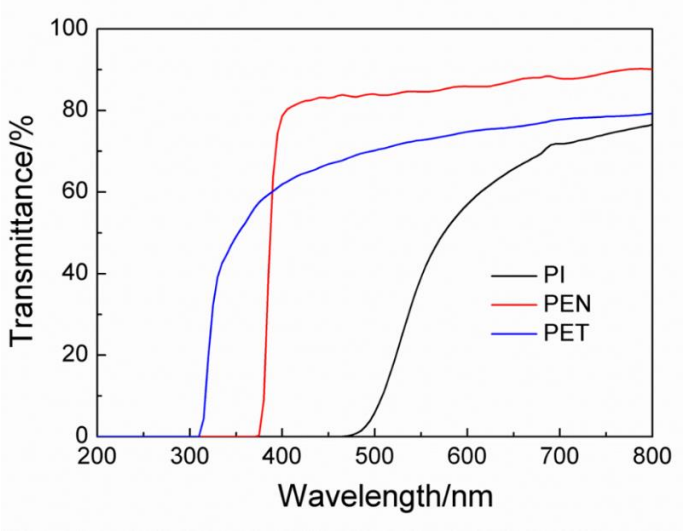

Figure 3.9 Transmittance spectra of PI, PEN, and PET substrates.

Figure 3.10 shows the resistivity evolution of sintered Cu patterns on heat-sensitive PEN and PET substrates. The resistivity of sintered Cu patterns on the two kinds of substrates is decreased with the applied IPL energy, a same trend seen in the case of PI substrate. The time of low temperature welding shows negligible function when the enough flash light energy is used. Moreover, due to the particular thermophysical properties of PEN and PET substrates, the supply of maximum energy for sintering Cu particles on these substrates is limited. High energy would cause the delamination of Cu patterns from the substrates (**Figure 3.11**) due to photo-chemical damage to the underlying substrates [9]. As shown in the Fig. 6, the PEN substrate can endure the maximum energy of 1273 mJ/cm^2 and a low resistivity of 1.65×10^{-5} Ω·cm was achieved while the PET substrate can endure a maximum energy of 1080 mJ/cm^2 and a low resistivity of 2.7×10^{-5} Ω·cm was achieved. The slightly higher resistivity, compared with that of sintered Cu patterns on the PI substrate, is due to the limited supply of flash light energy, which has been reported in most of previous literatures [9, 16]. However, the slightly higher resistivity is much lower than those resistivities reported in most of previous literatures even though nano-Cu particles were used in their studies.

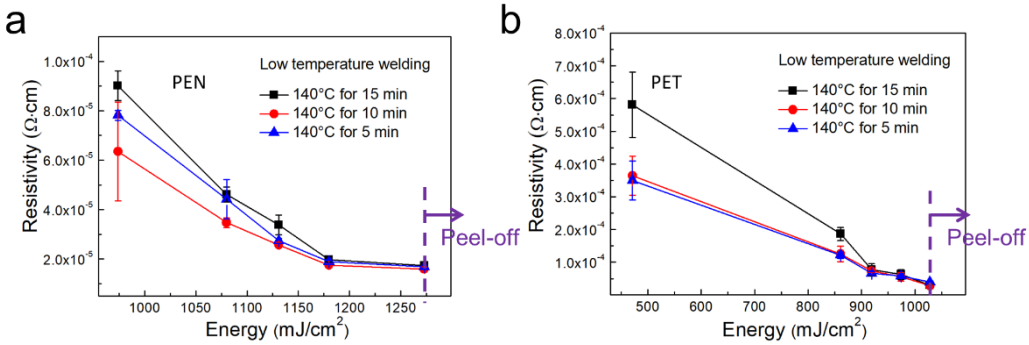

Figure 3.10 Resistivity evolution of sintered Cu patterns on PEN and PET substrates as function of time of low temperature welding and IPL energy.

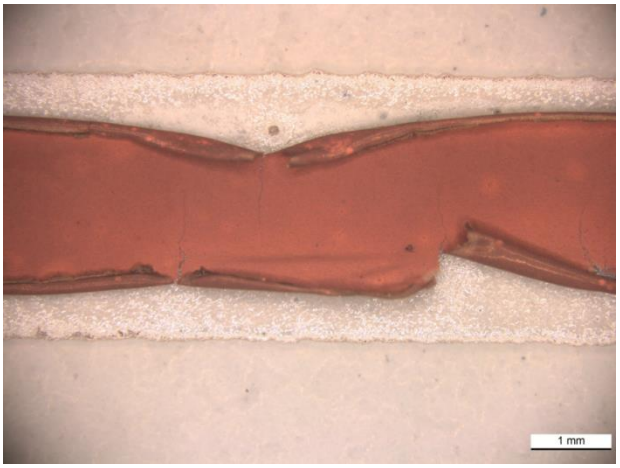

Figure 3.11 Sintered Cu pattern peeled off from the substrate due to photo-chemical damage to the underlying substrate.

Various studies of sintered Cu patterns for flexible electronic devices have been published, using different ink materials, substrates and heat treatment methods. **Table 3.1** shows an overview in comparison with this study. As shown in the **Table 3.1**, three kinds of Cu inks are studied by researchers: Cu particle ink, Cu precursor ink and hybrid Cu ink. It should be noted that Cu nanoparticles (<100 nm) and high heat-resistant PI substrate are typically used by most researchers. Due to the limitation of endurable IPL energy, the resistivity of sintered Cu nanoparticles patterns on heat-sensitive PET substrate was as high as 5.1×10^{-5} Ω·cm [9]. Contrastively, in our study, submicron Cu particles with average size of 250 nm were used and a lower resistivity of 2.7×10^{-5} Ω·cm is easily achieved on PET substrate by the optimized two-

step process. The result implies that modification of sintering process and design of Cu particle ink with suitable additive are crucial to obtain high conductive Cu patterns on transparent and flexible substrates. Furthermore, it is noteworthy that similar Cu ink including Cu particles and Cu precursor to make conductive Cu patterns on PI substrate by flash light sintering was reported [5]; however, the achieved resistivity of sintered Cu patterns was as high as 2.7×10^{-5} Ω·cm, which is about 4 times higher than our result (7.2×10^{-6} Ω·cm). The reason is that the decomposition of these Cu precursor (e.g., Cu(II) chloride, Cu(II) nitrate trihydrate, and Cu(II) sulfate pentahydrate) is finished during a short time and result in poor microstructure due to the dramatically evaporation of a large amount of by-product gas [4, 7]. Also, the used Cu precursors with high decomposition temperatures need high flash light energy for making conductive Cu patterns which cannot be accomplished on heat-sensitive substrates such as PEN and PET substrates. In our study, the additive of Cuf-AMP complex can decompose at 140 °C and transform into fresh and active metallic Cu nanoparticles, which in-situ covers on the surface of submicron Cu particles and promotes their contact during low temperature heat-welding process. The subsequent IPL further improves the sintering of these submicron Cu particles with the assistant of active Cu nanoparticles to form dense microstructure and therefore generates low resistivities of 7.2×10^{-6} Ω·cm, 1.6×10^{-5} Ω·cm and 2.7×10^{-5} Ω·cmcm on PI, PEN and PET substrates under low IPL energies of 2073 mJ/cm^2, 1273 mJ/cm^2 and 1080 mJ/cm^2, respectively.

Table 3.1 Overview of the reported conductive Cu ink patterns with respect to materials, substrate, heat treatment method, and conductivity.

Ink material	Liquid/ Particle size	Substrate	Heat treatment	Resistivity/ 10^{-6} Ω·cm	Ref
Cu particle	35-60 nm	PI	275-325 °C	11.5-92.0	[17]
Cu particle	5 nm	PI	Flash light	5.0	[2]
Cu particle	30 nm	PI	Flash light	173.0	[3]
Cu particle	20-50 nm	PI	Flash light	72.0	[18]
Cu precursor	liquid	PI	Flash light	3.2−5.3	[7]

Cu particle	20–50 nm/2μm	PI	Flash light	80.0	[19]
Cu particle	20-50 nm	PI	Flash light	94.0	[20]
Cu precursor/particle	liquid/10-70 nm	PI	Flash light	27.3	[5]
Cu particle	45 nm	PI	Flash light	8.6	[21]
Cu particle	<100 nm	PET	Flash light	51.2	[9]
Cu particle	<100 nm	PI	Flash light	7.0	[22]
Cu/Cu10Sn3 particle	20−60 nm	PEN	Flash light	16.0	[16]
Cu precursor/particle	Liquid/250nm	PI/PEN/PET	140 °C and Flash light	7.2/15.9/26.5	This study

3.5 Effect of Cu particle size on the microstructure and conductivity of printed Cu patterns

Figure 3.12 shows the microstructure evolution of printed Cu patterns prepared from 350 nm Cu particles. A low input energy of 1700 mJ/cm^2 has resulted in local sintering between adjacent Cu particles although their surface does not show any significant change (**Figure 3.12a**). The corresponding cross-section image also confirms that a weak network structure in small range is obtained (**Figure 3.12d**). With the increase of input energy, the contact areas between adjacent Cu particles are clearly enlarged even though the interfaces between them are still clear (**Figure 3.12b** and **3.12e**). When the input energy increases to 3300 mJ/cm^2, the interfaces between Cu particles seem to be disappeared, and meanwhile large necks between Cu particles have been observed (**Figure 3.12c**). The cross-section also confirms that the grains are further grown to form a strong network structure (**Figure 3.12f**).

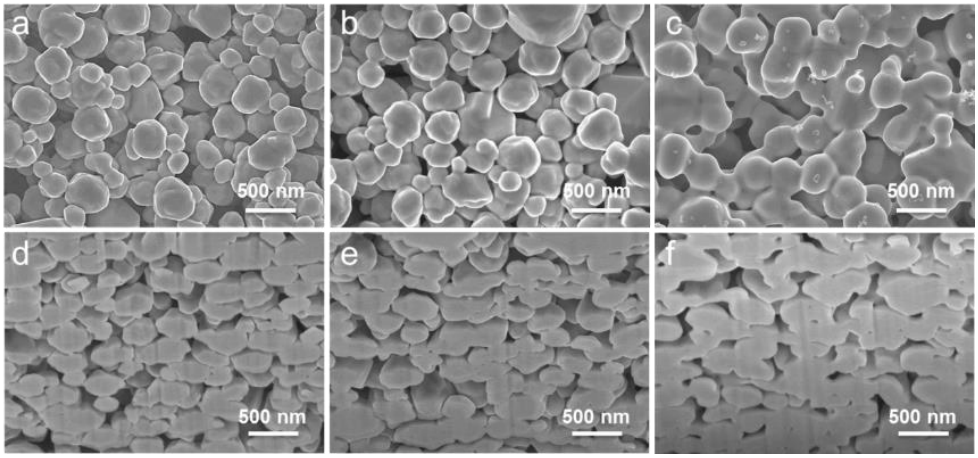

Figure 3.12 (a)-(f) Microstructures of printed Cu patterns after IPL sintering with input energies of 1700 mJ/cm^2, 2400 mJ/cm^2, and 3300 mJ/cm^2, respectively. Surface microstructures are shown in a-c, and the corresponding cross-section microstructures are shown in d-f. The size of Cu particle is 350 nm.

Figure 3.13 shows the microstructure evolution of the printed Cu pattern from 800 nm Cu particles. The microstructure evolution is similar to that prepared from particles with a size of 350 nm. However, there are two different features that should be noted. Firstly, under input energies lower than 2400 mJ/cm^2, there are many Cu nanoparticles existing on the surface of submicron Cu particles (**Figure 3.13a-b** and **Figure 3.13d-e**), which is likely to help joining adjacent submicron particles. Secondly, when the input energy increases to 3300 mJ/cm^2, Cu nanoparticles have been well-fused into submicron Cu particles resulting in interfaces formation between adjacent particles. However, these submicron Cu particles still retain their original morphology (**Figure 3.13c** and **f**).

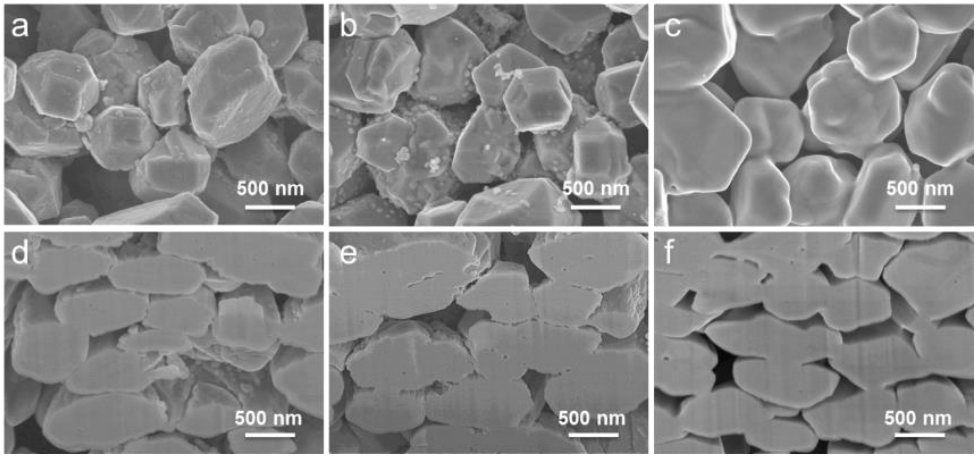

Figure 3.13 (a)-(f) Microstructures of printed Cu patterns after IPL sintering with input energies of 1700 mJ/cm^2, 2400 mJ/cm^2, and 3300 mJ/cm^2, respectively. Surface microstructures are shown in a-c, and the corresponding cross-section microstructures are shown in d-f. The size of Cu particle is 800 nm.

The conductivity of Cu patterns prepared from two kinds of Cu particle/Cu complex inks was investigated as a function of the of IPL energy as shown in **Figure 3.14**. It is clear that the resistivity of printed Cu patterns decreases with the increase of the input energy, and printed Cu patterns with smaller size Cu particles tend to achieve a lower resistivity. For example, when the input energy is 2400 mJ/cm^2, the resistivity of the printed Cu patterns from 350 nm Cu particles is 1.1×10^{-5} Ω·cm while that of printed Cu patterns from 800 nm Cu particles is as high as 2.3×10^{-5} Ω·cm, about two times higher than the former. A high input energy of 3300 mJ/cm^2 can further decrease the resistivity of printed Cu films prepared from Cu particles with a size of 350 nm to 5.8×10^{-6} Ω·cm though the same treatment exhibits little improvement for 800 nm Cu particles. This can be related to the sintering kinetics of particles [23]. Compared with large Cu particles, small Cu particles need a lower driving force for the surface atom diffusion because of the relative high specific surface area and high surface energy [24, 25]. In addition, the light absorption of small particles is stronger than that of big particles, which increases the absorption efficiency of flash light energy and therefore improves the sintering efficiency [26]. These results are consistent to the microstructures of printed Cu films. For example, after flash light sintering with input energy of 3300 mJ/cm^2, the 800 nm Cu particles retain their original shape even though many necks have been formed among particles due to the contribution of in-

situ formed Cu nanoparticles. In contrast, at the same input energy of 3300 mJ/cm^2, the shape of 350 nm Cu particles has been substantially changed and fused with the in-situ formed Cu nanoparticles. Therefore, printed Cu films prepared from submicron particles with a smaller size tend to achieve a lower resistivity.

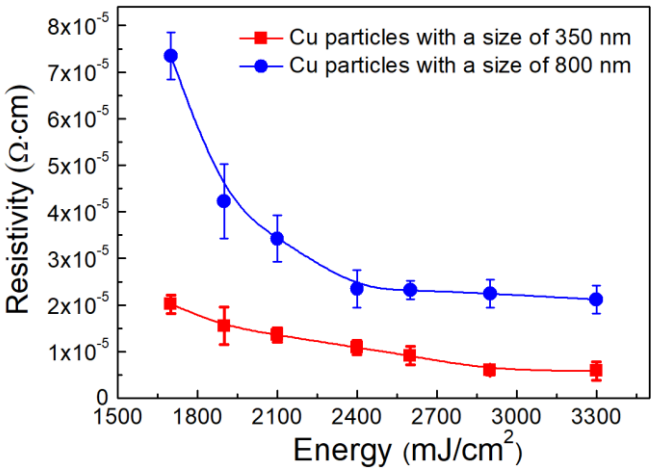

Figure 3.14 Resistivity of sintered Cu films as a function of the input energy of flash light sintering.

3.6 Long-term reliability of Cu patterns

3.6.1 Bending fatigue test

Flexible conductive patterns should possess a high reliability and especially maintain their electrical performance during different mechanical deformations. Therefore, the sintered Cu patterns on PET, PEN and PI substrates under tensile and compressive loading conditions were investigated in detail for evaluating their mechanical/electrical characteristics. Outer bending test and inner bending test correspond to tensile loading and compressive loading conditions respectively. **Figure 3.15a** shows the change of relative resistance of sintered Cu patterns on PET, PEN and PI substrates as function of the outer bending radius. The radius is decided by moving distance, as shown in **Figure 3.16**. The relative resistance (R/R_o) of sintered Cu patterns on all kind of substrates increases with the decrease of the bending radius. The electrical performance of Cu patterns formed on PET and PEN substrates is well maintained under bending radius above 10 mm while that of Cu patterns formed on PI substrate is well maintained

even under a harsh bending radius of 7 mm. When the bending radius decreases to about 3.5 mm, the relative resistances of sintered Cu patterns on PET, PEN and PI substrates are 1.5, 1.4 and 1.3 respectively. It should be noted that the outer bending test of the sintered Cu patterns was performed directly without acceptable surface protection and adjustment of the neutral plane to minimize the mechanical stress applied to the patterns, thus such a mechanical and electrical reliability can be further improved by suitable surface protection and coordination with a stress-free neutral plane in practical electronic devices [16]. Outer/inner bending fatigue tests were also conducted and results show that the sintered Cu patterns have high reliability without evident degradation of electrical performances, as shown in **Figure 3.15b-d**. The rapid increase in initial stage for all samples is attributed to the release of structural stress inside the patterns, which can be easily found in flash light sintered metallic patterns [7, 9, 27].The change of relative resistance for inner bending fatigue test is always smaller than that for outer bending fatigue test, which is related to the different type of stress during corresponding fatigue test because some cracks are accelerated under tensile stress in outer bending but retarded under compressive stress in inner bending [28]. The relative resistance of Cu patterns prepared on PET, PEN and PI substrates after 1000 bending test is below 1.8, showing a high mechanical/electrical reliability. Particularly, for the inner bending fatigue test the relative resistance of Cu pattern prepared on PI substrate is merely below 1.1 due to the original low resistivity [29]. It is believed that the high electrical reliability can be achievable due to the fully densified microstructure and well adhesion between sintered patterns and substrates. Flash light can soften substrate locally [30] and therefore improve adhesion between sintered pattern and substrates as shown in **Figure 3.17**.

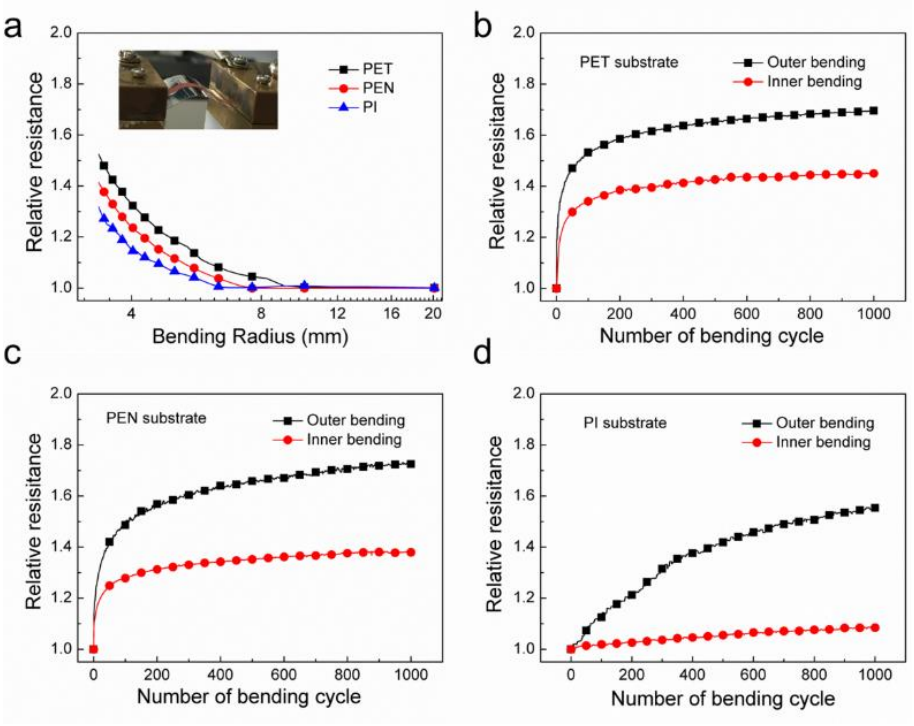

Figure 3.15 (a) Changes of relative resistance of sintered Cu patterns on PET, PEN and PI substrates as function of the outer bending radius. (Inset) Photograph of the specimen for outer bending test. (b)-(d) Changes of relative resistance of sintered Cu patterns during a repeated bending test at a bending radius of 10 mm on PET, PEN and PI substrates, respectively. Low temperature welding of 140 °C for 10 min and subsequent IPL using energy of 1080 mJ/cm^2, 1273 mJ/cm^2, and 2073 mJ/cm^2 were used to make sintered Cu patterns on PET, PEN, and PI substrates, respectively.

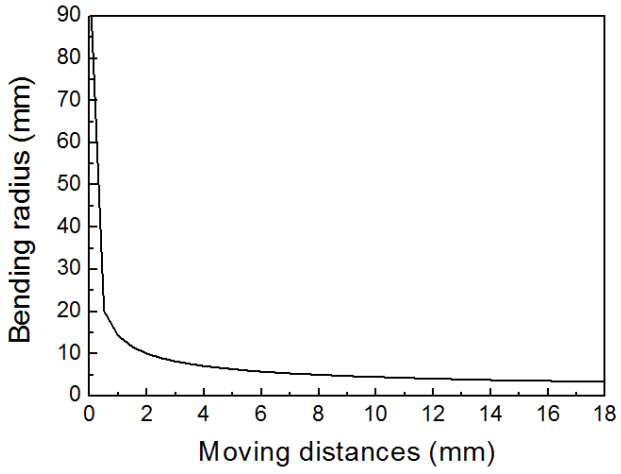

Figure 3.16 Relationship between bending radius and moving distance.

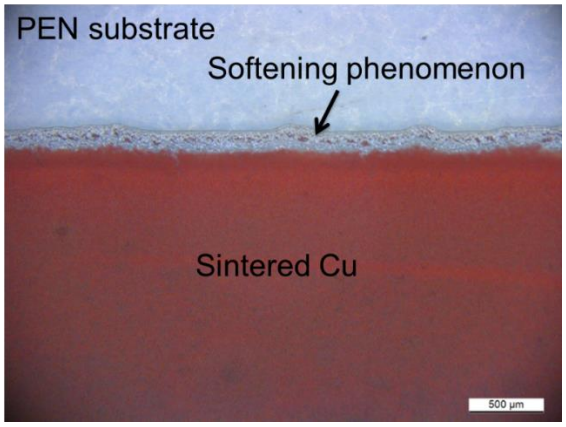

Figure3.17 Softening phenomenon of sintered Cu pattern on PEN substrate.

3.6.2 Oxidation resistance test

The oxidation protection of printed Cu films presents significant challenges for their practical applications in electronic devices [10, 31, 32]. In order to evaluate the long-term stability of the current printed Cu patterns, they were exposed to high temperatures in air. **Figure 3.18a, b** and **c** show the changes of the relative resistance of the printed Cu films as a function of exposure time at high temperatures of 140 °C, 180 °C and 220 °C, respectively. At 140 °C, the resistance of both sample A (Cu particles of 350 nm in size) and sample B (Cu particles of 800 nm in size) keeps stable values during the initial 5 h and then begins to increase. The resistance of sample A shows a higher increase rate than that of sample B. After 64 h, the relative resistance of sample A increases to about 2.4 while that of sample B only have a slight value less than 1.3. This difference indicates that the printed Cu patterns with large size particles are more stable than those with small size particles. In contrast, at 180 °C, the resistance of both sample A and B show a high increase rate. The relative resistances of sample A and B increase to high values of 12 and 9 after 64 h, respectively. At 220 °C, the relative resistances of both sample A and B sharply increase to above 10 only after 5 h. These results indicate that the printed Cu patterns are quite sensitive beyond 200 °C. The degeneration in electrical conductivity of the printed Cu patterns can be explained by the oxidation of Cu films under the high temperatures. As shown in **Figure 3.18d**, after oxidation at 140 °C, a Cu_2O peak clearly appears in the XRD pattern of Sample A and with the increase of oxidation temperature the

relative intensity of Cu_2O peaks in all XRD patterns become stronger. In addition, a high temperature exposure at 220 °C induces a formation of CuO phase.

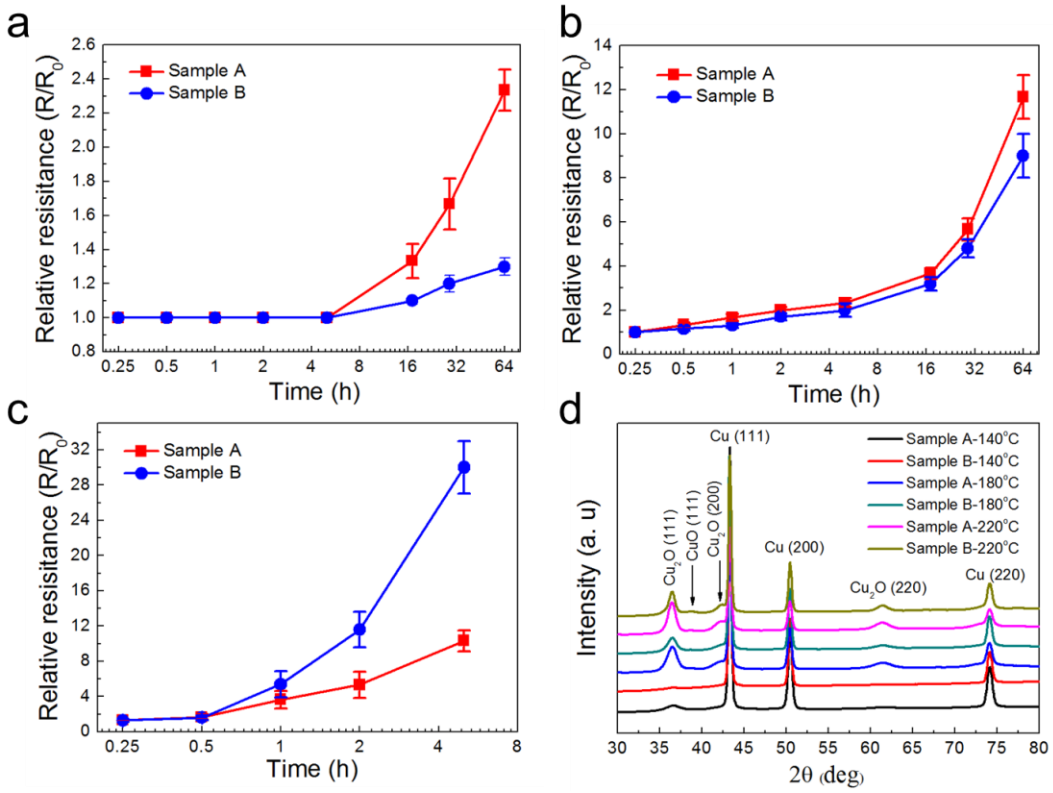

Figure 3.18 Change of relative resistance (R/R_0) of printed Cu films at temperatures of (a) 140 °C, (b) 180 °C, and (c) 220 °C, respectively, in air. R_0 is the original resistance of the printed patterns and R is the resistance of the printed patterns after oxidation at high temperatures. (d) XRD patterns of printed Cu films after oxidation in high temperatures for 5 hours. Low temperature heating of 140 °C for 10 min and IPL sintering using energy of 3300 mJ/cm^2 were used to fabricate printed Cu patterns.

Figure 3.19 shows the surface microstructures of the printed Cu patterns after oxidation exposure for 5 h at various temperatures. It is clear that there are many oxide particles formed on the surface of the printed Cu patterns (**Figure 3.19a-f**). At 140 °C, the size of the oxide particles is fine ranging from 5 to 50 nm (**Figure 3.19a, d**). With increasing temperature, the small oxide particles grow into larger ones. After oxidation for 5 h at 220 °C, the oxide particles on the printed Cu patterns grow into 100 nm-200 nm (**Figure 3.19c, f**). Thus, it can be said that

the Cu oxides are easily generated on the surface of printed Cu films and a high temperature can accelerate the formation of oxide layer (**Figure 3.19c**). The oxides formed such as CuO and Cu_2O are semi-conductive or insulating, so they seriously degrade the electrical property of printed Cu films.

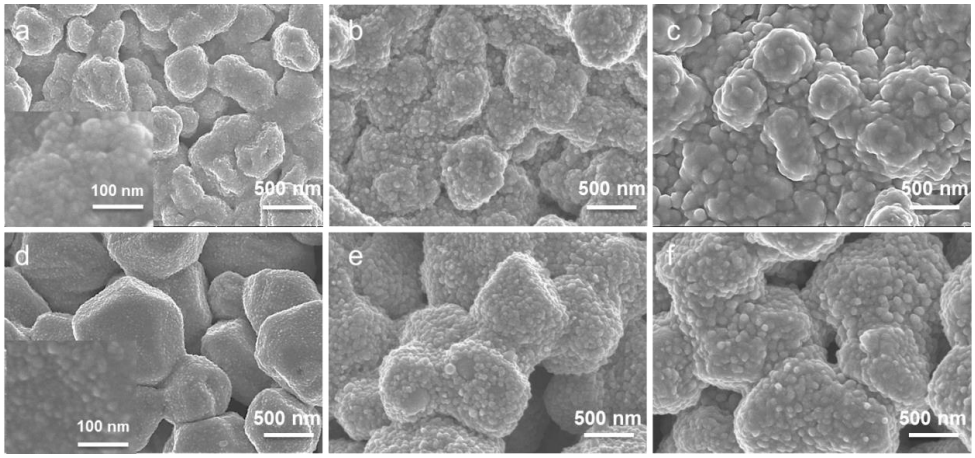

Figure 3.19 Surface microstructures of printed Cu patterns after oxidation for 5h at (a, d) 140 °C, (b, e) 180 °C, and (c, f) 220 °C, respectively. The printed Cu patterns prepared from Cu particle ink with an average size of 350 nm are shown in a-c and those prepared from Cu particle ink with an average size of 800 nm are shown in d-f.

The oxidation behaviors of printed Cu patterns were further investigated by the analysis of their chemical composition. The areas under XRD peaks of Cu (1 1 1), Cu_2O (1 1 1), and CuO (1 1 1) were measured to estimate the mass fractions of Cu, Cu_2O and CuO in the printed Cu patterns. **Figure 3.20** shows the change of mass fractions of Cu, Cu_2O and CuO in printed Cu patterns as a function of oxidation time, oxidized at 140 °C, 180 °C, and 220 ºC, respectively. At 140 ºC, only Cu_2O and Cu phases are found in the printed Cu patterns. With the increase of oxidation time, the mass fraction of Cu decreases and that of Cu_2O increases (**Figure 3.20a**). When the oxidation temperature is increased to 180 ºC, a CuO phase appears after oxidation for 5h. However, its mass fraction keeps as low as about 1 % even though the oxidation time is prolonged to 64 h. A higher oxidation temperature of 220 ºC causes a similar result that the most of the Cu is oxidized to Cu_2O rather than CuO even though the oxidation time has been prolonged to 64 h. Based on the previous studies [33], it is found that Cu is transfer to Cu_2O

and then CuO during the oxidation. The rapid transformation of Cu into Cu_2O can happen at a temperature below 200 °C while the rapid transformation of Cu_2O into CuO needs a really high temperature above 350 °C. In the current experiment, the highest temperature is 220 °C, thus the transformation of Cu_2O into CuO is supported to be slow. Therefore, even though the oxidation is as long as 64 h, the fraction of CuO is still small. In addition, there are two points to be noted: (1) In all cases, the printed Cu patterns prepared from 800 nm particles exhibit a higher oxidation resistance than those prepared from 350 nm particles, and (2) compared with the oxidation of Cu nanoparticles reported in the previous study [10, 34], the printed Cu patterns from submicron Cu particles exhibit much greater oxidation resistance.

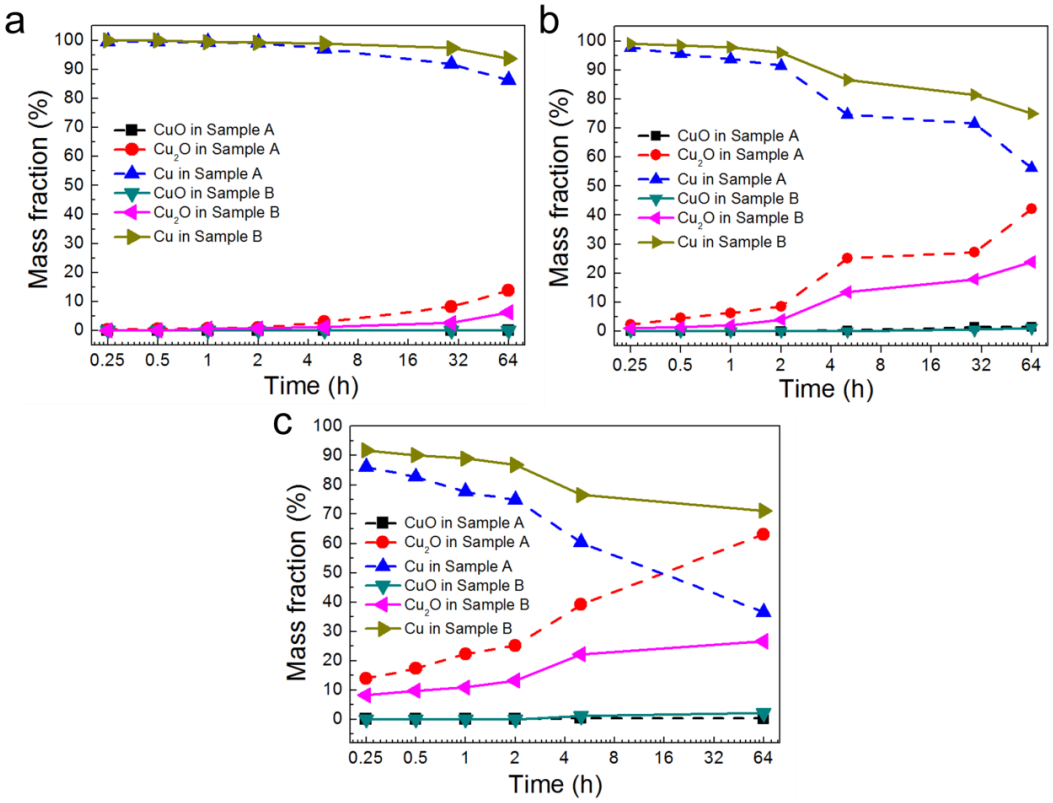

Figure 3.20 Mass fractions of CuO, Cu_2O and Cu in printed Cu patterns as a function of time, oxidized at (a) 140 °C, (b) 180 °C, and (c) 220 °C, respectively. Sample A and Sample B mean the printed Cu patterns prepared from Cu particles with average sizes of 350 nm and 800 nm, respectively.

At 220 °C, the initial Cu particle size effect changes drastically. The relative resistance of

printed Cu patterns prepared with 800 nm particles rapidly increases much faster than that with 350 nm (Figure 3.18c), which is opposite to the results both at 140 °C and at 180 °C (Figure 3.18a, b). This can be explained by the differences both of chemical composition and of microstructure evolution of the printed Cu patterns in oxidation. At 140 °C and at 180 °C, the excellent stability of the printed Cu patterns is attributed to the thick and strong conductive pathways formed inside the Cu films, even when the outer surface layer of Cu particles is oxidized (**Figure3.21a-b** and **d-e**). The resistance change of printed Cu patterns also depends on the gradual change of chemical composition such as Cu into Cu_2O and then CuO. The oxidation prefers to occur at particle boundaries due to their high Gibbs free energy [35]. Because the printed Cu patterns with large Cu particles contain a smaller number of particle boundaries than the patterns fabricated from small Cu particles, they show a higher oxidation resistance and thus a higher stability. On the other hand, when the printed Cu patterns are oxidized at a higher temperature of 220 °C, the printed Cu pattern prepared from particles with a size of 350 nm show a higher stability because rapid oxidation causes their microstructure to become dense, which in turn reduce the space of oxygen inside the printed Cu patterns (**Figure 3.21c**). In contrast, the loose structure with many large voids in the patterns fabricated from 800 nm particles provides sufficient space for the oxygen. The sufficient oxygen accelerates the oxidation of Cu to Cu_2O and then to CuO [36], which is consistent with the result shown in Figure 3.20c that the content of CuO in patterns fabricated form 800 nm particles becomes higher than that fabricated form 350 nm particle at 220 °C. Especially, the serious oxidation of Cu around the voids accelerates the break of pathways between adjacent Cu particles. In other words, the initial Cu-Cu metallic bond between the sintered Cu particles was broken by the formation of Cu oxides layer at the interface (**Figure 3.21f**). At this condition, the rapid increase of electrical resistance of printed Cu films depends heavily on the degradation of microstructures not the change of chemical composition. The similar phenomenon also occurred in the sintered Cu joint, in which the formation of Cu_2O oxidation layer between Cu particles heavily decreased the shear strength of Cu joint [37]. Therefore, the long-stability of printed Cu films is attributed to not only the change of chemical composition, but also to the microstructure evolution. It is possible to improve the long-stability of printed Cu patterns by

tailoring the particle size and guaranteeing a dense microstructure for printed Cu patterns.

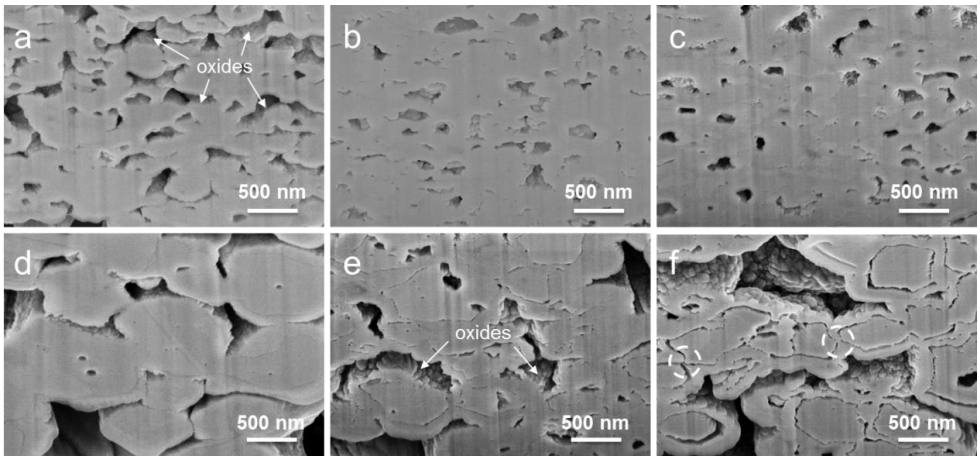

Figure 3.21 Cross-sectional microstructures of printed Cu patterns after oxidation for 5h at (a, d) 140 °C, (b, e) 180 °C, and (c, f) 220 °C, respectively. The printed Cu patterns prepared from Cu particles with an average size of 350 nm are shown in a-c and that prepared from Cu particles with an average size of 800 nm are shown in d-f.

3.7 Application

To demonstrate the applicability of the submicron Cu particle ink for flexible electronic devices, the sintered Cu patterns were used as conductive wires to light up a LED during the bending, folding and twisting, as shown in **Figure 3.22**. The LED illumination intensity remains constant without significant degradation. It strongly suggested that the present Cu ink can be used in flexible printed electronic devices or next-generation electronics [38, 39]. Also, V-shape dipole Cu antenna patterns were successfully fabricated, as shown in **Figure 3.23a**. The patterns are 30 mm length and 5mm width with an angle of about 30^{o}. The resonant frequency and return loss of the printed Cu antennas were measured, as shown in **Figure 3.23b**. The resonant frequency is a natural frequency at which it is easiest to get the radio wave signal. The S11 parameter of return loss means the loss of signal power during signal reflection in the antenna and low S11 parameter indicates high antenna sensitivity which is influenced by resistivity and surface roughness of printed antenna patterns [40, 41]. As shown in the results, the return losses of printed Cu antennas on PI, PEN and PET substrates are -52 dB, -35 dB and -18 dB, receptively, which correspond to the resistivities of sintered Cu patterns. Because a return loss

of less than -10 dB indicates an acceptable sensitivity [42, 43], the printed antennas on PI, PEN and PET substrates are expected to be high sensitivity. Also, the Cu-tape foil antenna on PEN substrate was evaluated for comparison. Its return loss is about -22 dB which is higher than that of printed Cu antennas on PI and PEN substrates, confirming that our printed Cu antennas are high sensitive. A future Internet of Things (IoT) society, especially in the field of wireless communication devices [38, 41], requires technologies for the mass production of high-performance flexible antennas. Our printed flexible antenna with high sensitivity can meet the demand and exhibit high potential as future wireless communication devices.

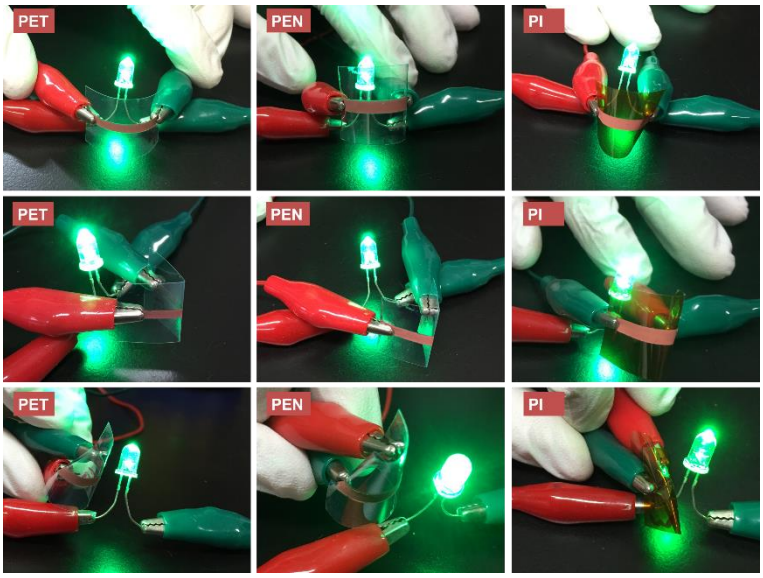

Figure 3.22 Photographs of the LED circuit with a 20 mm-long printed conductive pattern on PET, PEN, and PI substrates during the bending, folding, and twisting tests.

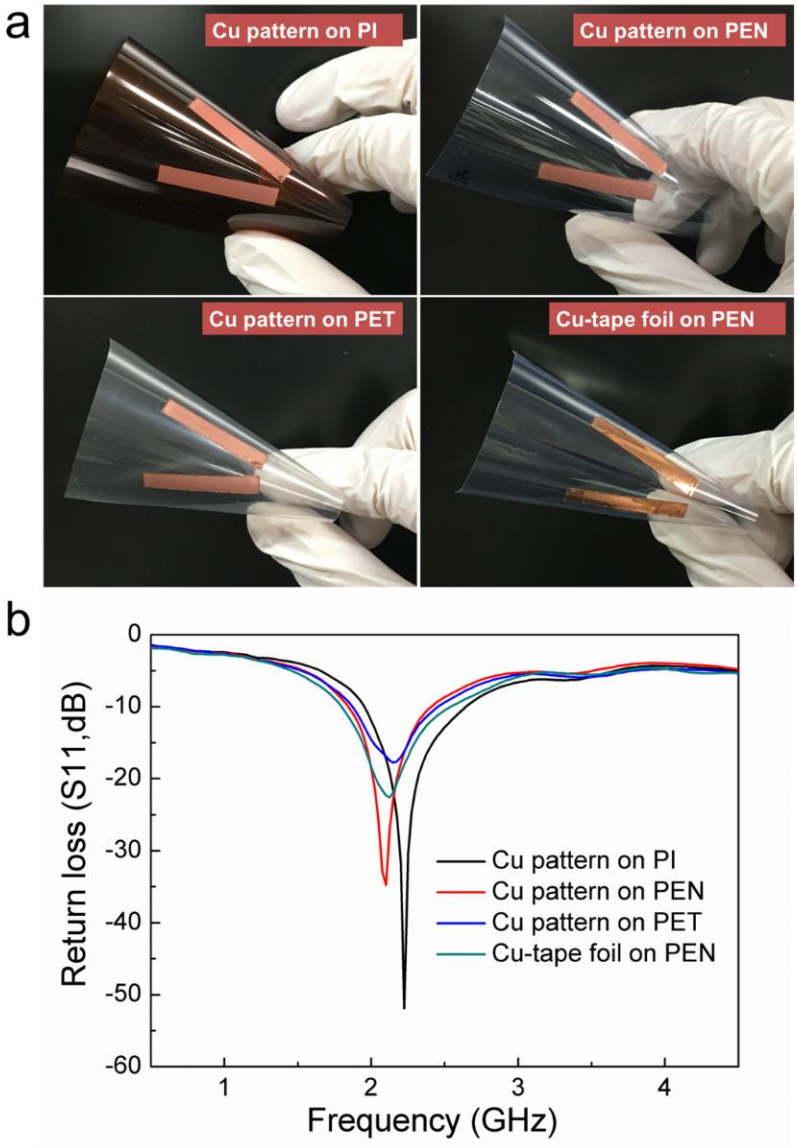

Figure 3.23 (a) Photographs of 30 mm-long dipole antennas and (b) their return losses.

3.8 Conclusion

In the chapter, IPL is successfully used to not only reinforce the bonding between submicron Cu particle and in-situ formed Cu nanoparticles but also improve the adhesion between films and substrates. Highly conductive and reliable Cu patterns are easily achieved on various flexible substrates by optimized low temperature heat welding and subsequent IPL sinter-reinforcement. The conductivity of printed Cu pattern is about 5.8-7.2×10^{-6} Ω·cm. It should be noted that compared with previous IPL sintering, the two-step sintering process in our work overcomes the weak-point of high IPL energy, enabling highly conductive Cu patterns

to be fabricated on inexpensive transparent heat-sensitive PET and PEN substrates. The bending fatigue test indicates that the sintered Cu patterns have high mechanical/electrical reliability due to the robust sintered Cu microstructure and strong adhesion between Cu patterns and substrates. The oxidation resistance test indicates the printed Cu patterns from submicron Cu particles with Cu complex exhibit excellent oxidation resistance and are superior to those from Cu nanoparticles. The degeneration of electrical conductivity of printed Cu patterns at high temperatures is attributed to not only the rapid oxidation of Cu to Cu_2O but also to the microstructure evolution, particularly the breaking of the necks joining adjacent particles. Their potential accessibility for flexible electronic device applications was demonstrated with a flexible and folding LED circuit and a flexible dipole antenna for wireless power transmission. It is believed that the use of big and low-cost Cu particles to create highly reliable and highly conductive Cu patterns by a suitable curing process would pave the way for ubiquitous smart, flexible and wearable devices.

References

1. Lim, H. S.; Kim, S. J.; Jang, H. W.; Lim, J. A., Intense pulsed light for split-second structural development of nanomaterials. *Journal of Materials Chemistry C* **2017,** *5* (29), 7142-7160.

2. Kim, H.-S.; Dhage, S. R.; Shim, D.-E.; Hahn, H. T., Intense pulsed light sintering of copper nanoink for printed electronics. *Applied Physics A* **2009,** *97* (4), 791.

3. Won-Suk, H.; Jae-Min, H.; Hak-Sung, K.; Yong-Won, S., Multi-pulsed white light sintering of printed Cu nanoinks. *Nanotechnology* **2011,** *22* (39), 395705.

4. Araki, T.; Sugahara, T.; Jiu, J.; Nagao, S.; Nogi, M.; Koga, H.; Uchida, H.; Shinozaki, K.; Suganuma, K., Cu salt ink formulation for printed electronics using photonic sintering. *Langmuir* **2013,** *29* (35), 11192-11197.

5. Chung, W.-H.; Hwang, H.-J.; Kim, H.-S., Flash light sintered copper precursor/nanoparticle pattern with high electrical conductivity and low porosity for printed electronics. *Thin Solid Films* **2015,** *580* (Supplement C), 61-70.

6. Rosen, Y. S.; Yakushenko, A.; Offenhäusser, A.; Magdassi, S., Self-reducing copper

precursor inks and photonic additive yield conductive patterns under intense pulsed light. *ACS Omega* **2017,** *2* (2), 573-581.

7. Wang, B.-Y.; Yoo, T.-H.; Song, Y.-W.; Lim, D.-S.; Oh, Y.-J., Cu Ion Ink for a Flexible substrate and highly conductive patterning by intensive pulsed light sintering. *ACS Applied Materials & Interfaces* **2013,** *5* (10), 4113-4119.

8. Li, W.; Cong, S.; Jiu, J.; Nagao, S.; Suganuma, K., Self-reducible copper inks composed of copper-amino complexes and preset submicron copper seeds for thick conductive patterns on a flexible substrate. *Journal of Materials Chemistry C* **2016,** *4* (37), 8802-8809.

9. Oh, S.-J.; Jo, Y.; Lee, E. J.; Lee, S. S.; Kang, Y. H.; Jeon, H.-J.; Cho, S. Y.; Park, J.-S.; Seo, Y.-H.; Ryu, B.-H.; Choi, Y.; Jeong, S., Ambient atmosphere-processable, printable Cu electrodes for flexible device applications: structural welding on a millisecond timescale of surface oxide-free Cu nanoparticles. *Nanoscale* **2015,** *7* (9), 3997-4004.

10. Rager, M. S.; Aytug, T.; Veith, G. M.; Joshi, P., Low-thermal-budget photonic processing of highly conductive Cu interconnects based on CuO nanoinks: potential for flexible printed Electronics. *ACS Applied Materials & Interfaces* **2016,** *8* (3), 2441-2448.

11. Jeon, E.-B.; Joo, S.-J.; Ahn, H.; Kim, H.-S., Two-step flash light sintering process for enhanced adhesion between copper complex ion/silane ink and a flexible substrate. *Thin Solid Films* **2016,** *603* (Supplement C), 382-390.

12. Kang, H.; Sowade, E.; Baumann, R. R., Direct intense pulsed light sintering of inkjet-printed copper oxide layers within six milliseconds. *ACS Applied Materials & Interfaces* **2014,** *6* (3), 1682-1687.

13. Ryu, J.; Kim, H.-S.; Hahn, H. T., Reactive sintering of copper nanoparticles using intense pulsed light for printed electronics. *Journal of Electronic Materials* **2011,** *40* (1), 42-50.

14. Dharmadasa, R.; Jha, M.; Amos, D. A.; Druffel, T., Room temperature synthesis of a copper Ink for the intense pulsed light sintering of conductive copper films. *ACS Applied Materials & Interfaces* **2013,** *5* (24), 13227-13234.

15. Paglia, F.; Vak, D.; van Embden, J.; Chesman, A. S. R.; Martucci, A.; Jasieniak, J. J.; Della Gaspera, E., Photonic sintering of copper through the controlled reduction of printed CuO nanocrystals. *ACS Applied Materials & Interfaces* **2015,** *7* (45), 25473-25478.

16. Oh, S.-J.; Kim, T. G.; Kim, S.-Y.; Jo, Y.; Lee, S. S.; Kim, K.; Ryu, B.-H.; Park, J.-U.; Choi, Y.; Jeong, S., Newly designed Cu/$Cu_{10}Sn_3$ core/shell nanoparticles for liquid phase-photonic sintered copper electrodes: large-area, low-cost transparent flexible electronics. *Chemistry of Materials* **2016,** *28* (13), 4714-4723.

17. Jeong, S.; Woo, K.; Kim, D.; Lim, S.; Kim, J. S.; Shin, H.; Xia, Y.; Moon, J., Controlling the thickness of the surface oxide layer on Cu nanoparticles for the fabrication of conductive structures by ink-jet printing. *Advanced Functional Materials* **2008,** *18* (5), 679-686.

18. Hyun-Jun, H.; Wan-Ho, C.; Hak-Sung, K., In situ monitoring of flash-light sintering of copper nanoparticle ink for printed electronics. *Nanotechnology* **2012,** *23* (48), 485205.

19. Sung-Jun, J.; Hyun-Jun, H.; Hak-Sung, K., Highly conductive copper nano/microparticles ink via flash light sintering for printed electronics. *Nanotechnology* **2014,** *25* (26), 265601.

20. Joo, S.-J.; Park, S.-H.; Moon, C.-J.; Kim, H.-S., A Highly reliable copper nanowire/nanoparticle ink pattern with high conductivity on flexible substrate prepared via a flash light-sintering technique. *ACS Applied Materials & Interfaces* **2015,** *7* (10), 5674-5684.

21. Niittynen, J.; Sowade, E.; Kang, H.; Baumann, R. R.; Mäntysalo, M., Comparison of laser and intense pulsed light sintering (IPL) for inkjet-printed copper nanoparticle layers. *Scientific Reports* **2015,** *5*, 8832.

22. Hwang, Y.-T.; Chung, W.-H.; Jang, Y.-R.; Kim, H.-S., Intensive plasmonic flash light sintering of copper nanoinks using a band-pass light filter for highly electrically conductive electrodes in printed electronics. *ACS Applied Materials & Interfaces* **2016,** *8* (13), 8591-8599.

23. Campbell, C. T.; Parker, S. C.; Starr, D. E., The effect of size-dependent nanoparticle energetics on catalyst sintering. *Science* **2002,** *298* (5594), 811-814.

24. Jang, S.; Seo, Y.; Choi, J.; Kim, T.; Cho, J.; Kim, S.; Kim, D., Sintering of inkjet printed copper nanoparticles for flexible electronics. *Scripta Materialia* **2010,** *62* (5), 258-261.

25. Tam, S. K.; Ng, K. M., High-concentration copper nanoparticles synthesis process for screen-printing conductive paste on flexible substrate. *Journal of Nanoparticle Research* **2015,** *17* (12), 466.

26. Solanki, A.; Gentile, P.; Calvo, V.; Rosaz, G.; Salem, B.; Aimez, V.; Drouin, D.; Pauc, N., Geometrical control of photocurrent in active Si nanowire devices. *Nano Energy* **2012,** *1* (5),

714-722.

27. Jo, Y.; Oh, S.-J.; Lee, S. S.; Seo, Y.-H.; Ryu, B.-H.; Moon, J.; Choi, Y.; Jeong, S., Extremely flexible, printable Ag conductive features on PET and paper substrates via continuous millisecond photonic sintering in a large area. *Journal of Materials Chemistry C* **2014,** *2* (45), 9746-9753.

28. Byoung-Joon, K.; Hae, A. S. S.; Ji-Hoon, L.; Young-Chang, J., Effect of cyclic outer and inner bending on the fatigue behavior of a multi-layer metal film on a polymer substrate. *Japanese Journal of Applied Physics* **2016,** *55* (6S3), 06JF01.

29. Jiu, J.; Wang, J.; Sugahara, T.; Nagao, S.; Nogi, M.; Koga, H.; Suganuma, K.; Hara, M.; Nakazawa, E.; Uchida, H., The effect of light and humidity on the stability of silver nanowire transparent electrodes. *RSC Advances* **2015,** *5* (35), 27657-27664.

30. Jiu, J.; Sugahara, T.; Nogi, M.; Araki, T.; Suganuma, K.; Uchida, H.; Shinozaki, K., High-intensity pulse light sintering of silver nanowire transparent films on polymer substrates: the effect of the thermal properties of substrates on the performance of silver films. *Nanoscale* **2013,** *5* (23), 11820-11828.

31. Lee, S.-K.; Hsu, H.-C.; Tuan, W.-H., Oxidation behavior of copper at a temperature below 300 °C and the methodology for passivation. *Materials Research* **2016,** *19*, 51-56.

32. Hai, H. T.; Takamura, H.; Koike, J., Oxidation behavior of Cu–Ag core–shell particles for solar cell applications. *Journal of Alloys and Compounds* **2013,** *564*, 71-77.

33. Figueiredo, V.; Elangovan, E.; Gonçalves, G.; Barquinha, P.; Pereira, L.; Franco, N.; Alves, E.; Martins, R.; Fortunato, E., Effect of post-annealing on the properties of copper oxide thin films obtained from the oxidation of evaporated metallic copper. *Applied Surface Science* **2008,** *254* (13), 3949-3954.

34. Yabuki, A.; Tanaka, S., Oxidation behavior of copper nanoparticles at low temperature. *Materials Research Bulletin* **2011,** *46* (12), 2323-2327.

35. Ul-Hamid, A., A microstructural study of preferential oxidation at the grain boundaries of Ni–Cr alloys. *Oxidation of Metals* **2002,** *57* (3), 217-230.

36. Schmidt-Whitley, R. D.; Martinez-Clemente, M.; Revcolevschi, A., Growth and microstructural control of single crystal cuprous oxide Cu2O. *Journal of Crystal Growth* **1974,**

23 (2), 113-120.

37. Liu, X.; Zhou, S.; Nishikawa, H., Thermal stability of low-temperature sintered joint using Sn-coated Cu particles during isothermal aging at 250 °C. *Journal of Materials Science: Materials in Electronics* **2017,** *28* (17), 12606-12616.

38. Joohee, K.; Mi-Sun, L.; Sangbin, J.; Minji, K.; Sungwon, K.; Kukjoo, K.; Franklin, B.; You, H. S.; Jang-Ung, P., Highly transparent and stretchable field-effect transistor sensors using graphene–nanowire hybrid nanostructures. *Advanced Materials* **2015,** *27* (21), 3292-3297.

39. Alexander, K.; Shlomo, M., Conductive nanomaterials for printed electronics. *Small* **2014,** *10* (17), 3515-3535.

40. Komoda, N.; Nogi, M.; Suganuma, K.; Kohno, K.; Akiyama, Y.; Otsuka, K., Printed silver nanowire antennas with low signal loss at high-frequency radio. *Nanoscale* **2012,** *4* (10), 3148-3153.

41. Koga, H.; Inui, T.; Miyamoto, I.; Sekiguchi, T.; Nogi, M.; Suganuma, K., A high-sensitivity printed antenna prepared by rapid low-temperature sintering of silver ink. *RSC Advances* **2016,** *6* (87), 84363-84368.

42. M., A. A.; K., K. H.; E., B. M., Design of compact directive ultra wideband antipodal antenna. *Microwave and Optical Technology Letters* **2006,** *48* (12), 2448-2450.

43. Ghorbani, K.; Waterhouse, R. B., Dual polarized wide-band aperture stacked patch antennas. *IEEE Transactions on Antennas and Propagation* **2004,** *52* (8), 2171-2175.

Chapter 4

Highly stable Cu-Ag alloy patterns fabricated form Cu particle/Ag complex inks

4.1 Introduction

Using micron or submicron Cu particles instead of Cu nanoparticles is an approach that can improve the oxidation resistance of sintered Cu patterns, but these larger particles are difficult to sinter at low temperatures, and they still oxidize eventually because of the intrinsic low oxidation resistance of Cu materials [1, 2]. Coating a non-oxidizable graphene shell or a Ag shell onto Cu nanoparticles can improve the oxidation resistance of synthesized Cu nanoparticles. However, the addition of graphene destroys the purity of the metallic Cu pattern and results in a high resistivity—about 5 orders of magnitude higher than that of bulk Cu [3]; the Ag shell still cannot protect Cu from oxidation over the long term because Ag shell is easily broken by the simultaneous coalescence of the Cu cores and ripening of the Ag shell [4, 5].

On the other hand, alloying Cu with Ti, Mg, Al, Pd, Ag, Ni, Cr, or Zr can increase the oxidation resistance of Cu by several orders of magnitude [6-9]. This is attributed to the fact that alloying elements in Cu can act as dopants and change the concentration of point defects, which govern the mobility of Cu ions and reduce the contact with oxygen [7]. Among Cu-based alloys, Cu-Ag alloy is regarded as the best solution to enhance the oxidation resistance of sintered Cu patterns because of the large improvement in their oxidation resistance along with only a slight reduction in the electrical conductivity [10]. Because of the limited solid solubilities of the Cu-Ag system under equilibrium conditions, many non-equilibrium processing methods have been devised to prepare Cu-Ag alloys. For example, quenching a molten Cu-Ag mixture at a high cooling rate can produce a Cu-Ag alloy by preventing the normal process of nucleation and growth of equilibrium phases [11]; a Cu-Ag alloy layer can be realized by rapid mutual dissolution of Cu and Ag atoms at their interface with ion beam bombardment [12]; and mechanical alloying can produce Cu-Ag alloy particles by the repeated cold welding and fracture of Cu-Ag particles [13, 14]. A vacuum co-deposition method has also been used to create a Cu-Ag alloy layer by inducing the nucleation and growth [15-17]; In addition, chemical co-reduction of a Cu salt and a Ag salt under a strong reductant can create a Cu-Ag nanoalloy [18-20]. However, these methods demand high temperatures, high pressures,

long processing times, and/or high vacuum conditions, and sometimes cause environmental pollution (toxic chemicals). None of them can feasibly meet the requirements of printed electronics under low temperature in an air atmosphere.

In this chapter, we develop Cu particle/Ag complex inks and realize the highly stable Cu-Ag alloy patterns on flexible substrates at a low temperature in the air by using the two-step sintering method. The fabrication process of Cu-Ag alloy patterns is studied in detail. Especially, the alloying process is discussed and a possible alloying mechanism is proposed. In addition, the long-term stabilities of Cu-Ag alloy patterns including high temperature oxidation resistance and bending fatigue property are studied. Results show that fabricated Cu-Ag alloy electrodes have ultrahigh oxidation resistance that remains stable in air at 180 and 200 °C and show great potential for practical use in the fabrication of highly reliable and cost-effective printed electronic devices.

4.2 Experimental

4.2.1 Materials

Silver nitrate ($AgNO_3$), sulfuric acid (H_2SO_4), diethyl ether ($C_4H_{10}O$), and diethanolamine ($C_4H_{11}NO_2$) were purchased form Wako Pure Chemical Industries, Ltd. Ethyl-2-methylacetoacetate ($C_7H_{12}O_3$) was purchased from Tokyo Chemical Industry Co., Ltd. Sodium hydroxide (NaOH), 2-amino-2-methyl-1-propanol ($C_4H_{11}NO$), and isopropyl alcohol (C_3H_8O) were purchased form Nacalai Tesque, Inc. Submicron Cu particles with an average size of 350 nm were provided by Mitsui Mining & Smelting Co., Ltd. Polyimide (PI) substrate with a thickness of 77.5 μm was purchased from Du Pont Toray Co., Ltd.

4.2.2 Synthesis of Ag (I) β-ketocarboxylate

Ag (I) β-ketocarboxylate was synthesized as described previously [21]. Briefly, 1.5 g of sodium hydroxide was dissolved in 15 g of deionized water, and then 4.7 g of ethyl-2-methylacetoacetate was added drop-wise to the resulting solution at 60 °C with a stirring speed of 200 rpm. After 60 min, 28.5 g of diethyl ether ($C_4H_{10}O$) was added to the above solution, and then the obtained mixture was cooled in an ice bath, followed by the addition of 1.76 g of

sulfuric acid. After about 3 min, an obvious stratification phenomenon occurred in the mixture and the supernatant layer was saved in a beaker. Next, 3.31g of diethanolamine dissolved in 5 g of deionized water was added to the beaker. After about 3 min, the stratification phenomenon occurred again in the baker and the supernatant layer was removed. Finally, 4.84 g of silver nitrate dissolved in 30 g of deionized water was added drop-wise to the beaker, and the white Ag (I) β-ketocarboxylate precipitate was created. The Ag (I) β-ketocarboxylate was filtered and washed with water and with isopropyl alcohol, and then dried in vacuum for 180 min.

4.2.3 Preparation of Cu particle/Ag complex inks, screen-printing, and sintering process

The Cu particle/Ag complex inks were prepared as follows: First, the Ag (I) β-ketocarboxylate was added to 2-ethylhexylamine solvent with a fixed molar ratio of 1:2 and stirred for 5 min at room temperature to ensure the complete formation of the Ag complex. Then, submicron Cu particles were introduced to the Ag-amino complex at different mass ratios, and alcohol solvent was also introduced to adjust the metal load of the Cu-Ag hybrid inks to 35.9 wt%. Finally, the ink was mixed by a hybrid mixer (HM-500) for 20 min to obtain homogeneous Cu particle/Ag complex ink. To facilitate the presentation, we denominate pure Cu, Cu-5Ag, Cu-13Ag, Cu-20Ag, and Cu-30Ag, which represent the Ag content in the obtained Cu-Ag patterns are 0 wt.%, 5 wt.%, 13 wt.%, 20 wt.%, and 30 wt.% respectively.

PI film was used as the flexible substrate in this work. To remove any contamination from the surface, the PI was cleaned in ethanol and distilled water under an ultrasonicator for 10 min. Then the Cu particle/Ag complex inks were printed onto the PI substrates using a screen-printing method. The thickness of the screen is 50 μm. The printed Cu particle/Ag complex inks were sintered by a simple two-step method under an air atmosphere; the printed inks were heated to a temperature of 140 °C for 10 min followed by intense pulsed light (IPL) sintering. The information about this IPL system can be found in chapter 3. In this study, the duration time was fixed at 2100 μs and the electrical voltage was changed from 220 V to 340 V to supply optical energies ranging from 1400 mJ/cm^2 to 4900 mJ/cm^2.

4.2.4 Characterization methods

The thermal behaviors of the prepared Cu particle/Ag complex inks were investigated by thermogravimetric-differential thermal analysis (TGA-DTA, NETZSCH) at a heating rate of 10 °C/min. The temperature evolution on the surface of the printed Cu-Ag patterns during IPL sintering was evaluated by the simulation software installed in PulseForge 3300 (Novacentrix, Austin, TX, USA). The surface and cross-section of sintered Cu-Ag patterns were characterized by optical microscopy (OM) and field-emission scanning electron microscopy (FESEM, Hitachi SU8020, Hitachi High Technologies America, Inc.) A focused ion beam (FIB, FB2100, Hitachi) was used to cut the cross-section samples with a diameter of 80 μm and standard current of 0.30-0.60 nA. Transmission electron microscopy (TEM, JEOL-2100, JEOL Ltd.), together with elemental mapping, was used to further analyze the microstructure and detailed composition of the resulting Cu-Ag alloys. Crystal structures of sintered Cu-Ag patterns were determined by an X-ray diffractometer (XRD, Rigaku) using Cu Kα radiation (λ = 0.15418 nm). Based on the X-ray diffraction patterns, the solid solubility of Cu into Ag, and Ag into Cu were estimated by the Vegard formula, as shown in equation 4.1 [22].

$$x = \frac{a-a_1}{a_2-a_1} \times 100\ \% \tag{4.1}$$

Where a_1 and a_2 are the lattice parameters of the pure solvent element and solute element, respectively; a is the lattice parameter of the solution alloy; and x is the solid solubility. The electrical resistivity was measured by a four-point-probe analyzer (LorestaGP T610, Mitsubishi Chemical Analytech Co. Ltd.). The long-term stability of the Cu-Ag alloy patterns was evaluated by exploring them under high temperatures of 180 °C and 200 °C in air. The flexibility of printed Cu-Ag alloy patterns was evaluated by adhesion test and bending fatigue test. The adhesion test was performed based on a tape peeling test. The printed Cu pattern was cross-cut into individual squares with about 0.5 mm width. Then, 3M tape was pressed on top of the Cu pattern and then manually torn off. The method of bending fatigue test has been described in section 3.2.3.

4.3 Fabrication of Cu-Ag alloy patterns

Figure 4.1 show the schematic diagram of directly printing Cu-Ag alloy patterns. Firstly, the Cu particle/Ag complex inks were printed onto the PI substrates using a screen-printing

method (**Figure 4.1a**). Under a low pre-curing temperature of 140 °C, the printed ink can transform in situ into a special Cu-Ag nanoparticle core-shell structure (**Figure 4.1b**), which is the prerequisite for the formation of Cu-Ag alloy. After that, rapid mutual diffusion between the Cu core and the Ag nanoparticle shell can be triggered by supplying the necessary energy [11, 12, 14]. Considering the light absorption of metal particles, especially nanoparticles, we use an IPL sintering technology to drive the rapid diffusion between the Cu core and the Ag nanoparticle shell, and achieve a Cu-Ag alloy on flexible substrates under an air atmosphere **(Figure 4.1c**).

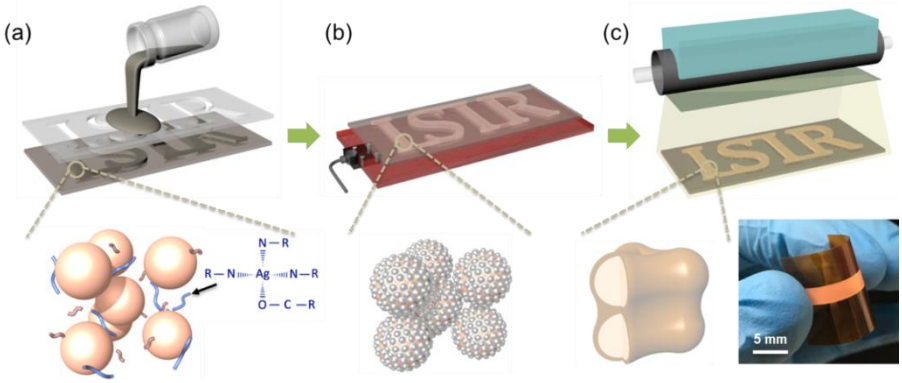

Figure 4.1 Schematic diagram: (a) screen-printing and fabrication of Cu-Ag alloy patterns or circuits by (b) low-temperature pre-curing and (c) rapid IPL sintering under an air atmosphere. The inset in the lower right corner is a photograph of the flexible Cu-Ag alloy pattern on a polyimide (PI) substrate.

Ion beam bombardment and mechanical alloying are possible methods that can be employed to form Cu-Ag alloys, but they are time-consuming and laborious for printed electronics. If a thin Ag nanoparticle shell can be deposited on the surface of a Cu core, applying suitable energy will drive the rapid diffusion between Cu and Ag to ensure the formation of Cu-Ag alloy. Hence, the first-step is to create a Ag nanoparticle shell on a Cu core. The in situ thermal decomposition of a Ag salt to create Ag metallic nanoparticles is a simple method. Normally, the thermal decomposition of Ag salt into metallic Ag is a continuous and random nucleation process with formation of both large and small Ag particles [23, 24]. If some seeds

exist, such as the submicron Cu particles in this work, the nucleation of metallic Ag occurs preferentially on the surface of these Cu particles; this is called heterogeneous nucleation [25]. This process will induce the uniform deposition of a Ag nanoparticle shell on the existing Cu particles because of the low interface energy between the Ag-nanoparticle layer and the Cu-core particles [24, 25].

Moreover, the chemical properties, especially the decomposition temperature of the Ag salt, determine the application range and the properties of obtained metallic Ag. Importantly, in the current study, the decomposition temperature of the chosen Ag salt should be low enough, and the reaction should not cause significant organic residues that would interfere subsequent sintering and application in printed electronics. Therefore, a Ag-amino complex made from Ag (I) β-ketocarboxylate and 2-ethylhexylamine was selected. The decomposition of the Ag (I) β-ketocarboxylate takes place according to the following reaction [21].

$$CH_3COCH(CH_3)COOAg \rightarrow Ag\ (s) + CO_2(g) + CH_3COCH_2CH_3(g)$$

Based on the results of thermal gravimetric analysis and differential thermal analysis (TGA-DTA) and X-ray diffraction (XRD) (**Figure 4.2**), the Ag complex could be decomposed and reacted to pure Ag without significant residues. Moreover, in the XRD pattern of pure Cu ink after 10 min at 140 °C (**Figure 4.3a**), only the peaks of Cu are found; while in the XRD results of Cu-Ag hybrid inks, the peaks of Ag appear. The relative peak intensities of Ag are increased with the increase of Ag complex, which confirms that the Ag complex in the hybrid ink has been decomposed and reduced to pure Ag after 10 min at 140 °C.

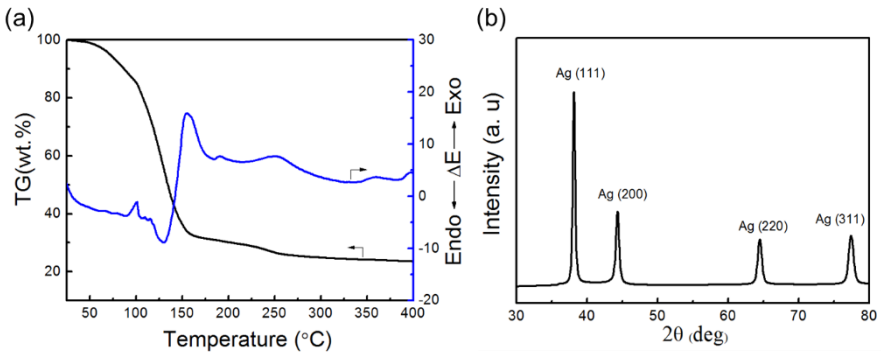

Figure 4.2 (a) TG-DTA plots of Ag complex under air atmosphere and (b) XRD pattern of received Ag.

The scanning electron microscope (SEM) images provide visual evidence of Cu-Ag nanoparticle core-shell structures. **Figure 4.3b** shows the microstructure of pure Cu ink after 10 min at 140 °C, where the surfaces of Cu particles remain smooth, and the interfaces between every particle are clear. When the Ag complex is added, the surfaces of Cu particles are uniformly coated with Ag nanoparticles (**Figure 4.3c-f**). The size range of the Ag nanoparticles is small—from 5 nm to 80 nm—and the average size is about 20 nm. With low Ag content, the surface of each Cu particle is partly coated with Ag nanoparticles (**Figure 4.3c-d**). When the Ag content increases to 20 wt.%, the in-situ-formed Ag nanoparticles can almost cover the entire surfaces of the Cu particles (**Figure 4.3e**). When excessive Ag complex is added, the generated Ag nanoparticles become dense, and in some areas these Ag nanoparticles have become connected to form a continuous layer (**Figure 4.3f**).

On the other hand, these in situ Ag nanoparticles have bonded the adjacent Cu particles to form some weak pathways. The resistivities of the patterns prepared from Cu-5Ag ink, Cu-13Ag ink, Cu-20Ag ink, and Cu-30Ag ink after 10 min at 140 °C are as high as 'nonconducting', 10^{0} Ω·cm, 10^{-3} Ω·cm, and 4×10^{-4} Ω·cm, respectively. Therefore, they need further sintering under a higher temperature or for a longer time. However, it is difficult to achieve high-conductivity Cu-Ag patterns by traditional sintering methods because of the dilemma that the efficient sintering of Ag particles needs a certain content of oxygen [26] while sintering of Cu must avoid the existence of oxygen [27]. Furthermore, a long time at high temperature results in a structural and phase separation of the Cu-Ag core-shell structures [4, 5]; thus, Cu-Ag alloy cannot be obtained. Using a rapid sintering method such as photonic sintering in air should be a possible method to solve the above problems. In contrast to the conventional thermal sintering technique in which the sample is exposed to high temperatures for a long time, the photonic sintering utilizes the light absorption of metal particles and the plasma effects to realize rapid sintering in only a few microseconds in an air atmosphere [28, 29]. Because of the very short treatment time, not only will the separation of Cu-Ag core-shell structures be prevented, but also the oxidation of Cu will be reduced. Moreover, the short time-exposure also avoids damaging the substrates [29].

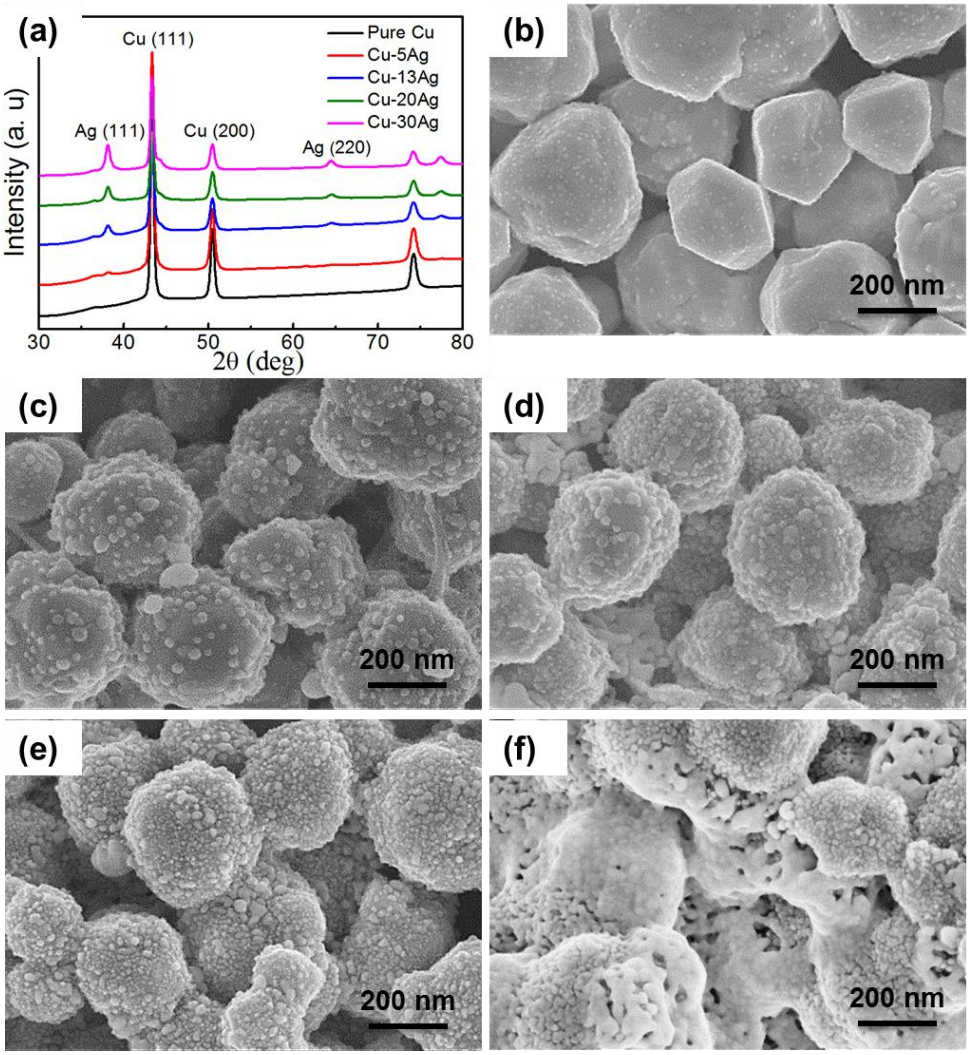

Figure 4.3 Crystal phase and microstructure of printed inks after 10 min at 140 °C under an air atmosphere. (a) XRD patterns of printed inks; SEM images of (b) Pure Cu ink; (c) Cu-5Ag ink; (d) Cu-13Ag ink; (e) Cu-20Ag ink; and (f) Cu-30Ag ink.

Figure 4.4a shows the resistivity evolution of printed Cu-Ag patterns on PI substrates after IPL sintering using different input energies. Printed pure Cu ink, Cu-5Ag ink, and Cu-13Ag ink endure the maximum energies of 2700 mJ/cm^2, 3400 mJ/cm^2, and 4100 mJ/cm^2, and achieve resistivities of 2.6×10^{-5} Ω·cm, 7.4×10^{-6} Ω·cm, and 5.4×10^{-6} Ω·cm, respectively. When the supplied energy exceeds the energy that can be endured, the resistivity of the sintered patterns begins to increase because the excessive energy during a short time may cause a huge thermal shock and make the metal particles fall off the substrate (**Figure 4.5a-b**). On the other hand, printed Cu-20Ag ink and Cu-30Ag ink can endure a higher energy of 4900 mJ/cm^2 and achieve

the very low resistivities of 3.4×10^{-6} Ω·cm and 4.2×10^{-6} Ω·cm, respectively, which is only two or three times that of bulk Cu. It should be noted that the printed Cu-Ag hybrid inks can endure a higher energy than that for printed pure Cu ink, which may relate to the pre-bonding between Cu particles by in-situ-formed Ag nanoparticles, as shown in Figure 4.3c-f. The in-situ-formed Ag nanoparticles help bond the Cu particles, and enough connection between these Cu particles can enable them to endure high energies/thermal shock while retaining a good surface (**Figure 4.5c-d**). Therefore, the patterns prepared from Cu-Ag hybrid inks under IPL sintering can possess a lower resistivity than those prepared from pure Cu ink.

The microstructural transformation of printed Cu-Ag patterns after IPL sintering was investigated to support their resistivity evolution. Under a low energy of 1800 mJ/cm^2, metallic Ag nanoparticles have begun to fuse with Cu particles, and local connection/sintering between adjacent particles is clearly observed, although these large Cu particles still retain a globose morphology (**Figure 4.4b**). The cross-section image confirms that a short-range network structure has occurred with some clear pores (**Figure 4.4c**). Upon increasing the energy to 2700 mJ/cm^2, the Ag nanoparticles and Cu particles are fused into an integral whole and obvious necking growth has begun to form large grains (**Figure 4.4d**); meanwhile, an evolved dense microstructure is formed at the bottom of the pattern with a few pores (**Figure 4.4e**), which corresponds closely to the resistivity evolution of printed Cu-Ag patterns in Figure 4.4a. When the supplied energy increases to 4100 mJ/cm^2, the surface of the printed Cu-Ag pattern become very dense without any pores (**Figure 4.4f**). The cross-section image also gives a very dense and bulk-like microstructure without pores (**Figure 4.4g**), which corresponds to the low resistivity of 3.4×10^{-6} Ω·cm shown in Figure 4.4a. The dense, fused structure also confirms the feasibility of IPL sintering of Cu-Ag patterns even within the short time of 2.1 ms. During IPL sintering, the light energy is selectively absorbed by metal particles, especially Ag nanoparticles, because these nanoparticles have a high surface/volume ratio. This is expected to quickly increase the temperature, which will induce surface melting and atomic diffusion to realize the rapid necking growth between adjacent particles depending on light intensity [28, 30, 31]. It is known that the sintering of submicron Cu particles is difficult. However, in the present work, the in-situ-formed Ag nanoparticles adsorb light energy by a self-heating effect; and, thanks to

the high thermal conductivity of Ag and Cu, the heat can be transferred rapidly to the Cu core. This means that the Ag nanoparticle shell can play the role of a nano-welder to assist in the sintering of adjacent submicron Cu particles [1, 32]; which in turn also explains why the patterns prepared from Cu-Ag hybrid inks can possess a lower resistivity than those prepared from pure Cu ink.

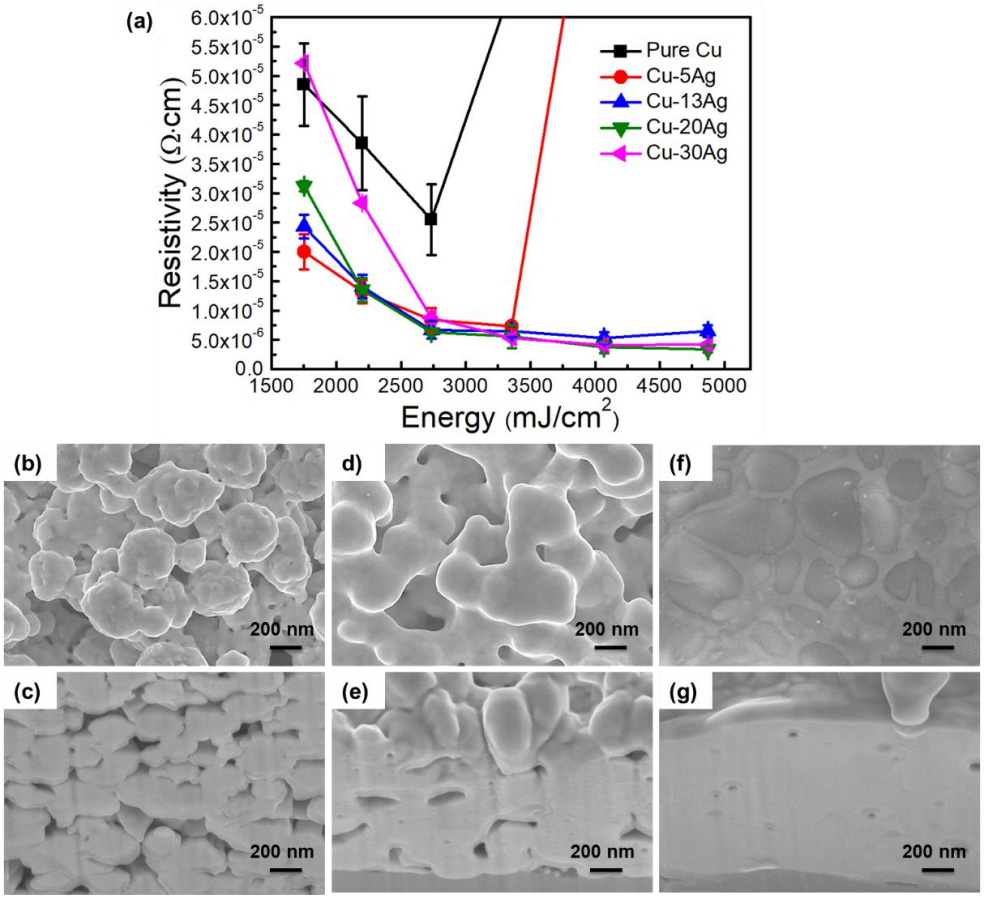

Figure 4.4 (a) Resistivity evolution of a printed pure Cu pattern and Cu-Ag patterns as function of supplied energy of IPL sintering (Number of pulses: 1; On-time: 2.1 ms). (b-g) Microstructure of printed Cu-20Ag inks after IPL sintering using energies of 1800 mJ/cm^2, 2700 mJ/cm^2, and 4100 mJ/cm^2, respectively. Top-view images are shown in b, d, and f; and the corresponding cross sections are shown in c, e, and g. Before the IPL sintering, all the printed patterns had been heated at 140 °C for 10 min under an air atmosphere.

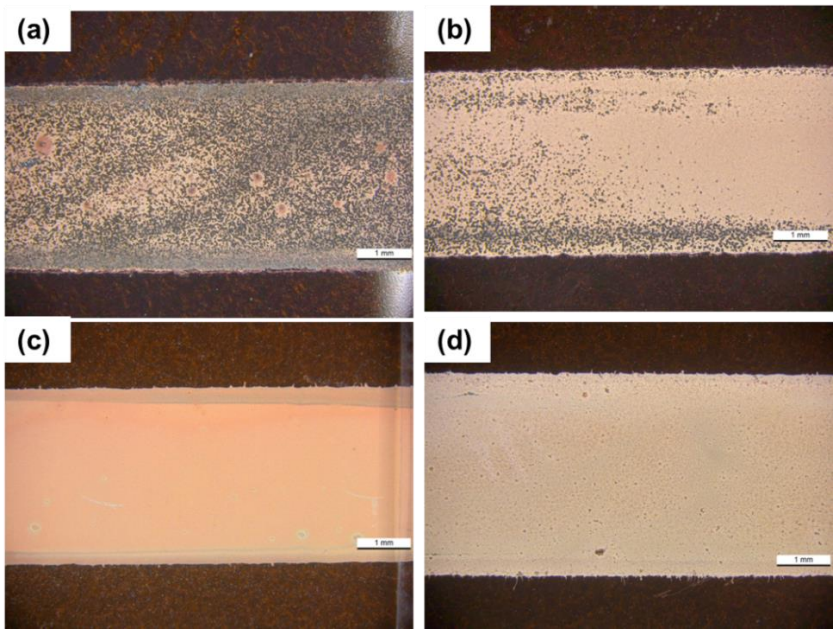

Figure 4.5. Photographs of printed patterns after IPL sintering with different energies. (a) Printed patterns prepared from pure Cu ink after IPL sintering using the energy of 3400 mJ/cm^2; (b) Printed pattern prepared from Cu-5Ag ink after IPL sintering using the energy of 4100 mJ/cm^2; (c) Printed pattern prepared from Cu-20Ag ink after IPL sintering using the energy of 3400 mJ/cm^2; (d) Printed pattern prepared from Cu-20Ag ink after IPL sintering using the energy of 4900 mJ/cm^2.

The crystal phases in the sintered Cu-Ag patterns were further investigated by XRD. **Figure 4.6**a shows the XRD patterns of sintered Cu-Ag patterns after IPL sintering with different energies. Only Cu and Ag peaks are found in the XRD patterns, which indicates that the obtained patterns have high metallic purity without any oxides. Specially, an interesting point should be noted that the Cu and Ag peaks have shifted significantly compared to those of pure metals when the supplied energy of IPL sintering was greater than 3400 mJ/cm^2. In order to ascertain that the peak shifts are not due to residual stress in the flexible patterns, a pure Ag pattern and a pure Cu pattern were also prepared using the same technique with a supplied energy of 4100 mJ/cm^2, and no shifted peaks can be found in the results (**Figure 4.7**). The formation of Cu-Ag alloy may be a suitable and reasonable explanation because the peak shift in the XRD patterns is a feature frequently observed for solution alloy materials [33].

For more details, **Table 4.1** collects the 2θ positions and interplanar spacing of Ag(1 1 1), Ag(2 0 0), Ag(2 2 0), Cu(1 1 1), Cu(2 0 0), and Cu(2 2 0) diffraction peaks in the Cu-Ag patterns after IPL sintering. **Figure 4.6b** and **Figure 4.6c** show the 2θ positions and interplanar spacing of Ag(1 1 1) and Cu(1 1 1) diffraction peaks, respectively, after IPL sintering. With increasing energy of IPL sintering, the Ag(111) peak (38.16°) shifts to the right-hand side (38.89°), while the Cu(111) peak (43.34°) shifts to the left-hand side (43.02°) (Figure 4.6b). At the same time, the interplanar spacing of the Ag(111) direction (2.3511 Å) decreases to 2.3145 Å, but that of the Cu(111) direction (2.0862 Å) increases to 2.1007 Å (Figure 4c). It should be noted that the shifted directions of the Ag(1 1 1) and Cu(1 1 1) peaks and the variation trends of their interplanar spacing are opposite. These results are related to the different atomic radii of Cu (0.14 nm) and Ag (0.17 nm). On the basis of the Hume-Rothery rules, elements Cu and Ag can form substitutional binary alloys [33]. Since the Cu atom is smaller than the Ag atom, the dissolution of Cu atoms into a Ag matrix causes lattice contraction while the dissolution of Ag atoms into a Cu matrix cause lattice expansion (**Figure 4.8**). This indicates that the present Cu-Ag alloy is a mixture of Cu atoms in a Ag matrix and Ag atoms in a Cu matrix.

Moreover, the solid solubilities of Cu in Ag and Ag in Cu were estimated by using the Vegard formula [22], together with the average lattice constants obtained from the Ag(111), (200), and (220) diffraction peaks and the Cu(111), (200), and (220) diffraction peaks. As shown in **Figure 4.6d**, dissolution of Cu into Ag occurs at a low energy of photonic sintering (1400 mJ/cm^2), and with the increase of energy, the solubility of Cu in Ag increases rapidly and finally achieves a saturation value of about 14.78 at.%. On the other hand, the Ag is essentially insoluble in Cu until the applied energy exceeds 2700 mJ/cm^2. The highest solubility of Ag in Cu, 4.75 at. %, is achieved when the energy increases to 4900 mJ/cm^2; this might be related to the sizes of Cu and Ag atoms. On the other hand, the enthalpy of dissolving Cu into Ag is reported to be 0.25 eV per atom, and the enthalpy of dissolving Ag into Cu is 0.39 eV per atom [34]. The smaller enthalpy of dissolving Cu into Ag crystals also explains why the dissolution of Cu atoms into Ag is easier, and the solubility of Cu into Ag is greater than that of Ag into Cu under IPL sintering with the same energy.

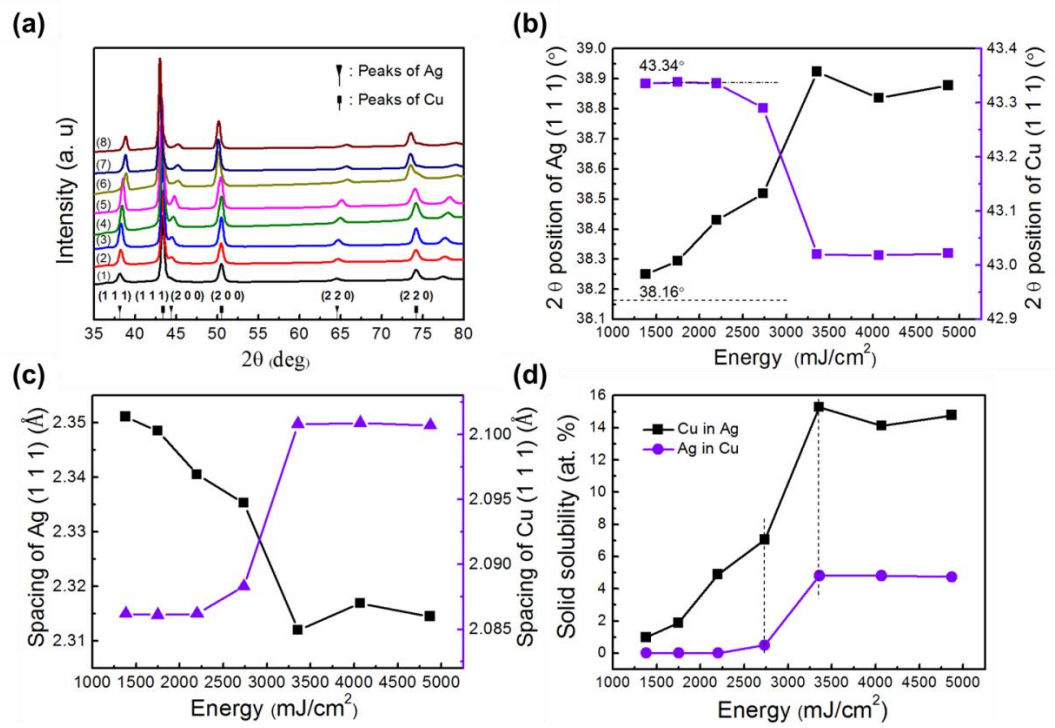

Figure 4.6 (a) XRD patterns of Cu-20Ag ink after IPL sintering with energies of (1) 0 mJ/cm^2, (2) 1400 mJ/cm^2, (3) 1800 mJ/cm^2, (4) 2200 mJ/cm^2, (5) 2700 mJ/cm^2, (6) 3400 mJ/cm^2, (7) 4100 mJ/cm^2, and (8) 4900 mJ/cm^2. Before the IPL sintering, all the samples had been heated at 140 °C for 10 min in air. (b) 2θ positions of Ag(111) and Cu(111) diffraction peaks; (c) Spacing of Ag(111) and Cu(111) diffraction directions; (d) Theoretical calculated solid solubility of Cu in Ag, and Ag in Cu.

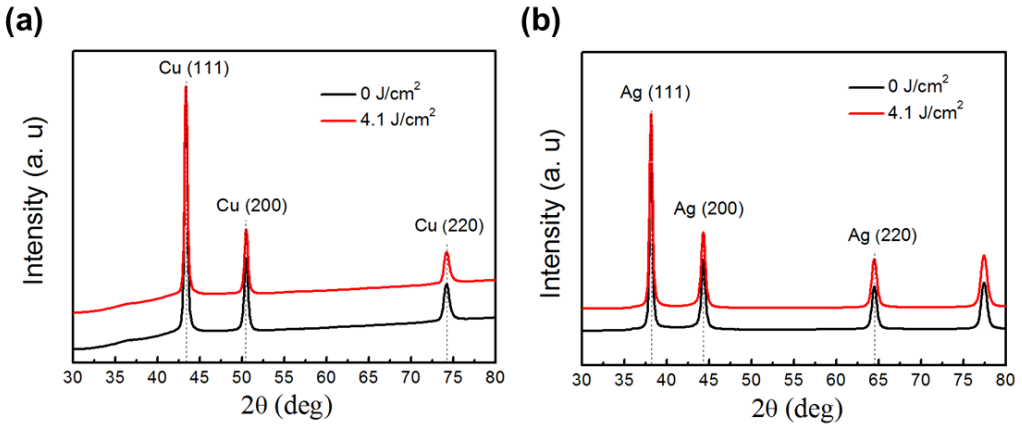

Figure 4.7 XRD patterns of (a) pure Cu and (b) pure Ag after IPL sintering using the energy of 4100 mJ/cm^2.

Table 4.1 2θ positions and interplanar spacing (d) of Ag(1 1 1), Ag(2 0 0), Ag(2 2 0), Cu(1 1 1), Cu(2 0 0) and Cu(2 2 0) diffraction peaks. The samples prepared from IPL sintering with different energies.

	Ag(1 1 1)		Ag(2 0 0)		Ag(2 2 0)	
Energy (mJ/cm^2)	2θ (°)	d (Å)	2θ (°)	d (Å)	2θ(°)	d (Å)
0	38.160	2.3564	44.402	2.0385	64.530	1.4429
1400	38.250	2.3511	44.423	2.0377	64.665	1.4402
1800	38.294	2.3485	44.46	2.0360	64.754	1.4385
2200	38.43	2.3405	44.644	2.0281	64.980	1.4340
2700	38.518	2.3353	44.776	2.0224	65.159	1.4305
3400	38.923	2.312	45.227	2.0032	65.835	1.4174
4100	38.836	2.3169	45.225	2.0034	65.701	1.4200
4900	38.878	2.3145	45.226	2.0033	65.789	1.4183
	Cu(1 1 1)		Cu(2 0 0)		Cu(2 2 0)	
Energy (mJ/cm^2)	2θ (°)	d (Å)	2θ (°)	d (Å)	2θ (°)	d (Å)
0	43.377	2.0843	50.490	1.8061	74.205	1.2769
1400	43.335	2.0862	50.489	1.8061	74.160	1.2776
1800	43.338	2.0861	50.490	1.8061	74.200	1.2769
2200	43.336	2.0862	50.490	1.8061	74.204	1.2769
2700	43.290	2.0883	50.444	1.8076	74.070	1.2789
3400	43.020	2.1008	50.131	1.8182	73.530	1.2869
4100	43.018	2.1009	50.131	1.8182	73.529	1.2870
4900	43.022	2.1007	50.175	1.8167	73.531	1.2869

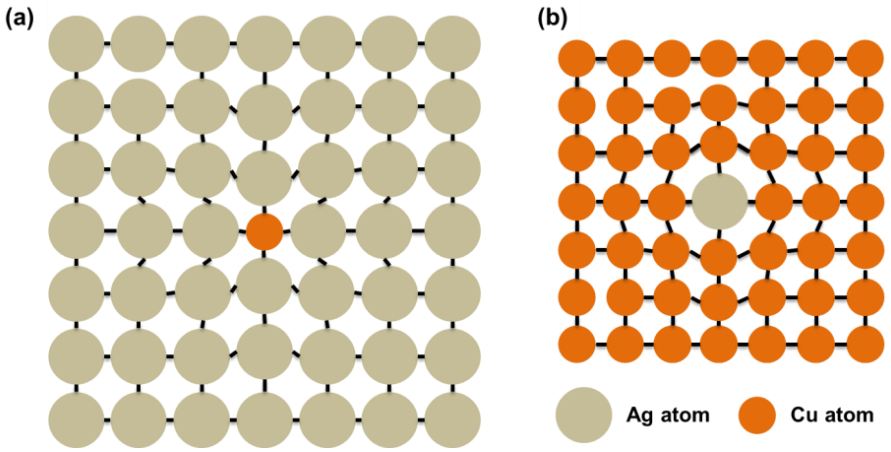

Figure 4.8 Schematic illustrating how the lattice is strained by the addition of Cu atom in Ag matrix and Ag atom in Cu matrix.

The formation and composition of the Cu-Ag alloy was further confirmed by scanning transmission electron microscopy (STEM). **Figure 4.9a** shows the STEM image of a Cu-Ag alloy pattern prepared from Cu-20Ag ink, where two contrast areas (bright area and dark area) are clearly seen, indicating two different phases. Elemental distribution analysis gives the detailed information (**Figure 4.9b-c**). The dark area corresponds to the Cu-rich phase, and the bright area is the Ag-rich phase. This confirms that Cu and Ag elements have diffused into each other to form solid solutions and to form core-shell structures consisting of Cu-rich cores and Ag-rich shells. Moreover, the detailed composition of the Cu-rich phase was determined by analyzing more than 20 spots, such as spots (A-C) marked in Figure 4.9a. All the spots are the Cu-rich phase, showing a high Cu content from 95.24 to 95.60 at.% and a weak Ag content from 4.40 to 4.76 at.%; their average composition is 95.41 at.% of Cu and 4.59 at.% of Ag (**Table 2**), which is consistent with the theoretical calculations based on XRD patterns (Figure 4.6d).

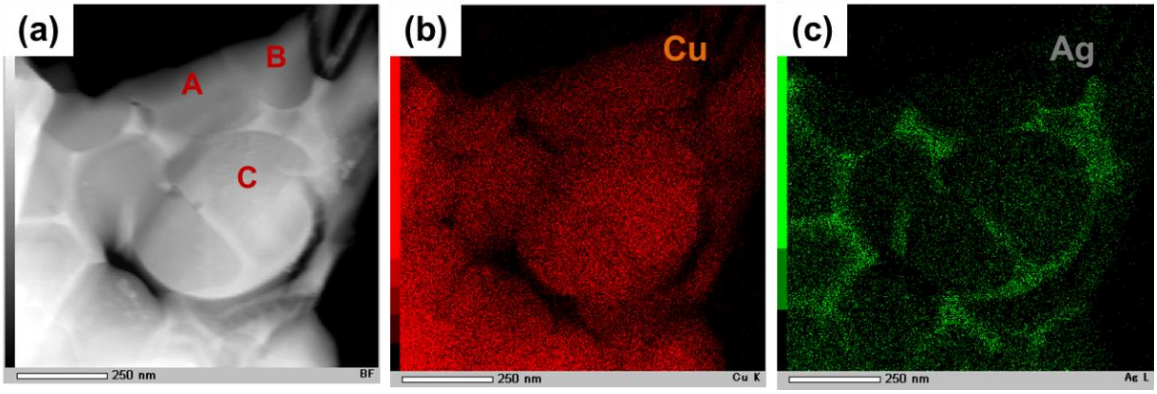

Figure 4.9 (a) STEM image of Cu-Ag alloy pattern prepared from Cu-20Ag ink and corresponding TEM mapping images of (b) elemental Cu and (c) elemental Ag. The sample was heated at 140 °C for 10 min, followed by the IPL sintering using an energy of 4900 mJ/cm^2.

Table 4.2 The detailed information of marked points in Figure 4.9a.

Point	Cu content (at %)	Average (at %)	Ag content (at %)	Average (at %)
A	95.60		4.40	
B	95.24	95.41	4.76	4.59
C	95.38		4.62	

The solid solubility of Ag into Cu is also realized in Cu-5Ag ink (about 3 at.% Ag). The Ag content in the pattern is lower than the maximum solubility of Ag in Cu obtained by the present process, thus it is anticipated that all the Ag atoms will dissolve into the Cu matrix and form a Cu-Ag alloy with only a Cu-rich phase. **Figure 4.10**a shows the XRD patterns of Cu-Ag patterns after IPL sintering using different energies. The peaks of Ag and Cu can be found in the XRD patterns under a low energy of IPL sintering (less than or equal to 1800 mJ/cm^2); while under a higher energy, the peaks of Ag cannot be found in the resulting XRD patterns; meanwhile the positions of the Cu peaks have been shifted to the left-hand side, which agrees with the formation of Cu-Ag alloy as discussed above. The disappearance of Ag peaks in the XRD patterns is related to the complete dissolution of Ag into Cu. The Cu-Ag alloy pattern was further examined by high-resolution TEM (HR-TEM) analysis (**Figure 4.10b**). The lattice spacing of 1.81 Å corresponds to the (200) plane of the Cu-rich phase. The selected area

electron diffraction (SAED) pattern from the TEM analysis (inset of Figure 6b) shows only a Cu-rich phase. **Figure 4.10c** shows the transmission electron microscopy (TEM) image of the Cu-Ag alloy, and the corresponding TEM mapping images are shown in **Figure 4.10d** and **4.10e**. The Ag is uniformly distributed in the Cu matrix without any Ag-rich phase, which confirms that uniform solid solubility of Ag into Cu can be realized by the present method.

Normally, in order to obtain Cu-Ag alloys from Cu-Ag nanoparticle core-shell structures, a high energy input is essential to drive the intermixing and mutual dissolution between adjacent Ag and Cu atoms. Under IPL sintering, incident photons are selectivity absorbed by Cu-Ag nanoparticle core-shell structures and converted into heat energy [35], which is expected to increase the temperature at the surface of Cu-Ag nanoparticle core-shell structure, especially those contact surfaces between Cu cores and Ag nanoparticles because of their strong light absorption [29, 36]. The high temperatures generated at the interfaces of Cu cores and Ag nanoparticles could induce surface melting [37] and drive the rapid atomic diffusion between Cu and Ag, realizing the mutual solution of Cu in Ag and Ag in Cu. The resulting solubilities of Cu in Ag and Ag in Cu are related to the temperature and corresponding rate of diffusion of Cu in Ag and Ag in Cu. Therefore, the average temperature on the surface of printed Cu-Ag patterns was evaluated by the simulation of temperature evolution on the Cu-Ag patterns using some parameters of thermal conductivity, specific heat, melt temperature and density of both Cu and PI substrate (**Table 4.3** and **Table 4.4**). The thickness of printed Cu film and PI substrate was set to 2 μm and 77.5 μm, respectively. Although this may be different from the actual temperature at some local surfaces between Cu cores and Ag nanoparticles, it can help us to understand the IPL sintering. According to the simulation results (**Figure 4.11**), the temperature on the surface of Cu-Ag patterns increases with increasing supplied photonic energy, and when the energy increases to 4100 mJ/cm^2, the temperature on the surface of Cu-Ag pattern reaches a value as high as about 850 °C. Considering the Cu-Ag phase diagram, this high temperature confirms the possibility of rapid mutual diffusion between Cu and Ag atoms and the dissolutions of Cu in Ag, and Ag in Cu. Therefore, rapid IPL sintering facilitates the creation of Cu-Ag alloy—i.e., a core-shell structure with a Cu-rich core and a Ag-rich shell—from the Cu-Ag nanoparticle core-shell structure. Also, because the IPL-sintering-induced Cu-Ag alloying takes

place primarily in the solid state, it avoids the liquid state miscibility gap and phase separation between Cu and Ag [33]; and thus can keep the dissolution of Ag in Cu and Cu in Ag to room temperature easily. Therefore, Cu-Ag alloy patterns can be easily obtained by using a Cu-Ag hybrid ink and the two-step sintering process. Moreover, it is noteworthy that the route can be extended to obtain various other alloy patterns/circuits such as Cu-Ni, Cu-Ti or Cu-Cr alloys on preferred substrates because of its readily adaptable process and simple mechanisms.

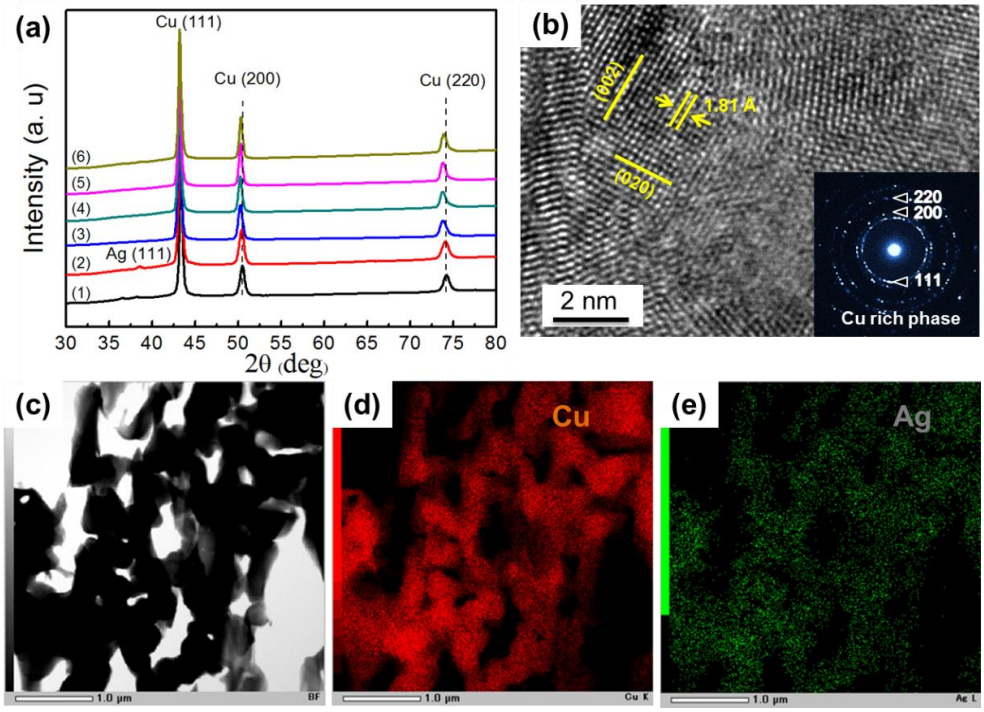

Figure 4.10 (a) XRD patterns of Cu-Ag prepared from Cu-5Ag ink after photonic sintering with energies of (1) 0 mJ/cm^2, (2) 1800 mJ/cm^2, (3) 2200 mJ/cm^2, (4) 2800 mJ/cm^2, (5) 3400 mJ/cm^2, and (6) 4100 mJ/cm^2; (b) HRTEM image of Cu-Ag solution alloy with a SAED pattern shown in the inset; (c) TEM image of Cu-Ag solution alloy, and corresponding TEM mapping images of (d) elemental Cu and (e) elemental Ag.

Table 4.3 Parameters of Cu-Ag electrode and PI substrate used in the simulation.

Material name	Thermal conductivity (W/mk)	Mass density (g/cm^3)	Specific heat (J/kg)	Melt temperature (°)
Cu	401	8.69	382.5	1084.6

PI	0.52	1.43	1150	340

Table 4.4 Parameters of IPL sintering.

Voltage (V)	Pulse duration (μs)	Pulse number	Pulse frequency (Hz)	Input energy (mJ/cm^2)
220	2100	1	1	1100
240	2100	1	1	1800
260	2100	1	1	2200
280	2100	1	1	2700
300	2100	1	1	3400
320	2100	1	1	4100
340	2100	1	1	4900

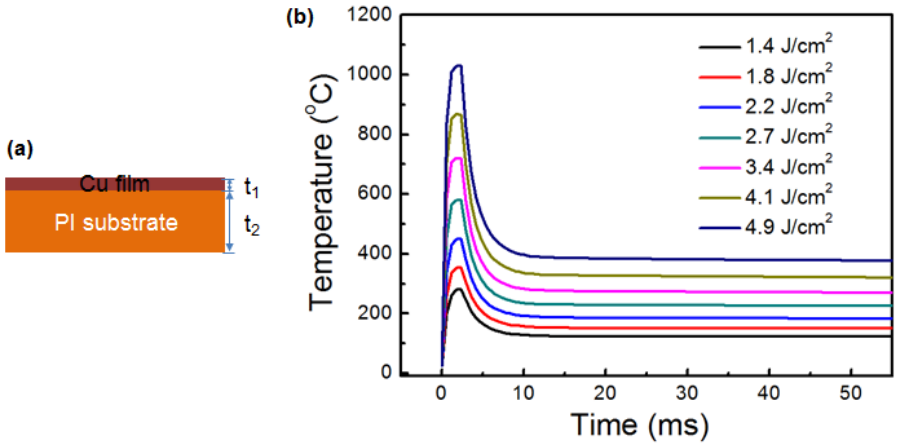

Figure 4.11 (a) Simulation model and (b) temperature evolution on the surface of Cu-Ag electrodes under different energy inputs of IPL sintering.

4.4 Long-term stability of Cu-Ag alloy patterns

The Cu-Ag alloy is considered to be a promising material to avoid oxidation and maintain high conductivity even at high temperatures and in an air atmosphere. **Figure 4.12**a shows the change of relative resistance of printed patterns at 180 °C in air. The patterns were prepared

using the optimized photonic energy based on the data in Figure 4.4a. The relative resistance of a pattern prepared from pure Cu ink rapidly increases to 24 after 64 h while the relative resistance of the Cu-Ag alloy patterns remains almost stable. After 128 h, the relative resistance of the pure Cu pattern increases to over 10^6 while that of Cu-Ag alloy patterns have only a slight increase to less than 8. This indicates that the preferential oxidation of Cu can be inhibited remarkably by the formation of Cu-Ag alloy. Moreover, the oxidation resistance of the Cu-Ag alloy depends on the amount of Ag. In terms of the free energy, the Ag-rich phase at the surface can be more stable than the Cu-rich phase because of the higher surface energy of Cu (1.85 J/m^2) compared to that of Ag (1.25 J/m^2) [38]; thus, the Cu-Ag patterns containing higher Ag content show higher oxidation resistance. In the current work, Cu-Ag alloy patterns prepared from Cu-20Ag ink and Cu-30Ag ink show similar oxidation resistant trends in which the relative resistance is less than 3 even after 128 h. Therefore, 20 wt.% Ag in the ink is deemed to be enough for the prevention of Cu oxidation.

Figure 4.12b shows the change of relative resistance of Cu-Ag alloy patterns prepared from Cu-20Ag ink with different energies of IPL sintering. They were also exposed to 180 °C in air. The relative resistance of printed patterns using an energy of IPL sintering below 2700 mJ/cm^2 rapidly increases above 150 after 128 h. However, once the energy of photonic sintering increases above 2700 mJ/cm^2, the obtained patterns become astonishingly stable and the relative resistance remains below 3 even after 128 h. This can be explained by the different alloy composition in the obtained patterns. When the energy of IPL sintering is below 2700 mJ/cm^2, the diffusion between Cu and Ag is inefficient, and the resulting patterns contain two kinds of phases: a Ag-rich phase containing Cu, and a pure Cu phase (Figure 4.6). The pure Cu can be easily oxidized during the oxidation aging, which results in a rapid increase in relative resistance. In contrast, when the energy increases beyond 2700 mJ/cm^2, the increased diffusion between Cu and Ag atoms is sufficient to activate the dissolution of Ag into Cu; thus, the composition of the resulting patterns transforms into a Ag-rich phase containing Cu and a Cu-rich phase containing Ag (Figure 4.6). The elimination of the pure Cu phase contributes to the further improvement of the oxidation resistance of the obtained Cu-Ag alloy patterns.

Further oxidation evaluations were conducted on patterns prepared from pure Cu ink and

Cu-20Ag ink at 180 °C and 200 °C as shown in Figure 4.12c and d. After 128 h at 200 °C, the relative resistance of the pattern prepared from pure Cu ink increased to 2.1×10^8, while patterns prepared from Cu-20Ag ink showed a very low increase of 14. Also, the oxidation resistance of our Cu-Ag alloy patterns is significantly better than those reported by other studies (Figure 4.12d). For example, the relative resistance of Cu-Ag hybrid patterns increases rapidly to 5 after only 2 h at 180 °C [39] while that of our obtained Cu-Ag alloy pattern remains unchanged until the oxidation time is longer than 64 h. This may be ascribed to the special structure in Cu-Ag alloy patterns where the Ag-rich phase shows a net-like structure and surrounds the Cu rich phase (Figure 4.9). In contrast, Cu-Ag hybrid patterns are a simple mixture of Cu particles and Ag particles that cannot realize a uniform coating of a Ag-rich phase on the surface of the Cu-rich phase [40].

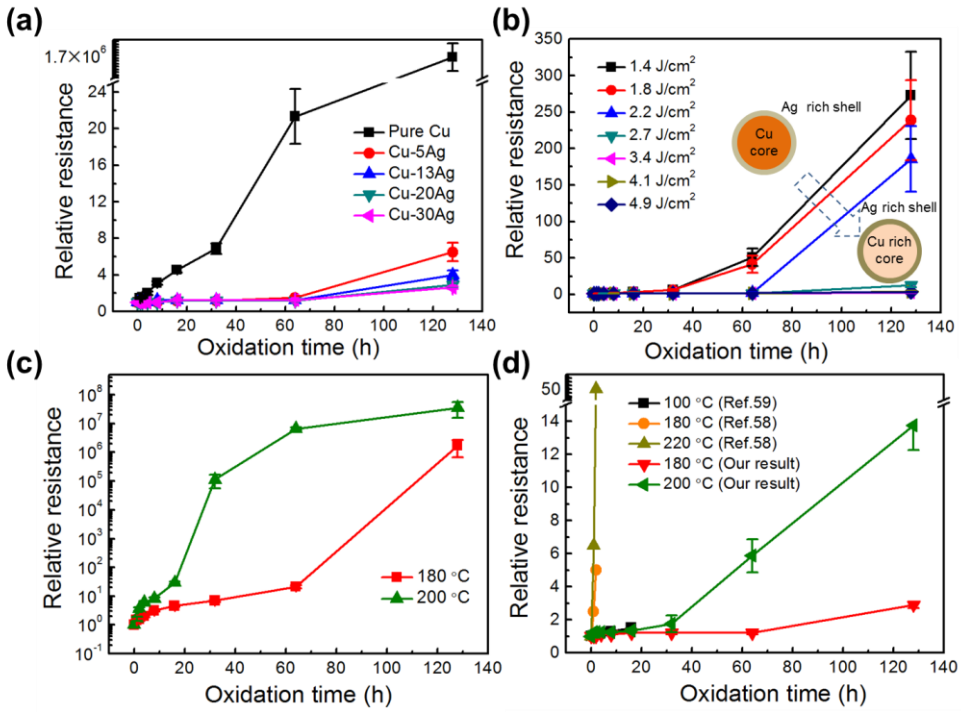

Figure 4.12 Oxidation resistance of printed pure Cu and Cu-Ag alloy patterns. Relative resistance (R/R_0) as a function of oxidation time at different temperatures in air. R_0 is the original resistance of printed patterns and R is the resistance of the printed patterns after oxidation under high temperatures. (a) Relative resistance of patterns prepared from pure Cu, Cu-5Ag, Cu-13Ag, Cu-20Ag, and Cu-30Ag at 180 °C; (b) Relative resistance of Cu-Ag

solution alloy patterns after different energies of IPL sintering at 180 °C; (c) Relative resistance of a pure Cu pattern at 180 °C and 200 °C; (d) Relative resistance of Cu-Ag solution alloy patterns prepared from Cu-20Ag ink at 180 °C and 200 °C, compared with reported values for Cu-Ag hybrid patterns.

In addition, the flexibility of printed Cu-Ag alloy patterns was evaluated by adhesion test and bending test. **Figure 4.13**a shows the result of the adhesion test of printed Cu-Ag alloy pattern. The pattern was prepared from Cu-20Ag ink after low pre-curing temperature of 140 °C and IPL sintering using energies of 2700 mJ/cm^2. Result shows that the Cu-Ag alloy pattern firmly adheres to the PI substrate and does not peel off at all; this indicates the printed Cu-Ag alloy pattern has a strong adhesion to the substrate. **Figure 4.13b** shows the results of the bending test of printed Cu-Ag alloy patterns. The change of resistance of printed Cu-Ag alloy patterns was measured during the bending fatigue test. The results show that printed Cu-Ag alloy patterns have highly mechanical bending properties without evident degradation of electrical performances. After 1000 cycles, the relative resistances of printed patterns keep below 1.2, 1.4 and 2.2 at bending radiuses of 5, 7 and 10 mm, respectively. It is believed that the high flexibility can be achievable due to the fully densified microstructure and well adhesion between printed patterns and substrate.

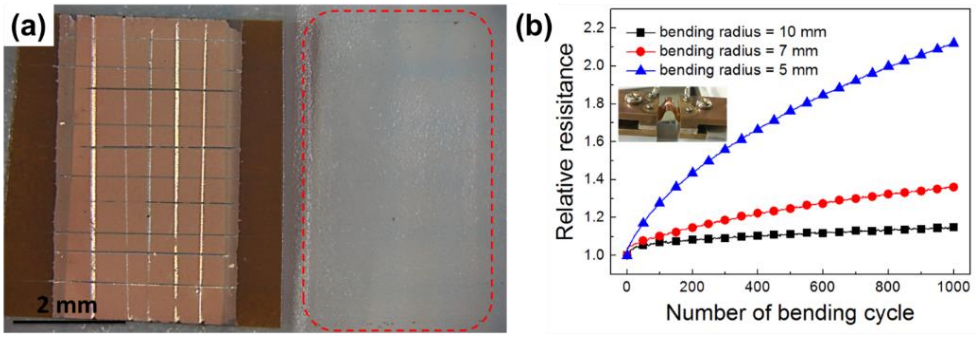

Figure 4.13 (a) Adhesion test and (b) Changes of relative resistance (R/R0) of printed Cu-Ag alloy patterns during a repeated bending test at bending radiuses of 5, 7 and 10 mm, respectively. R0 is the resistance of printed patterns before bending test and R is the resistance of the printed pattern during bending test. (Inset) Photograph of the specimen for bending test.

4.5 Conclusion

Printable and flexible Cu-Ag alloy patterns with high conductivity and ultrahigh oxidation resistance have been successfully fabricated by using a newly developed Cu particle/Ag complex ink and a simple two-step sintering process. The Cu particle/Ag complex ink firstly transforms into a Cu-Ag nanoparticle core-shell structure under a low temperature of 140 °C in air and then further transforms into Cu-Ag alloy under IPL sintering which induces rapid diffusion between the Cu core and the Ag nanoparticle shell. It was revealed that the obtained Cu-Ag alloy pattern has a bulk-like microstructure and shows a very low resistivity of 3.4×10^{-6} Ω·cm (50% of the bulk conductivity of Cu). Most importantly, it was clearly demonstrated that the Cu-Ag alloy has a special core-shell structure with a Cu-rich phase in the core and a Ag-rich phase in the shell, showing a high stability. The printed flexible Cu-Ag alloy patterns have ultrahigh oxidation resistance that remains stable in air at 180 °C and 200 °C and shows great potential for practical use in the fabrication of highly reliable and cost-effective printed electronic devices.

References

1. Li, W.; Zhang, H.; Gao, Y.; Jiu, J.; Li, C.-F.; Chen, C.; Hu, D.; Goya, Y.; Wang, Y.; Koga, H.; Nagao, S.; Suganuma, K., Highly reliable and highly conductive submicron Cu particle patterns fabricated by low temperature heat-welding and subsequent flash light sinter-reinforcement. *Journal of Materials Chemistry C* **2017,** *5* (5), 1155-1164.

2. Li, W.; Li, L.; Gao, Y.; Hu, D.; Li, C.-F.; Zhang, H.; Jiu, J.; Nagao, S.; Suganuma, K., Highly conductive copper films based on submicron copper particles/copper complex inks for printed electronics: Microstructure, resistivity, oxidation resistance, and long-term stability. *Journal of Alloys and Compounds* **2018,** *732*, 240-247.

3. Norman, A. L.; Evagelos, K. A.; Wendelin, J. S., Graphene-stabilized copper nanoparticles as an air-stable substitute for silver and gold in low-cost ink-jet printable electronics. *Nanotechnology* **2008,** *19* (44), 445201.

4. Grouchko, M.; Kamyshny, A.; Magdassi, S., Formation of air-stable copper-silver core-shell nanoparticles for inkjet printing. *Journal of Materials Chemistry* **2009,** *19* (19), 3057-

3062.

5. Tsai, C.-H.; Chen, S.-Y.; Song, J.-M.; Chen, I.-G.; Lee, H.-Y., Thermal stability of Cu@Ag core–shell nanoparticles. *Corrosion Science* **2013,** *74*, 123-129.

6. Li, J.; Li, Y.; Wang, Z.; Bian, H.; Hou, Y.; Wang, F.; Xu, G.; Liu, B.; Liu, Y., Ultrahigh oxidation resistance and high electrical conductivity in copper-silver powder. *Scientific Reports* **2016,** *6*, 39650.

7. Li, J.; Mayer, J.; Colgan, E., Oxidation and protection in copper and copper alloy thin films. *Journal of applied physics* **1991,** *70* (5), 2820-2827.

8. Kawamura, G.; Alvarez, S.; Stewart, I. E.; Catenacci, M.; Chen, Z.; Ha, Y.-C., Production of oxidation-resistant Cu-based nanoparticles by wire explosion. *Scientific Reports* **2015,** *5*, 18333.

9. An, B. W.; Gwak, E.-J.; Kim, K.; Kim, Y.-C.; Jang, J.; Kim, J.-Y.; Park, J.-U., Stretchable, transparent electrodes as wearable heaters using nanotrough networks of metallic glasses with superior mechanical properties and thermal stability. *Nano Letters* **2016,** *16* (1), 471-478.

10. Kim, K. O.; Kim, S., Surface morphology control of Cu–Ag alloy thin Film on W diffusion barrier by seedless electrodeposition. *Journal of Nanoscience and Nanotechnology* **2016,** *16* (11), 11701-11706.

11. Duwez, P.; Willens, R. H.; Jr, W. K., Continuous series of metastable solid solutions in silver-Copper Alloys. *Journal of Applied Physics* **1960,** *31* (6), 1136-1137.

12. Tsaur, B. Y.; Lau, S. S.; Mayer, J. W., Continuous series of metastable Ag-Cu solid solutions formed by ion-beam mixing. *Applied Physics Letters* **1980,** *36* (10), 823-826.

13. Klassen, T.; Herr, U.; Averback, R. S., Ball milling of systems with postive heat of mixing: effect of temperature in Ag-Cu. *Acta Materialia* **1997,** *45* (7), 2921-2930.

14. Ma, E.; Atzmon, M., Phase transformations induced by mechanical alloying in binary systems. *Materials Chemistry and Physics* **1995,** *39* (4), 249-267.

15. Grammatikopoulos, P.; Kioseoglou, J.; Galea, A.; Vernieres, J.; Benelmekki, M.; Diaz, R. E.; Sowwan, M., Kinetic trapping through coalescence and the formation of patterned Ag-Cu nanoparticles. *Nanoscale* **2016,** *8* (18), 9780-9790.

16. He, J. H.; Sheng, H. W.; Lin, J. S.; Schilling, P. J.; Tittsworth, R. C.; Ma, E., Homogeneity

of a supersaturated solid solution. *Physical Review Letters* **2002,** *89* (12), 125507.

17. Mader, S.; Nowick, A. S.; Widmer, H., Metastable evaporated thin films of Cu-Ag and Co-Au alloys—I occurrence and morphology of phases. *Acta Metallurgica* **1967,** *15* (2), 203-214.

18. Tsuji, M.; Hikino, S.; Tanabe, R.; Matsunaga, M.; Sano, Y., Syntheses of Ag/Cu alloy and Ag/Cu alloy core Cu shell nanoparticles using a polyol method. *CrystEngComm* **2010,** *12* (11), 3900-3908.

19. Taner, M.; Sayar, N.; Yulug, I. G.; Suzer, S., Synthesis, characterization and antibacterial investigation of silver-copper nanoalloys. *Journal of Materials Chemistry* **2011,** *21* (35), 13150-13154.

20. Tan, K. S.; Cheong, K. Y., Advances of Ag, Cu, and Ag–Cu alloy nanoparticles synthesized via chemical reduction route. *Journal of Nanoparticle Research* **2013,** *15* (4), 1537.

21. Hatamura, M.; Yamaguchi, S.; Takane, S.-y.; Chen, Y.; Suganuma, K., Decarboxylation and simultaneous reduction of silver(i) [small beta]-ketocarboxylates with three types of coordinations. *Dalton Transactions* **2015,** *44* (19), 8993-9003.

22. Xi, S.; Zuo, K.; Li, X.; Ran, G.; Zhou, J., Study on the solid solubility extension of Mo in Cu by mechanical alloying Cu with amorphous Cr(Mo). *Acta Materialia* **2008,** *56* (20), 6050-6060.

23. Nakano, M.; Fujiwara, T.; Koga, N., Thermal decomposition of silver acetate: physico-geometrical kinetic features and formation of silver nanoparticles. *The Journal of Physical Chemistry C* **2016,** *120* (16), 8841-8854.

24. Li, W.; Cong, S.; Jiu, J.; Nagao, S.; Suganuma, K., Self-reducible copper inks composed of copper-amino complexes and preset submicron copper seeds for thick conductive patterns on a flexible substrate. *Journal of Materials Chemistry C* **2016,** *4* (37), 8802-8809.

25. Kwon, S. G.; Krylova, G.; Phillips, P. J.; Klie, R. F.; Chattopadhyay, S.; Shibata, T.; Bunel, E. E.; Liu, Y.; Prakapenka, V. B.; Lee, B.; Shevchenko, E. V., Heterogeneous nucleation and shape transformation of multicomponent metallic nanostructures. *Nature Materials* **2014,** *14*, 215.

26. Lin, S.-k.; Nagao, S.; Yokoi, E.; Oh, C.; Zhang, H.; Liu, Y.-c.; Lin, S.-g.; Suganuma, K., Nano-volcanic eruption of silver. *Scientific Reports* **2016,** *6*, 34769.

27. Jeong, S.; Woo, K.; Kim, D.; Lim, S.; Kim, J. S.; Shin, H.; Xia, Y.; Moon, J., Controlling the thickness of the surface oxide layer on Cu nanoparticles for the fabrication of conductive structures by ink-jet printing. *Advanced Functional Materials* **2008,** *18* (5), 679-686.

28. Jiu, J.; Nogi, M.; Sugahara, T.; Tokuno, T.; Araki, T.; Komoda, N.; Suganuma, K.; Uchida, H.; Shinozaki, K., Strongly adhesive and flexible transparent silver nanowire conductive films fabricated with a high-intensity pulsed light technique. *Journal of Materials Chemistry* **2012,** *22* (44), 23561-23567.

29. Garnett, E. C.; Cai, W.; Cha, J. J.; Mahmood, F.; Connor, S. T.; Greyson Christoforo, M.; Cui, Y.; McGehee, M. D.; Brongersma, M. L., Self-limited plasmonic welding of silver nanowire junctions. *Nature Materials* **2012,** *11*, 241.

30. Shengyong, X.; Mingliang, T.; Jinguo, W.; Jian, X.; M., R. J.; W., C. M. H., Nanometerscale modification and welding of silicon and metallic nanowires with a high-intensity electron beam. *Small* **2005,** *1* (12), 1221-1229.

31. Qingzhou, C.; Fan, G.; Subhadeep, M.; Zhiyong, G., Joining and interconnect formation of nanowires and carbon nanotubes for nanoelectronics and nanosystems. *Small* **2009,** *5* (11), 1246-1257.

32. Sung-Jun, J.; Hyun-Jun, H.; Hak-Sung, K., Highly conductive copper nano/microparticles ink via flash light sintering for printed electronics. *Nanotechnology* **2014,** *25* (26), 265601.

33. Ma, E., Alloys created between immiscible elements. *Progress in Materials Science* **2005,** *50* (4), 413-509.

34. Gilmore, C. M., Materials science and engineering properties. Cengage Learning: Stamford, CT, 2015.

35. Richardson, H. H.; Carlson, M. T.; Tandler, P. J.; Hernandez, P.; Govorov, A. O., Experimental and theoretical studies of light-to-heat conversion and collective heating effects in metal nanoparticle solutions. *Nano Letters* **2009,** *9* (3), 1139-1146.

36. MacNeill, W.; Choi, C.-H.; Chang, C.-H.; Malhotra, R., On the self-damping nature of densification in photonic sintering of nanoparticles. *Scientific Reports* **2015,** *5*, 14845.

37. Joo, S.-J.; Park, S.-H.; Moon, C.-J.; Kim, H.-S., A Highly reliable copper nanowire/nanoparticle ink pattern with high conductivity on flexible substrate prepared via a

flash light-sintering technique. *ACS Applied Materials & Interfaces* **2015,** *7* (10), 5674-5684.

38. Malviya, K. D.; Chattopadhyay, K., Temperature- and size-dependent compositionally tuned microstructural landscape for Ag-46 Atom % Cu nanoalloy prepared by laser ablation in liquid. *The Journal of Physical Chemistry C* **2016,** *120* (48), 27699-27706.

39. Yim, C.; Sandwell, A.; Park, S. S., Hybrid copper–silver conductive tracks for enhanced oxidation Resistance under Flash Light Sintering. *ACS Applied Materials & Interfaces* **2016,** *8* (34), 22369-22373.

40. Wan-Ho, C.; Yeon-Taek, H.; Seung-Hyun, L.; Hak-Sung, K., Electrical wire explosion process of copper/silver hybrid nano-particle ink and its sintering via flash white light to achieve high electrical conductivity. *Nanotechnology* **2016,** *27* (20), 205704.

Chapter 5

Self-catalyzed Cu-Ag complex inks for ultra-low temperature fabrication of conductive patterns

5.1 Introduction

As found in chapter 4, printable and flexible Cu-Ag alloy patterns can be realized by using developed Cu particle/Ag complex ink and two-step sintering method, which can greatly improve the oxidation resistance of printed conductive patterns. However, it should be noted that the alloying process needs a high energy for inducing the mutual diffusion between Cu and Ag elements. It cannot be compatible with heat sensitive substrates such as PET, even though the rapid ILP sintering is used. On other hands, several other kinds of Cu/Ag hybrid inks have been proposed for improving the oxidation resistance of printed conductive patterns, such as Cu nanoparticle/Ag nanoparticle mixture inks [1, 2], Cu/Ag core-shell nanoparticle inks [3, 4], and Cu/Ag bimetallic nanoparticle inks [5]; however, all these particle-type inks need a high annealing temperature above 200 °C to remove organic compounds and sinter particles [3, 5], which limits their practical applications on heat-sensitive film substrates, such as textile, paper, PET.

To reduce the temperature, using metal complex inks is a possible approach. They are different from particle-type inks which need a high annealing temperature to promote necking among particles. Metal complex inks directly transform into pure metal patterns by a low temperature thermal decomposition process [6-9]. Schubert *et al*. reported a kind of Ag complex ink decomposed at 130 °C for 60 min to form highly conductive patterns (6.8×10^{-6} Ω·cm)[10]. Our previous work also demonstrated that the annealing temperature of Ag complex can be decreased to 100 °C by changing the complex groups [11, 12]. Besides these Ag complexes, Cu complexes possessing their own benefits have also been studied recently [13, 14]. Yabuki *et al*. reported various Cu complex inks composed of Cu formate and different amine solvents which can be annealed at 140 °C [15]. Farraj *et al*. investigated the decomposition mechanism of Cu complex inks and obtained the lowest resistivity of 1.05×10^{-5} Ω·cm at 190 °C [6]. Compared with Ag complex inks, Cu complex inks need a higher annealing temperature above 140 °C. The temperature is still harsh for most heat-sensitive substrates. Very recently, Farraj

et al. reported that low-pressure plasma could drive the decomposition of Cu complex to form metallic Cu at a temperature less than 70 °C [16]; however, the low-pressure plasma method is time-consuming and not compatible to rapid roll-to-roll mass production processes because of the high complexity, small irradiation area, and expensive equipment. It is known that metal nanoparticles, such as Pt, Au, Cu, and Ag nanoparticles, have excellent catalytic activity to accelerate the decomposition of metal complex into pure metal particles under mild and low-temperature conditions [17-19]. If the Cu and Ag complexes are mixed and annealed, the in-situ formed fresh metal nanoparticles are likely to play a role of catalyst that can promote decomposition and trigger the reduction of complexes at an ideal low temperature.

In this chapter, Cu-Ag complex inks are developed for printing conductive patterns of low cost, high stability, and high conductivity on heat-sensitive substrates such as polyethylene terephthalate (PET) substrate. The inks show an obvious self-catalyzed characteristic due to the in-situ formation of fresh metal nanoparticles which promote rapid decomposition and sintering of the inks at a low temperature below 100 °C. The temperature is 40-60 °C lower than those of general Cu complex inks and 100-120 °C lower than those of general Cu/Ag particle inks. Highly conductive Cu-Ag patterns of 2.80×10^{-5} Ω·cm and 6.40×10^{-5} Ω·cm have been easily realized at 100 °C and 80 °C, respectively. In addition, the printed Cu-based patterns not only show high oxidation resistance at high temperatures up to 140 °C (the maximum tolerable temperature of current PET substrate) but also show excellent stability at high humidity of 85 % because of the very uniform Cu-Ag hybrid structure. The printable patterns exhibit great potential application to various wearable devices on textiles, papers, and other heat-sensitive substrates.

5.2 Experimental

5.2.1 Materials

Cu (II) formate tetrahydrate ($C_2O_4H_2Cu\cdot4H_2O$) and 2-ethylhexylamine were purchased form Wako Pure Chemical Industries, Ltd. Ag (I) β-ketocarboxylate ($C_5O_3H_7Ag$) was provided by Toppan Forms Co., Ltd. and the synthesis can be found in chapter 4. PET substrate of 100 μm thick was purchased from Toray Industries, Inc.

5.2.2 Preparation of Cu-Ag complex inks

First, 0.50 g of Ag (I) β-ketocarboxylate was added into 0.57g 2-ethylhexylamine solvent followed by stirred for 2 min at room temperature to ensure the formation of the Ag complex (**Figure 5.1a**). Second, the 0.50 g of Cu (II) formate tetrahydrate was added into 0.57g 2-ethylhexylamine solvent and they were stirred for 10 min at room temperature to ensure the formation of the Cu complex (**Figure 5.1b**). Finally, Cu-Ag complex inks were prepared by mixing the Ag complex and the Cu complex with various weight ratios with a hybrid mixer (HM-500) for 2 min (**Figure 5.1c**). The prepared Ag complex and Cu/Ag complex inks were stored in refrigerator to keep their stability and were used within 5 h. For ease of description, they were denoted as Cu, Cu-30Ag, Cu-46Ag, Cu-63Ag, and Ag inks, in which figures represent Ag content: 30 wt%, 46 wt%, and 63 wt%, respectively.

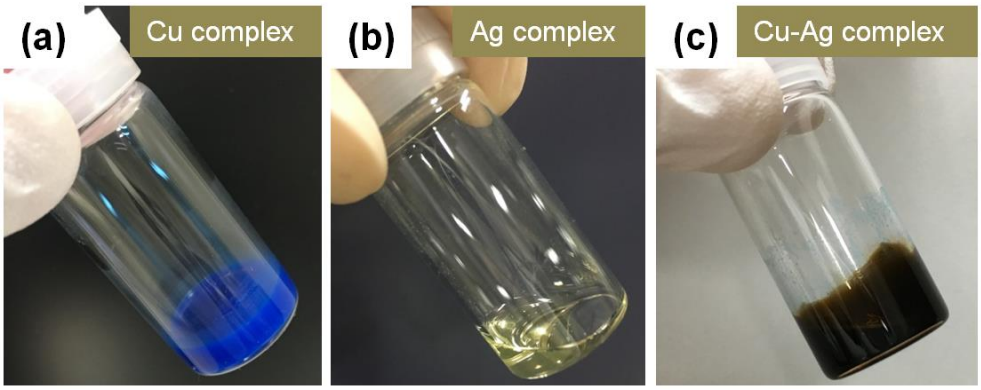

Figure 5.1 Photos of (a) Cu complex, (b) Ag complex, and (c) Cu-46Ag complex.

5.2.3 Screen-printing and simple annealing process

Polyethylene terephthalate (PET) films and glass sheets were used as substrates. To remove the contamination on their surfaces, they were cleaned by an ultrasonic bath in ethanol for 15 min followed by sequential rinsing with distilled water for 1 min. Then complex inks were printed onto the substrates by screen-printing method. Finally, the printed inks were cured by a simple annealing process at 80 °C, 100 °C, 120 °C, and 140 °C in a N_2 atmosphere to form metal patterns. The flow rate of N_2 is about 3 L min^{-1}.

5.2.4 Characterization methods

The electrical resistivity of printed patterns was measured by four probe analyzer (LorestaGP T610, Mitsubishi Chemical Analytech Co. Ltd.). The microstructure of conductive patterns was observed by field-emission scanning electron microscopy (FE-SEM, Hitachi SU8020, Hitachi High Technologies America, Inc.) and transmission electron microscopy (TEM, JEM-ARM200F, JEOL Ltd.), together with energy dispersive spectroscopy (EDS). To get pattern fragments for making TEM samples, some part of the printed pattern was firstly peeled off from the glass substrate with an adhesive tape and then separated from the tape using acetone solvent. A focused ion beam (FIB, FB2100, Hitachi) was used to cut the cross-section samples with a diameter of 40 μm and standard current of 0.06-0.15 nA. To prevent the sample surface from being damaged by ion beam, they were coated with a platinum layer of about 25 nm. Crystal structures of patterns were determined by X-ray diffractometer (XRD, Rigaku) using Cu Ka radiation. The thermal behaviors of complex inks were investigated by thermogravimetric analysis (TGA 2000SE, NETZSCH) and differential scanning calorimetry (DSC 204 F1, NETZSCH) at a heating rate of 10 °C min^{-1} in N_2. Finally, the long-term durability of metal patterns was evaluated by exploring them at high temperatures of 80 °C, 110 °C, and 140 °C in air and also at 85 °C with 85 % relative humidity (85 °C-85% RH).

5.3 Conductivity, microstructure, and chemical composition of printed Cu-Ag hybrid patterns

Electrical conductivity of printed patterns, especially after a low temperature annealing, is one of the most important factors to evaluate the conductive inks for the application to heat-sensitive substrates; thus, the resistivity evolution of patterns was studied firstly. **Figure 5.2a** shows the relationship between resistivity and annealing temperatures. It can be seen that conductive patterns have been achieved from pure Ag ink and Cu-46Ag and Cu-63Ag inks even at a low annealing temperature of 80 °C. When the temperature increases to 100 °C, significantly lower resistivity values of the order of 10^{-5} Ω·cm are reached from all inks except pure Cu ink. The pure Cu ink needs a high annealing temperature of 140 °C to obtain the similar resistivity. It is noteworthy that the Cu-46Ag ink gives the best conductivity at 100 °C and is

even superior to the pure Ag ink. Hence, the low temperature of 100 °C was selected to evaluate other parameters. **Figure 5.2b** shows the resistivity of patterns after annealing at 100 °C for different times. It is clear that the resistivity drastically decreases as the time increases, and patterns from Cu-46Ag always achieve the lowest resistivity. After 30 min, the resistivity of patterns prepared from all inks except pure Ag ink becomes constant with a small fluctuation. The further decrease for Ag pattern is related to the continuous sintering of Ag particles. Considering the expensive cost of pure Ag and high annealing temperature of pure Cu, the Cu-Ag complex inks show obvious advantages for wide applications to heat-sensitive substrates at low temperatures below 100 °C. The Cu-46Ag ink is believed as the best one, which gives a very low resistivity of 2.80×10^{-5} Ω·cm at 100 °C for 30 min. **Figure 5.2c** shows the detailed resistivity evolution of patterns prepared from the Cu-46Ag ink. The resistivity is dependent on both annealing temperature and time. A high temperature of 140 °C enables patterns to have a low resistivity of 2.14×10^{-5} Ω·cm in a very short time such as 5 min, which can be realized at 100 °C for 30 min (lower temperature and longer time). Hence, the Cu-Ag complex inks is highly free in practical applications for a variety of purposes.

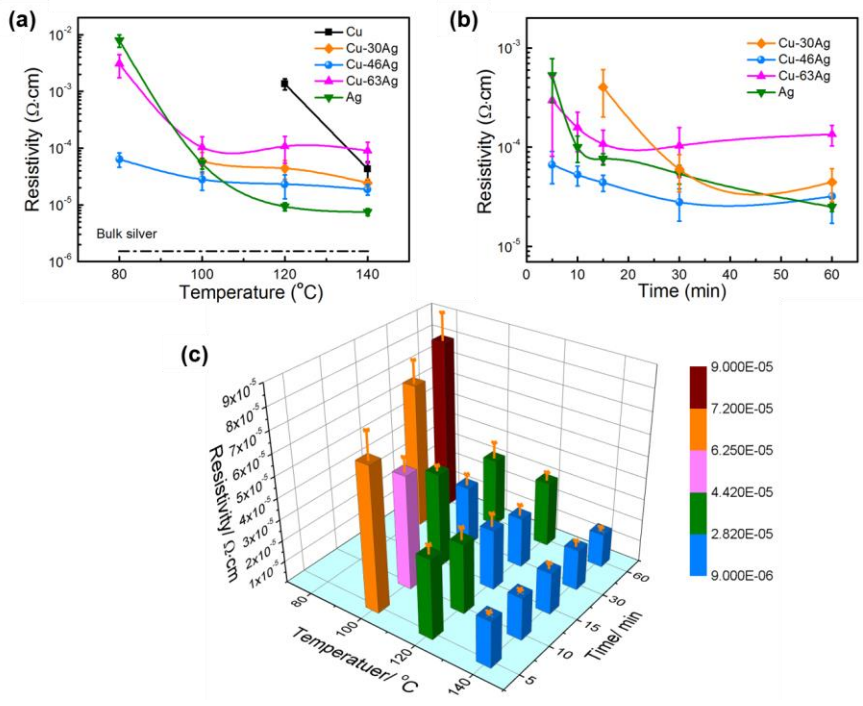

Figure 5.2 (a) Electrical resistivity of patterns annealed at different temperatures for 30 min, (b) electrical resistivity of patterns annealed at 100 °C with different times, and (c) electrical

resistivity of patterns using Cu-46Ag complex ink. The dashed line in Figure 5.2a indicates the resistivity of bulk Ag.

Table 5.1 compares the present work with those reported Cu-Ag patterns prepared from different Cu-Ag inks. It can be seen that the particle-type Cu-Ag inks (even the size of them decreases to about 20 nm) normally need a high annealing temperature above 200 °C and are usually applied on heat-resistant substrates, such as polyethersulphone (PES), polyimide (PI), and glass substrates. Although rapid photonic sintering is a highly efficient method to fabricate conductive Cu-Ag patterns with a resistivity value of order of 10^{-6} Ω·cm resulted from the light absorption of metal particles and the plasma effect [20-22], it can only apply to heat-resistant PI and glass substrates. In contrast, our Cu-Ag complex inks show an excellent low temperature sinterability and can easily achieve a low resistivity of 2.80×10^{-5} Ω·cm and 6.40×10^{-5} Ω·cm on heat-sensitive PET substrates after annealing at only 100 °C and 80 °C respectively. The annealing temperatures are 100-120 °C lower than that of general Cu/Ag particle inks. Therefore, the present complex ink with a simple low temperature process is considered as a revolution of conductive inks, which greatly expands their application to heat-sensitive paper, textile, and other low cost substrates.

Table 5.1 Literature survey of Cu-Ag patterns with respect to materials, heat treatment methods, substrates, and achieved resistivity.

Type of ink	Heat treatment	Substrate	Resistivity (Ω·cm)	Ref
Cu particle/Ag particle	200 °C	PES	2.36×10^{-5}	[1]
Cu particle/Ag particle	Photonic sintering	PI	4.06×10^{-6}	[2]
Cu/Ag core-shell particle	250 °C	Glass	3.20×10^{-5}	[3]
Cu/Ag core-shell particle	250 °C	Glass	2.42×10^{-5}	[4]
Ag/Cu bimetallic particle	350 °C	Glass	1.37×10^{-5}	[5]
Cu particles/Ag salt	Photonic sintering	Glass	3.00×10^{-4}	[21]
Cu particles/Ag complex	LTRS[a)]	PI	3.40×10^{-6}	[22]
Cu-Ag complex	80 °C	PET	6.40×10^{-5}	

Cu-Ag complex	100 °C	PET	2.80×10^{-5}	This
Cu-Ag complex	120 °C	PET	2.32×10^{-5}	study

[a)]LTRS= Low-temperature precuring followed by rapid photonic sintering.

The microstructure and chemical composition of patterns annealed at 100 °C for 30 min were studied to clarify their low resistivity property. **Figure 5.3a** shows the surface microstructure of pattern from pure Cu ink. As seen, there are many small particles with an average size of 55 nm. The corresponding X-ray diffraction (XRD) pattern in **Figure 5.3f** shows an obvious peak of Cu_2O (111) (PDF#05-0667). Therefore, it can be concluded that these Cu particles resulted from decomposition of pure Cu complex at low temperature of 100 °C have been partly oxidized even under the N_2 protection. Thus, they cannot be further sintered to form conductive pathways, resulting in a high resistivity (Figure 5.2a). The similar oxidation phenomenon has also been observed in previous researches [23, 24], which might be related to the decomposition process of Cu complex, including nucleation and growth process. When heated, Cu complex decomposes and fresh Cu nuclei form. These nuclei are very sensitive to oxygen even under N_2 protection due to their small size and high surface energy [25]. At low temperature of 100 °C, the nucleation and the growth speed are slow, so these newly formed Cu nuclei are easily oxidized and cannot be further sintered to form conductive pattern. In contrast, a high temperature above 140 °C can provide sufficient energy for rapid decomposition of Cu complex. The formation and growth of Cu nuclei are fast so that oxidation can be suppressed (**Figure 5.4a**). Also, due to the high temperature, the efficient sintering between these fresh Cu particles can occur easily to form a dense structure (**Figure 5.4b**). Therefore, in order to form high conductive pure Cu patterns without oxidation, a high annealing temperature is necessary. **Figure 5.3b** shows the microstructure of pattern prepared from Cu-30Ag ink. Small particles are also observed but most of them have been sintered with each other to form conductive pattern (5.92×10^{-5} Ω·cm). Particularly, the corresponding XRD pattern in Figure 5.3f shows peaks of pure Cu (PDF#04-0836) and Ag (PDF#04-0783) without any peak of Cu oxides. It means that the oxidation of Cu is suppressed in Cu-30Ag complex ink even at low temperature of 100 °C. **Figure 5.3c** shows the microstructure of pattern

prepared from Cu-46Ag ink. There are no isolated particles because they have been sintered with each other to form strong conductive pathways. This result enables the pattern to have a lower resistivity (2.80×10^{-5} Ω·cm) than that prepared from Cu-30Ag ink. Also, the corresponding XRD pattern in Figure 5.3f shows only Cu and Ag peaks, further supporting the fact that the oxidation of Cu has been successfully suppressed in the decomposition and sintering process of Cu-Ag complex inks. **Figure 5.3d** shows the microstructure of pattern prepared from Cu-63Ag ink. It is a very dense structure but has some micro-cracks; as result, the resistivity is relatively high (1.03×10^{-4} Ω·cm). The formation of micro-cracks is likely because the mismatch between the densification of Cu-rich and Ag-rich parts in the Cu-63Ag pattern causes a stress beyond the threshold value of cracks formation [26]. **Figure 5.3e** shows the microstructure of pattern prepared from pure Ag ink. It is similar to that of Cu-46Ag complex ink except for some small particles, thus the achieved resistivity (5.40×10^{-5} Ω·cm) is higher than that from Cu-46Ag complex ink. On the other hand, the cross-sections of corresponding patterns were also observed, as shown in the insets of Figure 5.3a-e. It confirms that the patterns have a very uniform microstructure. The porosities of Cu-30Ag, Cu-46Ag, and Cu-63Ag are about 5.9 %, 5.6 %, and 8.1 % respectively which are consistent with their conductivity. Printed Cu-Ag patterns with lower porosity have higher conductivity. Based on the above results, three points are noteworthy: 1) the microstructure and resistivity of printed patterns highly rely on the chemical composition of complex ink; 2) the Cu-46Ag ink is the best composition to achieve a dense microstructure with the lowest resistivity of 2.80×10^{-5} Ω·cm at 100 °C; 3) The oxidation of Cu is successfully suppressed in the decomposition and sintering process of Cu-Ag complex inks.

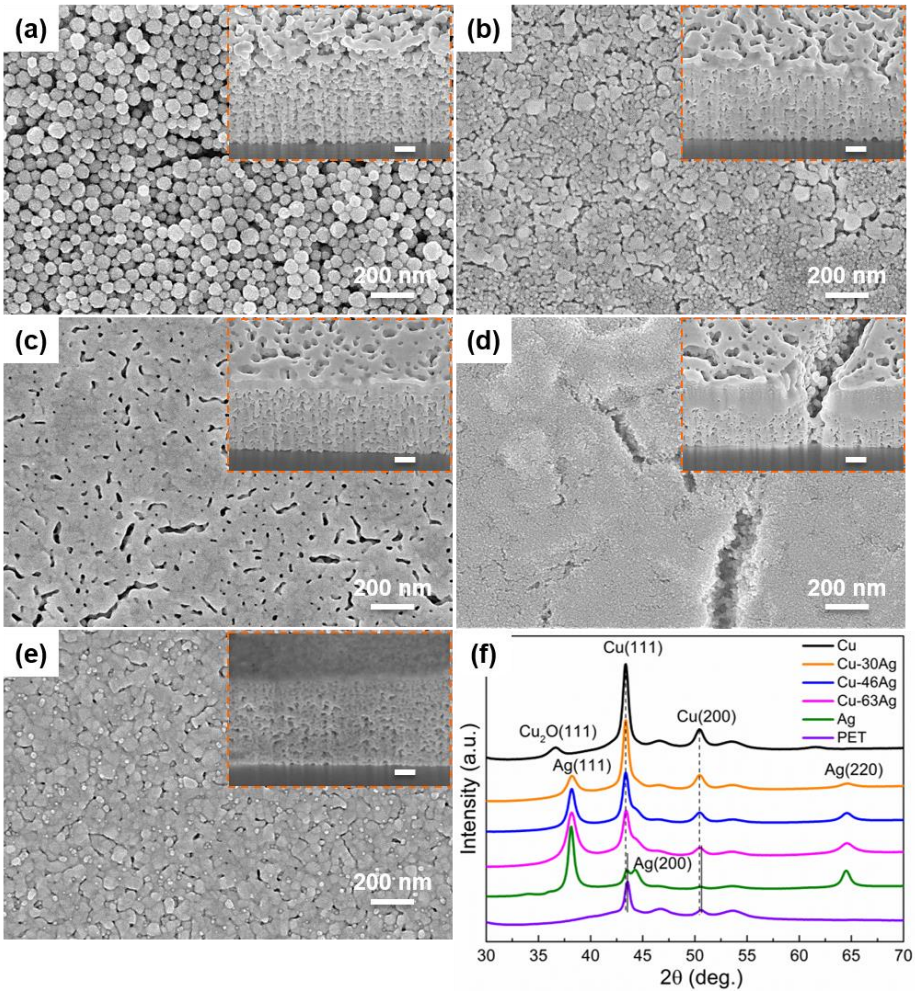

Figure 5.3 Microstructure of patterns prepared from (a) pure Cu, (b) Cu-30Ag, (c) Cu-46Ag, (d) Cu-63Ag, and (e) pure Ag complex inks; (f) corresponding XRD patterns. Insets in Figure 5.3a-e are corresponding cross-sections of patterns, respectively, which were taken on an angle of 30°. The scale bar in insets is 200 nm. The annealing process is 100 °C for 30 min.

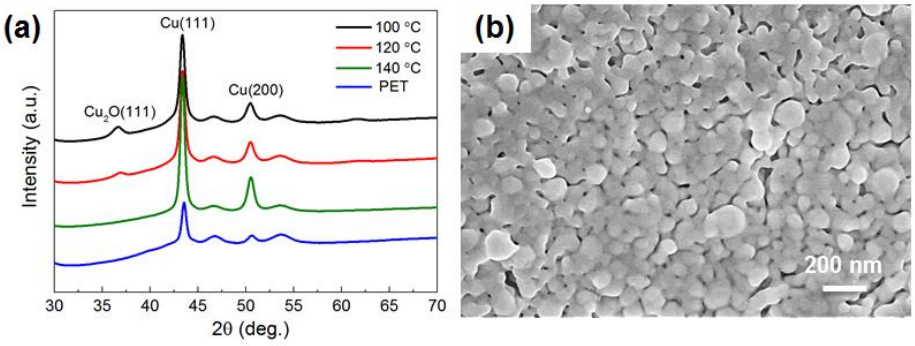

Figure 5.4 (a) XRD patterns of Cu pattern annealed at different temperatures for 30 min and (b) microstructure of Cu pattern annealed at 140 °C for 30 min.

Figure 5.5a shows the typical transmission electron microscopy (TEM) image of the pattern prepared from Cu-46Ag ink annealed at 100 °C for 30 min. As seen, the pattern is an aggregate of small particles with an average size of 35 nm. The value is much smaller than that (55 nm) in the pure Cu pattern (Figurer 5.3a), which indicates that the nucleation in Cu-46Ag ink is much faster than that in pure Cu ink. Clearly, these particles are connected with each other to form strong and conductive pathways (**Figure 5.5b**). The detailed microstructures were further examined by high-resolution TEM (HR-TEM) method (**Figure 5.5c**). The lattice spacing of 2.09 Å corresponds to the Cu (111) plane and that of 2.36 Å is assigned to Ag (111), which means that these particles contain both Cu phase and Ag phase. Furthermore, scanning TEM (STEM) image and corresponding mapping images confirm the uniform distribution of Cu phase and Ag phase (**Figure 5.5d-g**). It is believed that Cu phase and Ag phase have been uniformly mixed in nano-size and connected with each other. In other words, Cu and Ag phase have been fused with each other to form a very uniform Cu-Ag hybrid structure.

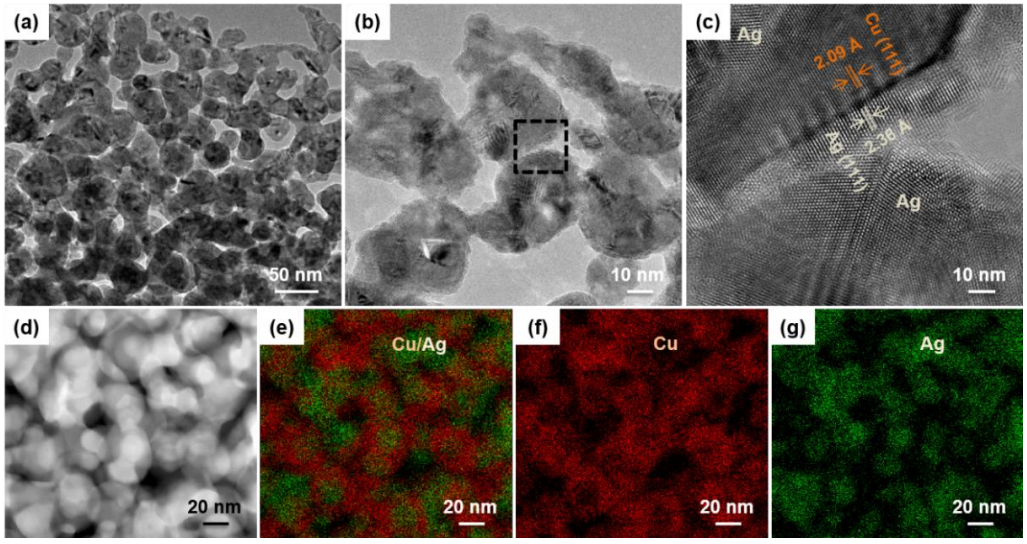

Figure 5.5 (a) TEM image of pattern prepared from Cu-46Ag ink, (b) magnified TEM image, and (c) corresponding HR-TEM image. (d) STEM image and corresponding mapping images of (e) Cu and Ag, (f) Cu, and (g) Ag element.

5.4 Self-catalyzed characteristics in Cu-Ag complex inks

In order to explain why Cu-Ag complex inks can form conductive patterns with a dense structure and a low resistivity at such low temperatures, the thermal behaviors of these Cu, Ag and Cu-Ag inks were investigated. **Figure 5.6a** shows the differential scanning calorimetry (DSC) results of pure Cu ink and pure Ag ink. The decomposition of them is accompanied by a series of exothermic and endothermic processes. The gaseous products during the decomposition of these complexes have been studied by many researchers based on the mass spectrometry and Fourier transform infrared analyses, which suggests that the exothermic peak at 130 °C in Cu complex and at 140 °C in Ag complex conforms to the carboxyl dissociation from the Cu (II) formate and Ag (I) β-ketocarboxylate, respectively, while the endothermic peak at 152 °C in both represents the dissociation of amine [6, 23, 24]. **Figure 5.6b** shows the DSC results of Cu-Ag complex inks. It can be clearly seen that the decomposition temperature of amine decreases with the increase of weight ratio of Ag to Cu. The endothermic peak at 175 °C in Cu-63Ag is likely attributed to the crystallization of Cu or Ag because there is no weight-loss in the range (**Figure 5.6c**). The thermogravimetric analysis (TG) results also confirm the decomposition process of Cu-Ag inks with a low temperature and rapid weight-loss. And from the differential TG (DTG) results, Cu-Ag inks show a faster decomposition rate at lower temperatures than that of pure Cu and Ag inks (Figure 5.6d). These results imply that there is an obvious accelerated process during the decomposition of Cu-Ag complexes, which might be related to the catalyzed characteristic of metal nanoparticles mentioned above [17-19].

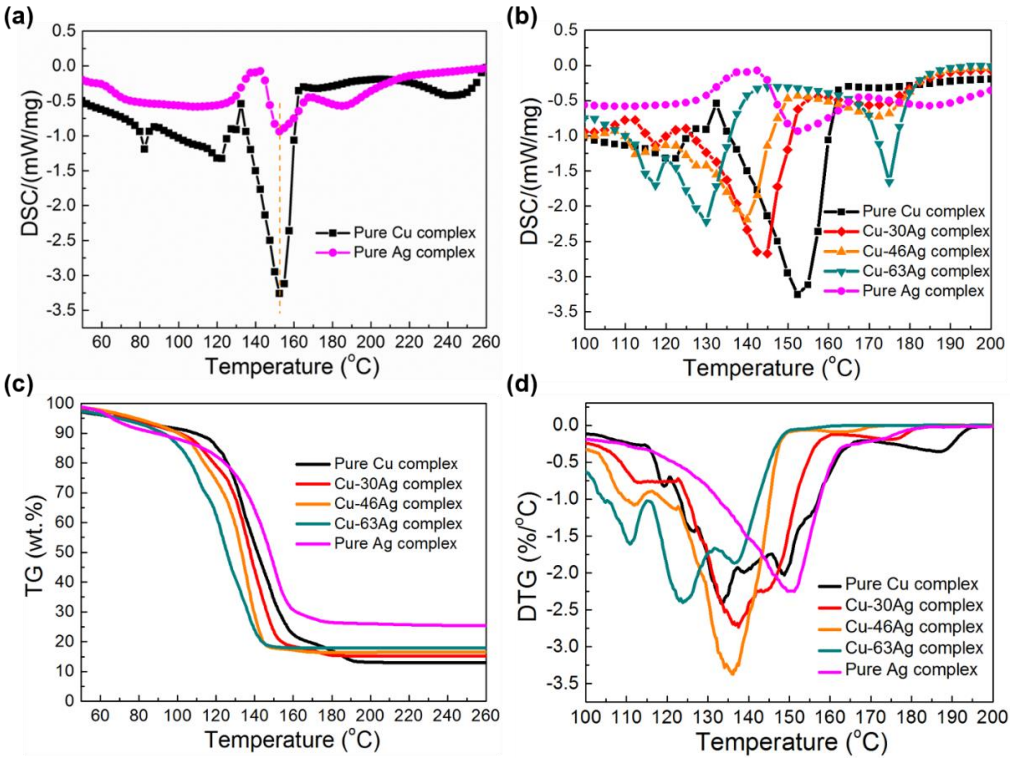

Figure 5.6 (a) DSC results of pure Cu and Ag inks; (b) DSC, (c) TG, and (d) differential TG (DTG) results of all inks.

To further understand the accelerated decomposition process of Cu-Ag complexes, the phase transition as a function of annealing time during the decomposition of complexes was investigated. **Figure 5.7a** shows the XRD patterns of pure Cu complex ink during the decomposition process. At the initial stage, all peaks correspond to Cu complex and by-products; there are no peaks of Cu and Cu oxide. After 5 min, peaks of Cu(111) and Cu(200) begin to appear in the pattern, which indicates the decomposition of Cu complex to Cu has occurred. When the time increase to 10 min, an obvious peak of Cu_2O(111) appears and becomes stronger with the increase of time. It means that during the decomposition process, some Cu particles are gradually oxidized even in the N_2 atmosphere. **Figure 5.7b** shows the XRD patterns of pure Ag complex ink. At the initial stage, there is only one peak of Ag_2CO_3(300) (PDF#31-1236). After 1 min, the peaks of Ag(111), Ag(200) and Ag(220) appear. With the increase of time, the relative intensity of Ag peaks becomes stronger and stronger while that of Ag_2CO_3(300) becomes weaker and weaker, but the Ag_2CO_3 (300) peak still exists when the time increases to

60 min. It means that the decomposition of the Ag complex is incomplete. **Figure 5.7c** shows the XRD results of Cu-46Ag complex ink. The peaks of Ag_2CO_3(300), Ag(111), Ag(200) and Ag(220) have been found at the initial stage, which strongly suggests the decomposition of Ag complex has occurred even at room temperature. After only 1 min, the peaks of Cu(111), and Cu (200) also appears, and that of Ag_2CO_3(300) disappears totally. With the increase of time, the relative intensity of Cu and Ag peaks increases, and until the end, no peaks of Cu oxides appear. These results strongly indicate that the Cu and Ag complexes are rapidly and completely decomposed within only 1 min in the mixed complex ink. The accelerated decomposition phenomenon is related to the catalytic activity of metal nanoparticles [27, 28]. When the Cu and Ag complexes are mixed, the Ag^+ would easily react with $HCOO^-$ to form metal Ag even at room temperature [29]. A simple experiment was designed to confirm this deduction. Formic acid of 5 wt.% was added into the Ag complex ink and its XRD pattern was measured immediately, where obvious Ag peaks are found (**Figure 5.8**). However, no Ag peaks are found in Ag complex ink, even stored at ambient conditions for one month. These results suggest that the Cu complex can accelerate the formation of Ag phase even at room temperature. TEM results also give solid evidence (**Figure 5.7d**); many Ag nanoparticles with sizes ranging from 2 nm to 20 nm (average size of 3.8 nm) are found in the Cu-46Ag complex ink at room temperature. These in-situ formed fresh Ag nanoparticles can catalyze the decomposition of Cu complex at 100 °C within only 1 min. The similar phenomenon was also reported by Magdassi *et al*., where pre-formed Ag nanoparticles with a size in the range of 4-15 nm could catalyze the synthesis of copper nanoparticles with decreasing reaction duration from 2 h to 10 min [19].

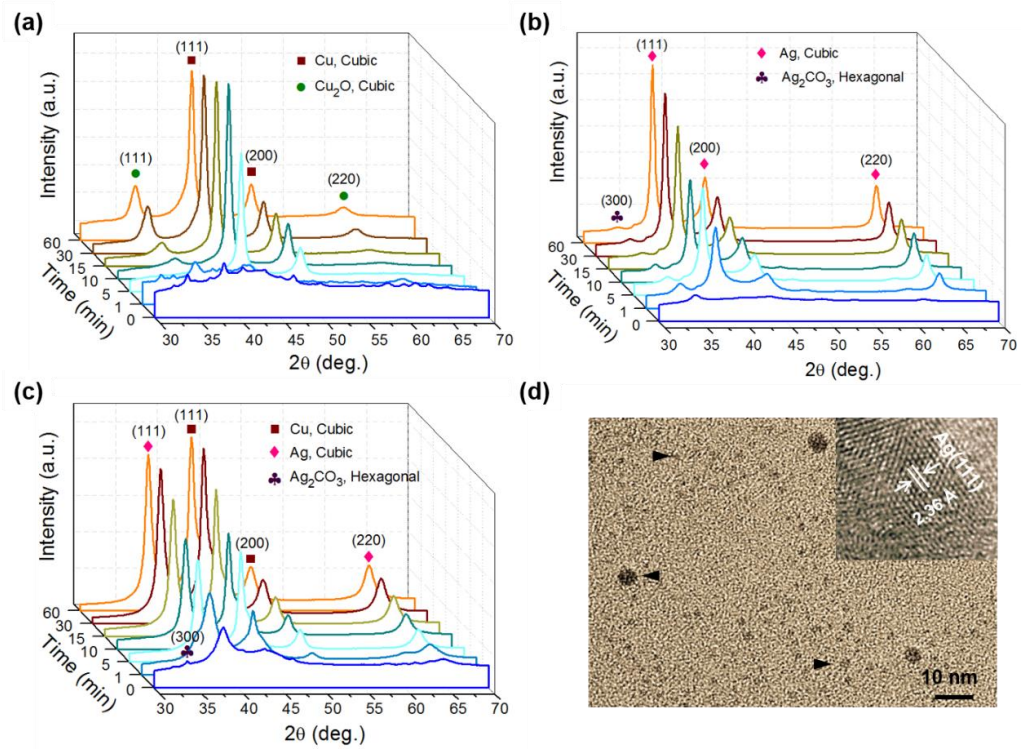

Figure 5.7 XRD patterns of (a) pure Cu, (b) pure Ag, and (c) Cu-46Ag complex inks; (d) TEM image and their HR-TEM image (inset) of in-situ formed Ag nanoparticles in Cu-46Ag complex ink.

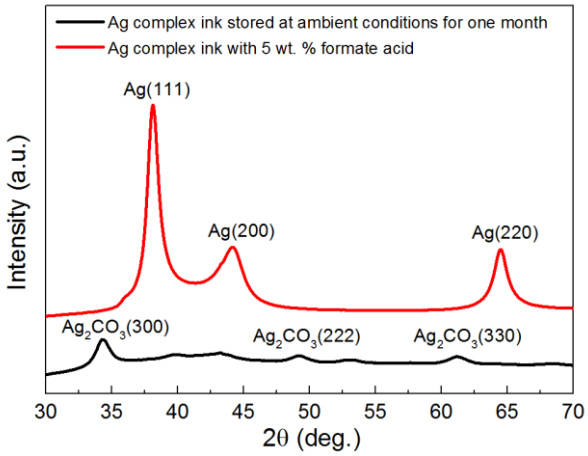

Figure 5.8 XRD patterns of Ag complex ink after storage in ambient conditions for one month and Ag complex ink with addition of 5 wt. % formate acid.

Figure 5.9 summarizes the self-catalyzed decomposition and sintering of Cu-Ag complex

inks. When the two metal complexes are mixed, some Ag nanoparticles form immediately due to the reaction between Ag+ and $HCOO^-$ (from Cu formate). These in-situ formed fresh Ag nanoparticles will catalyze the decomposition of Cu complex below 100 °C. This is a self-catalyzed decomposition process. During the annealing process, the Cu phase and Ag phase are continually formed from the decomposition of Cu-Ag complex. Ag phase is covered by newly formed Cu phase and then Cu phase is covered by the newly formed Ag phase again. In other words, the nucleation and growth of Cu and Ag are mutually dependent on each other to form a uniform Cu-Ag hybrid structures. This helps to avoid the oxidation of Cu and accelerate the sintering of Cu at low temperatures. Compared with the sintering of pure Cu and Ag complex inks, the sintering of Cu-Ag complex ink is accelerated to get a dense structure and a high conductivity of patterns at low temperatures for a short time. This is a self-catalyzed sintering process. Although the detailed mechanism is still unclear, it provides a valid strategy to achieve high conductive Cu-based patterns at low temperatures by selecting suitable catalysts.

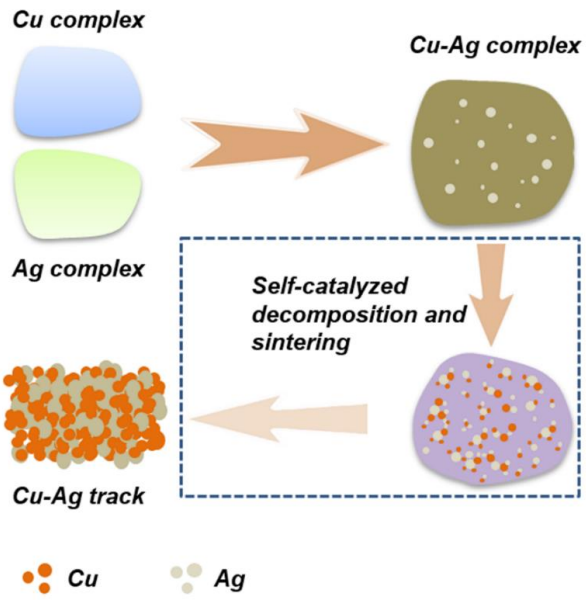

Figure 5.9 Schematic illustration of self-catalyzed decomposition and sintering of Cu-Ag complex inks.

5.5 Oxidation resistance of printed Cu-Ag hybrid patterns

The long-term stability of patterns presents significant challenges for their practical applications in printed electronic devices [30, 31]. Especially, the oxidation of Cu-based patterns in air would induce the heavy degradation of their electrical conductivity [32]. The stability of present patterns in air at different temperatures and humidity is shown in **Figure5.10** with the change of relative resistance (R/R_0, R_0 is the original resistance of pattern and R is the resistance after oxidation) of patterns. The samples were prepared from two kinds of annealing process (100 °C for 30 min and 140 °C for 30min). For distinction, different labels with information of annealing temperature are used. For example, the label of Cu-46Ag-140 means the sample prepared from Cu-46Ag complex ink using an annealing temperature of 140 °C. **Figure 5.10a** shows the R/R_0 evolution of patterns at 80 °C in air. The value of Cu patterns rapidly increases to 1.6 after 28 h, while those of Cu-Ag patterns remain stable or even have a little falling. The falling, especially in Cu-63Ag-100 patterns, is related to the further sintering of silver nanoparticles (**Figure 5.11**). As seen, the small particles have been sintered and grown to big particles, which is beneficial for the improvement of conductivity. After 64 h, R/R_0 of Cu patterns increases to about 2.0 while those of Cu-Ag patterns still remain stable or have only a slight increase to less than 1.2. A high temperature of 110 °C accelerates the rise of R/R_0 of printed patterns (**Figure 5.10b**). After 64 h, the R/R_0 of Cu patterns rises to about 20.0 while those of Cu-Ag patterns have a slight increase to less than 2.0. A high temperature of 140 °C (the maximum tolerable temperature of current PET substrate) is very harsh for the Cu patterns, resulting in the total loss of conductive ability after 32 h (Figure 5.10c). In contrast, the Cu-Ag patterns always show high oxidation resistance; the R/R_0 of all Cu-Ag patterns increases to less than 20 until 64 h (**Figure 5.10c**). **Figure 5.10d** shows the R/R_0 change of patterns at 85 °C-85% RH. The results are similar to that at 80 °C. The R/R_0 of Cu patterns increases rapidly to 3 after 64 h while those of Cu-Ag patterns have a slight increase to less than 1.3. The increase of R/R_0 is related to the oxidation of Cu in printed patterns (**Figure 5.12**). The oxides such as CuO and Cu_2O are semi-conductive, so they seriously degrade the electrical property of printed patterns [33]. Base on the above results, it is noteworthy that the high content of Ag in printed patterns enhances their oxidation resistance at high temperatures even in air. R/R_0 of Cu-30Ag patterns increases to more than 10 after 64 h at 140 °C, while those of Cu-46Ag and Cu-63Ag

patterns show a slight increase to less than 2. This phenomenon is attributable to high oxidation resistance of Ag phase as well as the very uniform distribution of them in Cu-Ag patterns (Figure 5.3 and 5.5). Even though it is not a solid solution alloy structure, the Ag phase uniformly surrounding the Cu phase can effectively protect Cu phase form oxidation and therefore enhance the overall oxidation resistance of printed patterns [22]. In the present work, Cu-Ag patterns prepared from Cu-46Ag and Cu-63Ag inks show a similar oxidation-resistant trend in which the R/R_0 is less than 2 even after 64 h at 140 °C. Therefore, 46 wt % Ag is enough for the prevention of Cu oxidation at temperature of 140 °C and below. In addition, it is noteworthy that except Cu-30Ag patterns, other two Cu-Ag patterns prepared from annealing temperatures of 140 and 100 °C show the similar oxidation-resistant trends. Therefore, it can be concluded that the Cu-Ag patterns could endure a high long-term stability at 140 °C, even after a low annealing temperature of 100 °C. The Cu-Ag patterns show a tempting prospect for the fabrication of highly reliable and cost-effective printed electronic devices on heat-sensitive substrates.

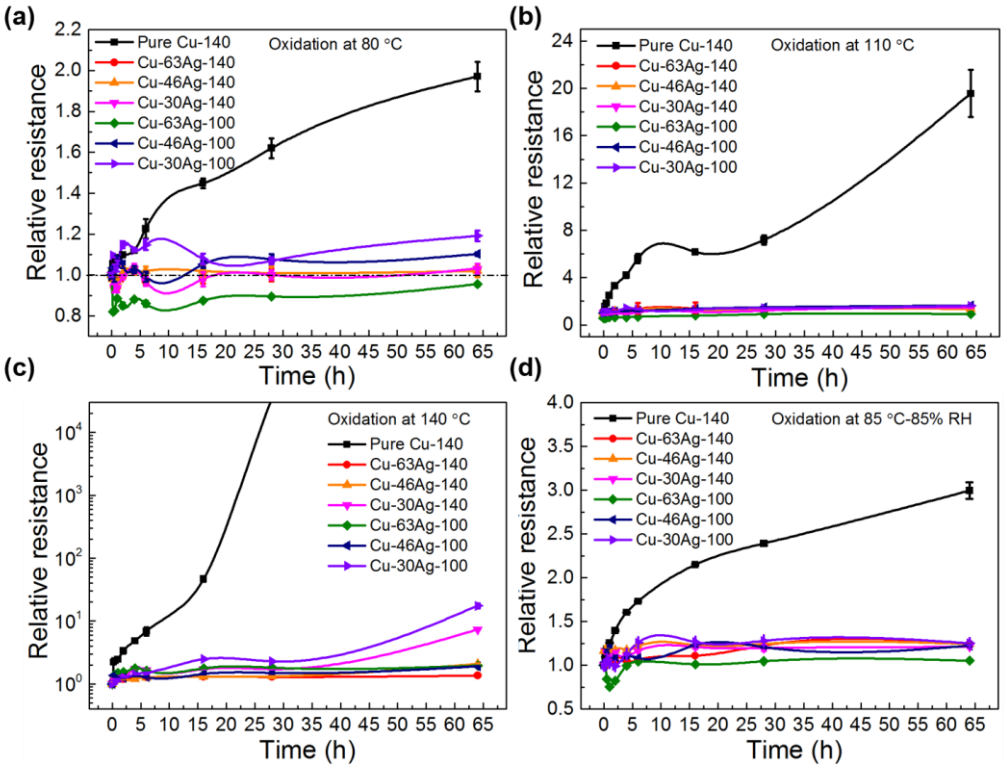

Figure 5.10 Changes in the relative resistance (R/R_0) of patterns prepared from pure Cu, Cu-30Ag, Cu-46Ag and Cu-63Ag complex inks in air at (a) 80 °C, (b) 110 °C, (c) 140 °C, and (d) 85 °C-85 % RH.

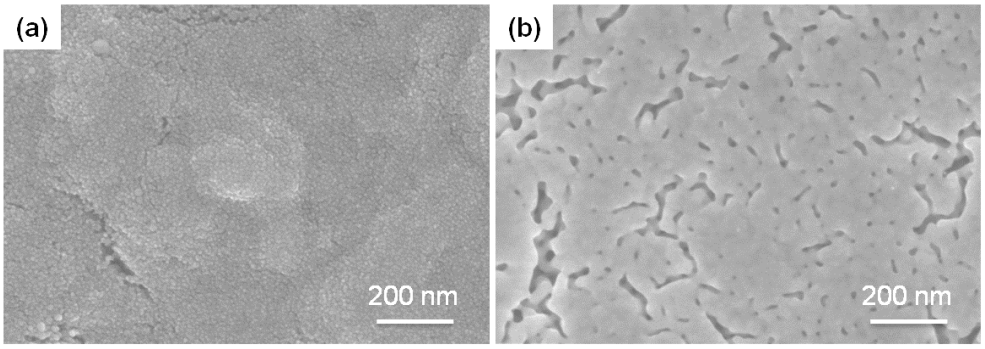

Figure 5.11 Microstructures of (a) original Cu-63Ag-100 pattern and (b) Cu-63Ag-100 pattern after aging at 80 for 2 h.

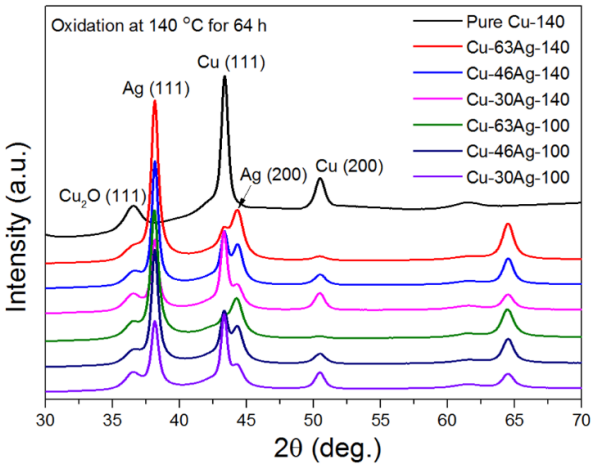

Figure 5.12 XRD patterns of printed patterns after oxidation at 140 °C for 64 h.

To demonstrate the long-term stability of Cu-Ag patterns in practical applications, the Cu pattern and Cu-46Ag pattern after oxidation at 140 °C in air were used as flexible conductive wires to light up a light-emitting diode (LED). With the increase of oxidation time, the Cu pattern causes the progressive dimming in the LED and fails to illuminate the LED after 180 min (**Figure 5.13a**). In contrast, the LED illumination intensity using printed Cu-46Ag pattern as a conductive wire remains almost constant after 180 min, which strongly suggests that the

Cu-46Ag patterns have a high long-term stability at 140 °C in air (**Figure 5.13b**). In addition, a bending fatigue test was conducted to evaluate the mechanical stability of the printed patterns (**Figure 5.14**). The relative resistance of printed conductors keeps below 1.3 after 1000 bending cycles at the bending radius of 7 mm. The result indicates that printed Cu-Ag patterns also have a high mechanical stability.

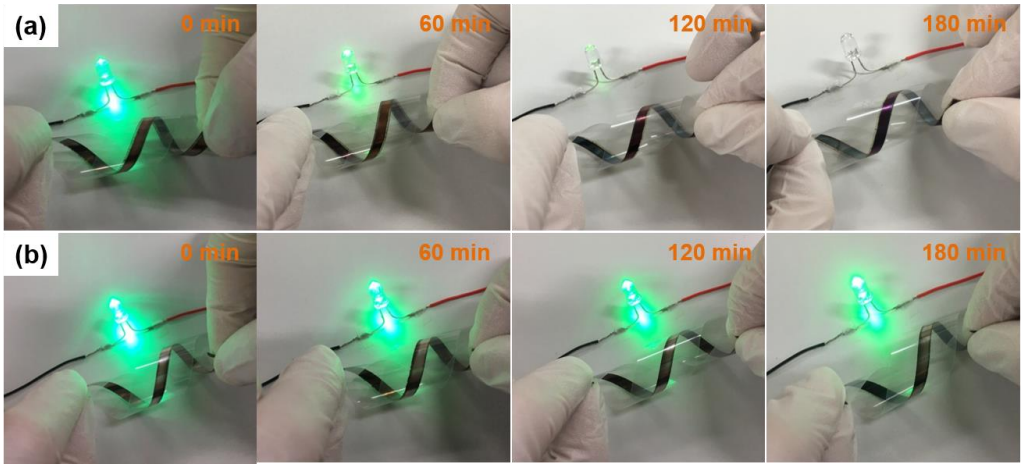

Figure 5.13 Photographs of the LED circuit with a 100 mm-long metal pattern prepared from (a) pure Cu and (b) Cu-46Ag complex inks on PET substrate after oxidation at 140 °C.

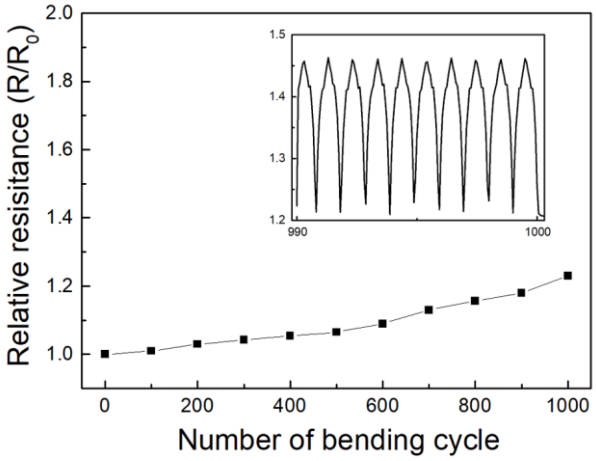

Figure 5.14 Change of relative resistance of the Cu-46Ag pattern during bending test. The bending radius is 7 mm. Inset graph shows the real-time relative resistance during the last ten cycles of bending and releasing process.

5.6 Conclusion

In this chapter, self-catalyzed C u-Ag complex inks have been successfully developed for low temperature fabrication of highly stable and conductive patterns on heat-sensitive substrates. The self-catalyzed characteristic can promote the rapid decomposition and efficient sintering of inks at such low temperatures of 100 °C and even 80 °C to form highly conductive patterns. The achieved resistivity of about 2.80×10^{-5} Ω·cm is even superior to that of pure Ag patterns at the same annealing conditions. The mechanism of low resistivity achievement at such low temperatures below 100 °C can be understood by two effects: 1) in-situ formed Ag nanoparticles in Cu-Ag complex inks can effectively catalyze the decomposition of Cu complex at lower temperatures; 2) the catalyzed decomposition process promotes the rapid nucleation and growth of Cu/Ag particles without any oxides at a low temperature below 100 °C, hence to accelerate their efficient sintering. Moreover, owing to the very uniform Cu-Ag hybrid structure, the printed Cu-Ag patterns show excellent stability at both high temperatures up to 140 °C (the maximum tolerable temperature of current PET substrate) and high humidity of 85 %. As a practical application example, printed patterns remain high conductivity after oxidation at 140 °C in air, which can be used as conductive wires to light up a LED.

References

1. Woo, K.; Kim, D.; Kim, J. S.; Lim, S.; Moon, J., Ink-jet printing of Cu−Ag-based highly conductive tracks on a transparent substrate. *Langmuir* **2009,** *25* (1), 429-433.

2. Wan-Ho, C.; Yeon-Taek, H.; Seung-Hyun, L.; Hak-Sung, K., Electrical wire explosion process of copper/silver hybrid nano-particle ink and its sintering via flash white light to achieve high electrical conductivity. *Nanotechnology* **2016,** *27* (20), 205704.

3. Grouchko, M.; Kamyshny, A.; Magdassi, S., Formation of air-stable copper-silver core-shell nanoparticles for inkjet printing. *Journal of Materials Chemistry* **2009,** *19* (19), 3057-3062.

4. Changsoo, L.; Na Rae, K.; Jahyun, K.; Yung Jong, L.; Hyuck Mo, L., Cu-Ag core–shell nanoparticles with enhanced oxidation stability for printed electronics. *Nanotechnology* **2015,** *26* (45), 455601.

5. Na Rae, K.; Yung Jong, L.; Changsoo, L.; Jahyun, K.; Hyuck Mo, L., Surface modification of oleylamine-capped Ag–Cu nanoparticles to fabricate low-temperature-sinterable Ag–Cu nanoink. *Nanotechnology* **2016,** *27* (34), 345706.

6. Farraj, Y.; Grouchko, M.; Magdassi, S., Self-reduction of a copper complex MOD ink for inkjet printing conductive patterns on plastics. *Chemical Communications* **2015,** *51* (9), 1587-1590.

7. Chun, S.; Grudinin, D.; Lee, D.; Kim, S.-H.; Yi, G.-R.; Hwang, I., Roll-to-roll printing of silver oxide pastes and low temperature conversion to silver patterns. *Chemistry of Materials* **2009,** *21* (2), 343-350.

8. Li, W.; Cong, S.; Jiu, J.; Nagao, S.; Suganuma, K., Self-reducible copper inks composed of copper-amino complexes and preset submicron copper seeds for thick conductive patterns on a flexible substrate. *Journal of Materials Chemistry C* **2016,** *4* (37), 8802-8809.

9. Hu, M.; Cai, X.; Guo, Q.; Bian, B.; Zhang, T.; Yang, J., Direct pen writing of adhesive particle-free ultrahigh silver salt-loaded composite ink for stretchable circuits. *ACS Nano* **2016,** *10* (1), 396-404.

10. Jolke, P.; Chris, E. H.; Antonius, W. M. d. L.; Ulrich, S. S., One-step inkjet printing of conductive silver tracks on polymer substrates. *Nanotechnology* **2009,** *20* (16), 165303.

11. Hatamura, M.; Yamaguchi, S.; Takane, S.-y.; Chen, Y.; Suganuma, K., Decarboxylation and simultaneous reduction of silver(i) [small beta]-ketocarboxylates with three types of coordinations. *Dalton Transactions* **2015,** *44* (19), 8993-9003.

12. Suganuma, K.; Wakuda, D.; Hatamura, M.; Nogi, M., Low-temperature wiring with ag nanoinks [Nanopackaging]. *IEEE Nanotechnology Magazine* **2010,** *4* (3), 20-23.

13. Araki, T.; Sugahara, T.; Jiu, J.; Nagao, S.; Nogi, M.; Koga, H.; Uchida, H.; Shinozaki, K.; Suganuma, K., Cu salt ink formulation for printed electronics using photonic sintering. *Langmuir* **2013,** *29* (35), 11192-11197.

14. Shin, D.-H.; Woo, S.; Yem, H.; Cha, M.; Cho, S.; Kang, M.; Jeong, S.; Kim, Y.; Kang, K.; Piao, Y., A Self-reducible and alcohol-soluble copper-based metal–organic decomposition ink for printed electronics. *ACS Applied Materials & Interfaces* **2014,** *6* (5), 3312-3319.

15. Yabuki, A.; Tanaka, S., Electrically conductive copper film prepared at low temperature by

thermal decomposition of copper amine complexes with various amines. *Materials Research Bulletin* **2012,** *47* (12), 4107-4111.

16. Farraj, Y.; Smooha, A.; Kamyshny, A.; Magdassi, S., Plasma-induced decomposition of copper complex ink for the formation of highly conductive copper tracks on heat-sensitive substrates. *ACS Applied Materials & Interfaces* **2017,** *9* (10), 8766-8773.

17. Haruta, M.; Daté, M., Advances in the catalysis of Au nanoparticles. *Applied Catalysis A: General* **2001,** *222* (1), 427-437.

18. Gawande, M. B.; Goswami, A.; Felpin, F.-X.; Asefa, T.; Huang, X.; Silva, R.; Zou, X.; Zboril, R.; Varma, R. S., Cu and Cu-based nanoparticles: synthesis and applications in catalysis. *Chemical Reviews* **2016,** *116* (6), 3722-3811.

19. Grouchko, M.; Kamyshny, A.; Ben-Ami, K.; Magdassi, S., Synthesis of copper nanoparticles catalyzed by pre-formed silver nanoparticles. *Journal of Nanoparticle Research* **2009,** *11* (3), 713-716.

20. Garnett, E. C.; Cai, W.; Cha, J. J.; Mahmood, F.; Connor, S. T.; Christoforo, M. G.; Cui, Y.; McGehee, M. D.; Brongersma, M. L., Self-limited plasmonic welding of silver nanowire junctions. *Nature Materials* **2012,** *11* (3), 241-249.

21. Yim, C.; Sandwell, A.; Park, S. S., Hybrid copper–silver conductive tracks for enhanced oxidation resistance under flash light sintering. *ACS Applied Materials & Interfaces* **2016,** *8* (34), 22369-22373.

22. Li, W.; Hu, D.; Li, L.; Li, C.-F.; Jiu, J.; Chen, C.; Ishina, T.; Sugahara, T.; Suganuma, K., Printable and flexible copper–silver alloy electrodes with high conductivity and ultrahigh oxidation resistance. *ACS Applied Materials & Interfaces* **2017,** *9* (29), 24711-24721.

23. Xu, W.; Wang, T., Synergetic effect of blended alkylamines for copper complex ink to form conductive copper films. *Langmuir* **2017,** *33* (1), 82-90.

24. Choi, Y.-H.; Hong, S.-H., Effect of the amine concentration on phase evolution and densification in printed films using Cu(ii) complex ink. *Langmuir* **2015,** *31* (29), 8101-8110.

25. Jeong, S.; Woo, K.; Kim, D.; Lim, S.; Kim, J. S.; Shin, H.; Xia, Y.; Moon, J., Controlling the thickness of the surface oxide layer on Cu nanoparticles for the fabrication of conductive structures by ink-jet printing. *Advanced Functional Materials* **2008,** *18* (5), 679-686.

26. Largiller, G.; Bouvard, D.; Carry, C. P.; Gabriel, A.; Müller, J.; Staab, T., Deformation and cracking during sintering of bimaterial components processed from ceramic and metal powder mixes. Part I: Experimental investigation. *Mechanics of Materials* **2012,** *53*, 123-131.

27. Back, S.; Yeom, M. S.; Jung, Y., Active sites of au and ag nanoparticle catalysts for CO_2 electroreduction to CO. *ACS Catalysis* **2015,** *5* (9), 5089-5096.

28. Dong, X.-Y.; Gao, Z.-W.; Yang, K.-F.; Zhang, W.-Q.; Xu, L.-W., Nanosilver as a new generation of silver catalysts in organic transformations for efficient synthesis of fine chemicals. *Catalysis Science & Technology* **2015,** *5* (5), 2554-2574.

29. Won, H. I.; Nersisyan, H.; Won, C. W.; Lee, J.-M.; Hwang, J.-S., Preparation of porous silver particles using ammonium formate and its formation mechanism. *Chemical Engineering Journal* **2010,** *156* (2), 459-464.

30. Paglia, F.; Vak, D.; van Embden, J.; Chesman, A. S. R.; Martucci, A.; Jasieniak, J. J.; Della Gaspera, E., Photonic sintering of copper through the controlled reduction of printed CuO nanocrystals. *ACS Applied Materials & Interfaces* **2015,** *7* (45), 25473-25478.

31. Aliprandi, A.; Moreira, T.; Anichini, C.; Stoeckel, M.-A.; Eredia, M.; Sassi, U.; Bruna, M.; Pinheiro, C.; Laia, C. A. T.; Bonacchi, S.; Samorì, P., Hybrid copper-nanowire–reduced-graphene-oxide coatings: A "green solution" toward highly transparent, highly conductive, and flexible electrodes for (opto)electronics. *Advanced Materials* **2017,** *29* (41), 1703225-n/a.

32. Jeong, S.; Lee, S. H.; Jo, Y.; Lee, S. S.; Seo, Y.-H.; Ahn, B. W.; Kim, G.; Jang, G.-E.; Park, J.-U.; Ryu, B.-H.; Choi, Y., Air-stable, surface-oxide free Cu nanoparticles for highly conductive Cu ink and their application to printed graphene transistors. *Journal of Materials Chemistry C* **2013,** *1* (15), 2704-2710.

33. Li, W.; Li, L.; Gao, Y.; Hu, D.; Li, C.-F.; Zhang, H.; Jiu, J.; Nagao, S.; Suganuma, K., Highly conductive copper films based on submicron copper particles/copper complex inks for printed electronics: Microstructure, resistivity, oxidation resistance, and long-term stability. *Journal of Alloys and Compounds* **2018,** *732*, 240-247.

Chapter 6

Summary

In this dissertation, novel low-cost Cu inks and post-treatment methods are successfully developed for fabrication of highly conductive and reliable Cu patterns on various plastic substrates, enabling these abundant and cheap Cu inks to replace or partly replace the noble Ag and Au inks in the application of printable and flexible electronics. Three strategies are proposed to address the oxidation problem of Cu inks and improve the conductivity and reliability of printed Cu patterns, including using submicron Cu particles instead of Cu nanoparticles, utilizing intense pulsed light (IPL) sintering, and introducing anti-oxidation Ag element.

In *chapter 1*, the emergence, development, and application of printed electronic is briefly described. The organic conductive polymers, metallic nanoparticle inks, and metallic complex inks have been reviewed with conducting mechanism, development, application, and technical limits. It is shown that metallic Ag inks exhibit the best performance; however, it cannot be satisfied with the need for low cost. Therefore, a purpose of developing low-cost Cu inks and three strategies for addressing the oxidation problem of Cu inks and improving the conductivity and reliability of printed Cu patterns are suggested.

In *chapter 2*, the concept that using in-situ formed fresh Cu nanoparticles to help sintering the submicron Cu particles has been proved feasible by the developed submicron Cu particle/Cu complex inks. During the low temperature heat treatment of 140 °C, fresh Cu nanoparticles decomposed from Cu complex can attach to the submicron Cu particles and activate their surface, which contributes to the connection and neck-growth between these submicron Cu particles to achieve conductive pathways. The effects of the size of submicron Cu particles and the ratio of the amount of Cu complex to particles on the conductivity and morphology of sintered Cu patterns are clarified, and the functions of the heat treatment temperature and holding time are investigated. Printed Cu patterns with a low resistivity of 1.1×10^{-5} Ω·cm can be easily obtained through heat treatment at 140 °C for only 15 min when the size of Cu particle is about 700 mm and the ratio of Cuf-AMP complex and Cu particles is 3: 1.

In *chapter 3*, IPL is utilized successfully to not only reinforce the sintering between

submicron Cu particle and in-situ formed Cu nanoparticles but also improve the adhesion between printed patterns and substrates, enabling the printed Cu patterns to have a high conductivity and high mechanical reliability. The best conductivity of printed Cu pattern is about 5.8×10^{-6} Ω·cm. The bending fatigue test indicates that the sintered Cu patterns have high mechanical/electrical reliability due to the robust sintered Cu microstructure and strong adhesion between Cu patterns and substrates. The oxidation resistance test indicates the printed Cu patterns from submicron Cu particles with Cu complex exhibit excellent oxidation resistance and are superior to those from Cu nanoparticles. The degeneration of electrical conductivity of printed Cu patterns at high temperatures is attributed to not only the rapid oxidation of Cu to Cu_2O but also to the microstructure evolution, particularly the breaking of the necks joining adjacent particles. Their potential accessibility for flexible electronic device applications was demonstrated with a flexible and folding LED circuit and a flexible dipole antenna for wireless power transmission. It is believed that the use of big and low-cost Cu particles to create highly reliable and highly conductive Cu patterns by a suitable curing process would pave the way for ubiquitous smart, flexible and wearable devices.

In *chapter 4*, in order to further improve the oxidation resistance of printed Cu patterns, printable and flexible Cu-Ag alloy patterns are successfully fabricated by using a newly developed Cu particle/Ag complex ink and a simple two-step sintering process. The Cu particle/Ag complex ink firstly transforms into a Cu-Ag nanoparticle core-shell structure under a low temperature of 140 °C in air and then further transforms into Cu-Ag alloy under IPL sintering which induces rapid diffusion between the Cu core and the Ag nanoparticle shell. It was revealed that the obtained Cu-Ag alloy pattern has a bulk-like microstructure and shows a very low resistivity of 3.4×10^{-6} Ω·cm (50% of the bulk conductivity of Cu). Most importantly, the printed flexible Cu-Ag alloy patterns have ultrahigh oxidation resistance that remains stable in air at 180 °C and 200 °C, showing great potential for practical use in the fabrication of highly reliable and cost-effective printed electronic devices.

In *chapter 5*, self-catalyzed Cu-Ag complex inks have been successfully developed for low temperature fabrication of highly stable and conductive patterns on heat-sensitive substrates such as PET. The self-catalyzed characteristic can promote the rapid decomposition

and efficient sintering of inks at such low temperatures of 100 °C and even 80 °C to form highly conductive patterns. The achieved resistivity of about 2.80×10^{-5} Ω·cm is even superior to that of pure Ag patterns at the same annealing conditions. The mechanism of low resistivity achievement at such low temperatures below 100 °C can be understood by two effects: 1) in-situ formed Ag nanoparticles in Cu-Ag complex inks can effectively catalyze the decomposition of Cu complex at lower temperatures; 2) the catalyzed decomposition process promotes the rapid nucleation and growth of Cu/Ag particles without any oxides at a low temperature below 100 °C, hence to accelerate their efficient sintering. Moreover, owing to the very uniform Cu-Ag hybrid structure, the printed Cu-Ag patterns show excellent stability at both high temperatures up to 140 °C (the maximum tolerable temperature of current PET substrate) and high humidity of 85 %. As a practical application example, printed patterns remain high conductivity after oxidation at 140 °C in air, which can be used as conductive wires to light up a LED.

Research achievements

A Journal papers

1. **Wanli Li**, Cai-Fu Li, Jinting Jiu, Minoru Ueshima, Zhi-Quan Liu and Katsuaki Suganuma, Self-catalyzed copper-silver complex inks for low-cost fabrication of highly oxidation-resistant and conductive copper-based tracks at a low temperature below 100 °C, Nanoscale, Vol. 10, pp. 5254-5263, February, 2018.

2. **Wanli Li**, Lingying Li, Yue Gao, Dawei Hu, Cai-Fu Li, Hao Zhang, Jinting Jiu, Shijo Nagao and Katsuaki Suganuma, Highly conductive copper films based on submicron copper particles/copper complex inks for printed electronics: microstructure, resistivity, oxidation resistance, and long-term stability, Journal of Alloys and Compounds, Vol. 732, pp. 240-247, January, 2018.

3. **Wanli Li**, Dawei Hu, Lingying Li, Cai-fu Li, Jinting Jiu, Chuantong Chen, Toshiyuki Ishina, Tohru Sugahara and Katsuaki Suganuma, Printable and flexible copper-silver alloy electrodes with high conductivity and ultrahigh oxidation resistance, ACS Applied Materials & Interfaces, Vol. 9, No 29, pp. 24711-24721, July, 2017.

4. **Wanli Li**, Hao Zhang, Yue Gao, Jinting Jiu, Cai-fu Li, Chuantong Chen, Dawei Hu, Yusuke Goya, Yutao Wang, Hirotaka Koga, Shijo Nagao and Katsuaki Suganuma, Highly reliable and highly conductive submicron Cu particle patterns fabricated by low temperature heat-welding and subsequent flash light sinter-reinforcement, Journal of Materials Chemistry C, Vol. 5, pp. 1155-1164, December, 2016.

5. **Wanli Li**, Shuren Cong, Jinting Jiu, Shijo Nagao and Katsuaki Suganuma, Self-reducible copper inks composed of copper-amino complexes and preset submicron copper seeds for thick conductive patterns on a flexible substrate, Journal of Materials Chemistry C, Vol. 4, pp. 8802-8809, August, 2016.

6. **Wanli Li**, Yang Yang, Bowen Zhang, Cai-Fu Li, Jinting Jiu, Katsuaki Suganuma, Highly densified Cu wirings fabricated from air-stable Cu complex ink with high conductivity, enhanced oxidation resistance, and flexibility, Advanced materials interface, accepted.

7. Hao Zhang, **Wanli Li**, Yue Gao, Hao Zhang, Jinting Jiu and Katsuaki Suganuma, Enhancing low-temperature and pressureless sintering of micron silver paste based on an ether-type solvent, Journal of Electronic Materials, Vol. 46, No. 8, pp. 5201-5208, April, 2017.

8. Yue Gao, Hao Zhang, **Wanli Li**, Jinting Jiu, Shijo Nagao, Tohru Sugahara and Katsuaki Suganuma, Die bonding performance using bimodal Cu particle paste under different sintering atmospheres, Journal of Electronic Materials, Vol. 46, No. 7, pp. 4575-4581, March, 2017.

B Conference proceedings

1. Lingying Li, **Wanli Li**, Jinting Jiu and Katsuaki Suganuma, Effects of oxygen containing groups on barrier layer on the stability of silver nanowire transparent electrodes, IEEE 17th International Conference on Nanotechnology, Pittsburgh, pp. 903-906, November, 2017.

C Presentations

1. **Wanli Li**, Jinting Jiu and Katsuaki Suganuma, Highly reliable Cu-Ag alloy electrodes for flexible electronics, International Conference on Flexible and Printed Electronics 2017, Jeju Island, Korea, September 5-7, 2017.

2. **Wanli Li**, Jinting Jiu and Katsuaki Suganuma, Low-temperature sintering of submicron copper particle ink, Japan Institute of Electronics Packaging 2017; Keio University, Japan, March 6-8, 2017.

3. **Wanli Li**, Jinting Jiu and Katsuaki Suganuma, Flexible copper patterns based on a novel copper ink composed of submicron copper particles and copper complexes under low temperature process, International Conference on Flexible and Printed Electronics 2016, Yonezawa, Japan, September 6-8, 2016.

D Patents

1. 配線作製方法，**李万里**，菅沼克昭，特願番号：2017-047241.

2. 銅銀合金の合成方法、および導通部の形成方法，菅沼克昭，**李万里**，酒金婷，上岛稔，特願番号：2017-144038.

Acknowledgement

Firstly, I would like to express my sincere gratitude to my advisor Prof. Katsuaki Suganuma for providing me an international and competitive research environment and for his inspiring guidance and steady support to my Ph. D. study and related research.

Besides my advisor, I would like to thank the rest of my thesis committee: Prof. Masaya Nogi and Assoc. Prof. Shijo Nagao, for their invaluable advice and encouraging comments, but also for the hard questions which incented me to widen my research from various perspectives. I also would like to thank Assoc. Prof. Hirotaka Koga for his invaluable advice and comments on my thesis.

I would like to thank Dr. Jinting Jiu, Professor Zhi-Quan Liu, Professor Hao Wang, Dr. Tohru Sugahara, Dr. Chuantong Chen, Dr. Cai-Fu Li, Dr. Hao Zhang, and Dr. Peng Xue for their valuable advice and comments on my research and publication activities. I thank all the members and alumni of Suganuma Laboratory, Dr. Chunhui Wu, Dr. Ekubaru Yusufu, Dr. Teppei Araki, Dr. Hao Zhang, Dr. Shuren Cong, Dr. Su Ding, Dr. Chun Pei, Dr. Aripuru Reira, Mr. Zhenghong Wang, Mr. Seungjun Noh, Mr. Yue Gao, Mr. Chanyang Choe, Mr. Zheng Zhang, Mr. Jeyun Yeom, Mr. Guiming Liu, Mr. Dong-Jin Kim, Mr. Hiroki Yoshikawa, Mr. Yusuke Goya, Ms. Bowen Zhang, Ms. Linying Li, Ms. Haoran Ding, Ms. Fengpei Lang, Mr. Taikun Fan, Mr. Dawei Hu, Mr. Akio Shimoyama, Mr. Norio Asatani, Mr. Koji Kimoto, Mr. Aishi Suetake, Ms. Emi Yokoi, Ms. Ming-Chun Hsieh, Ms. Noriko Kagami, Ms. Keiko Suzuki, Ms. Naomi Keenan, Ms. Seiyou Okuda, Ms. Sachiko Moribe. Without their encouragement and support, it would not be possible to conduct this research.

Also I thank my friends and colleagues in Osaka University, Dr. Xiangdong Liu, Dr. Jie Zhang, Dr. Xiaowei Shi, Dr. Xiaochao Liu, Mr. Jeong-Min Kim, Mr. Sang-Hoon, Jin, Mr. Bo Zhuang. In particular, I am grateful to Ms. Xin Zhang in South China University of Technology for her invaluable support and patience.

Finally, I would love to thank my family for inspiring me to realize my own potential and supporting me materially and spiritually throughout my life. All the encouragement, support, and love they have provided me over the years is the reason why I can do it today.